UNIVERSITY OF
LINCOLN

The development of a delivery method for a non-traditional antibiotic: Electrospun polymer nanofibers

Jasmine Ahad

MSc by Research

2020

The development of a delivery method for a non-traditional antibiotic: Electrospun polymer nanofibres

Jasmine Ahad

A thesis submitted in partial fulfilment of the requirements of the University of Lincoln for the degree of MSc by Research, School of Pharmacy

Supervisory team: Dr Emma J Wright, Dr Lorna Lancaster and Dr Nick Tucker

March 2020

I DECLARATION AND CERTIFICATE OF ORIGINALITY

I hereby certify that I am responsible for the work submitted in this thesis, that the original work is my own, except as specified in the acknowledgements and references, and that neither the thesis nor the original work contained herein has been previously submitted to any institution for a degree.

Signature: 

Name: Jasmine Ahad

Date: 19th March 2020

II ABSTRACT

Through electrospinning, a hydroxypropyl methylcellulose (HPMC) non-woven nanofibrous patch was formed. The effects of propylene glycol (PG) and dimethyl sulfoxide (DMSO) were investigated to determine the impact co-solvents would have in terms of rheological characterisation and properties; as well as the electrospinnability when incorporated into 5%, 7.5% and 10% (w/w) HPMC. The HPMC solutions were rheologically characterised to observe the rheological properties and it was found that the incorporation of the co-solvents overall increased the polymer's elasticity.

After electrospinning, nanofibres were visualised through SEM to measure bead diameters. The addition of both co-solvents reduced bead diameter, the most prominent decrease was from 0.73 µm (10% HPMC %w/w) to 0.36 µm (10% HPMC with 2% PG and 7.5% DMSO %w/w). The increase in elasticity allowed for the solution to be more stable without reaching gel point; as well as increasing hydrodynamic volume to reduce polymer-polymer interactions when electrospinning. Further work needs to be done to decrease and/or remove bead formation through altering more electrospinning parameters such as the electrospinning solution and environmental factors.

The production of bacteriocins was attempted through cloning cloacins in the hopes of incorporating them into the nanofibrous patch and to act as a novel antimicrobial. The aim of this was to provide an alternative to traditional antibiotics with a reduced risk of developing resistance. However, due to time restrictions, the synthesis of these bacteriocins did not progress past the restriction enzyme digestion phase.

III ACKNOWLEDGEMENTS

I would like to express my sincere appreciation to my supervisors: Drs Emma Wright, Lorna Lancaster and Nick Tucker. You all have guided and encouraged me throughout my thesis and provided limitless anecdotes which I will forever remember. Thank you for providing me with the opportunity to develop my skills and learn new techniques that have helped me to grow as a researcher and that I can take forward to the next stage of my scientific career.

I would like to express my endless gratitude to Dan Lloyd, Laura Rutledge and Dr James Flint for providing a helping hand and allowing for your brains to be picked. Thank you for supporting me in times when life decided to throw a spanner in the works. You provided me with the tools that I needed to complete my research.

I would also like to thank my friends Rohan Mosely, Samantha Ellis and Chris Weck for always being there and providing great support. I wish you all the best success for the future.

Lastly, I would like to thank Fielden Dawson for making sure I had a roof over my head, I was financially supported and that I always had someone to talk to. Thank you for everything.

IV TABLE OF CONTENTS

V LIST OF FIGURES

VI LIST OF TABLES

VII GLOSSARY AND ABBREVIATIONS

AR	Antimicrobial resistance
BHI	Brain heart infusion
EC	Ethylcellulose
DDS	Drug delivery system/s
DMSO	Dimethyl sulfoxide
DS	Degree of substitution
DTM HCl	Diltiazem hydrochloride
EDTA	Ethylenediaminetetraacetic acid
HMW	High molecular weight
HPC	Hydroxypropyl cellulose
HPMC	Hydroxypropyl methylcellulose
Kbp	Kilobase pairs
LMW	Low molecular weight
MC	Methylcellulose
Nosocomial	Hospital-acquired infections or diseases
OD	Optical density
PG	Propylene glycol
R.m.s	Root-mean-square
A	Surface area
A:V	Surface area to volume ratio
SEM	Scanning electron microscope/microscopy
Spp.	Species

1 INTRODUCTION

Antimicrobial resistance (AR) is one of the most prominent issues facing the 21st century and is a key threat to global health. It is predicted that by 2050, bacterial infections will lead to 10 million deaths and an economic loss of $100 trillion annually (Tangcharoensathien *et al.,* 2017). Therefore, it is imperative that an intervention is made and alternatives to traditional antibiotics are discovered, explored and introduced to the health systems. Wound care is one of the areas in which AR can have a major impact. Wound healing is a complex process and if interrupted – such as through infection – could lead to the formation of non-healing, chronic wounds. Infections within the wound are harder to combat or prevent when the infectious bacteria are resistant.

A hydroxypropyl methylcellulose (HPMC) nanofibrous patch with incorporated novel antimicrobials may be a viable alternative. The patch should be able to provide a physical barrier to the wound from the outside from contaminants while allowing oxygen to flow through. The incorporation of the novel antimicrobial should be able to help prevent infection while reducing the risk of resistance and helping the wound progress past the inflammatory phase and heal.

1.1 POLYMERS AND HYDROGELS

Hydrogels have been employed in the field of molecular biology aiding advances in treating a variety of diseases (Peppas *et al.,* 2000). For example, recently there have been developments in hydrogel-based drug delivery systems (DDS) for major infectious diseases such as Acquired Immune Deficiency Syndrome (AIDS), influenza and Ebola (Vashist *et al.,* 2016). Hydrogels are 3D, hydrophilic, polymeric networks which are capable of absorbing large volumes of water or biological fluids (Peppas *et al.,* 2000; Chai *et al.,* 2017). These 3D networks, held together by physical or chemical crosslinks, are extensive enough to make hydrogels insoluble in aqueous media (Peppas *et al.,* 2000; Maitra and Shukla, 2014).

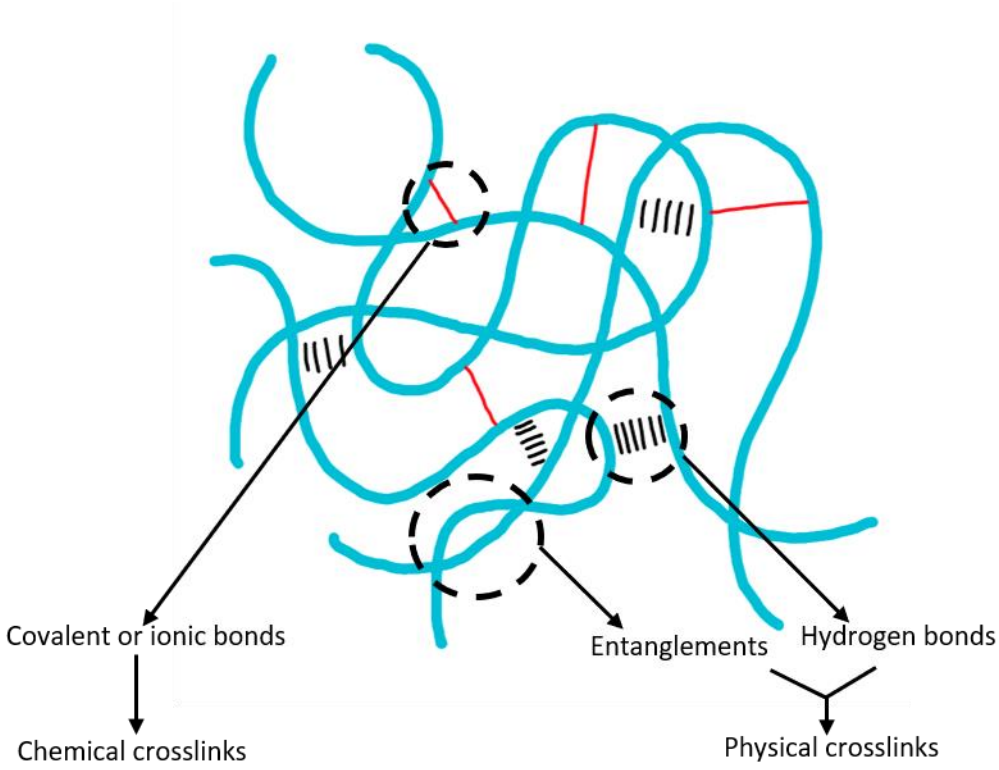

Figure 1: A schematic diagram showing the difference between physical crosslinks and chemical crosslinks. Physical crosslinks are entanglements (overlaps of long polymer chains) and hydrogen bonds (black dashed lines). Chemical crosslinks are covalent or ionic bonds (red lines).

Physical crosslinks consist of entanglements and hydrogen bonding and are key to the many features of polymers such as network structure and physical integrity (**Figure 1**) (Peppas *et al.,* 2000; Serpe and Craig, 2007). They impact the viscoelastic nature of a polymer gel; the more physical crosslinks present, the more elastic the polymer will be. Entangled chains are chains which overlap – almost as a knot – and are hindered in their ability to slide over each other. The number of entanglements within a polymer gel can be linked to chain length (Brostow *et al.,* 1995). The simplest measure of the polymer chain is the contour length nl, this is the length of the stretched-out molecule with a chain of n bonds of length l (Kremer *et al.,* 2005). However, as polymer chains can be coiled up when in a molten or dilute state – as well as if the conformation changes due to thermal motion – the contour length is not a realistic measure of polymer chain length (Kremer *et al.,* 2005). Taking these into consideration there are two other useful average measures for polymer coil dimensions: r.m.s (root-mean-square) and radius of gyration. The r.m.s is the unperturbed end-to-end distance of the polymer chains between two neighbouring crosslinks (Peppas *et al.,* 2000), denoted as **Equation 1**, where <> indicates thermal change. Alongside this, there is also the radius of gyration, which is the average distance of a chain segment from the centre of the mass of the polymer coil, denoted as **Equation 2**. In the simplest of models for polymer coils, the chains consist of N volume-less C-C segments

(Kuhn segments) of length b (Kuhn lengths) which can rotate freely in space (Doi and Edwards, 1986; Kremer *et al.,* 2005). As the Kuhn segments can adopt any orientation, the polymer coil executes a random walk configuration (**Equation 3**) (Doi and Edwards, 1986; Kremer *et al.,* 2005). Meaning the polymer chain can coil back and overlap itself several times, leading to a dense and entangled structure (Kremer *et al.,* 2005).

$$< r^2 >_0^{1/2}$$

Equation 1

$$< R_g^2 >_0^{1/2}$$

Equation 2

$$< R^2 >= Nb^2$$

Equation 3

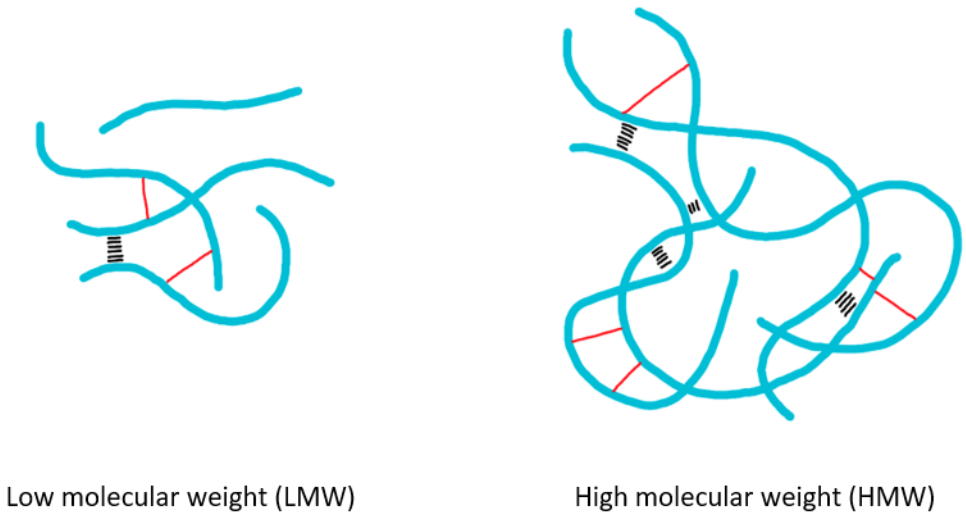

Figure 2: A schematic diagram showing the difference between low molecular weight (LMW) polymer chains and high molecular weight (HMW) polymer chains. Physical crosslinks are entanglements (overlaps of long polymer chains) and hydrogen bonds (black dashed lines). Chemical crosslinks are covalent or ionic bonds (red lines).

Polymers which have shorter chains (low molecular weight (LMW)) are less likely to lead to entanglements, while polymers with longer chains (high molecular weight (HMW)) are more likely to entangle as they will occupy more space (**Figure 2**) (Xiao *et al.,* 2017). As more chains are entangled with each other this gives rise to the effects of high elasticity and the chains are harder to "pull apart" (Barnes *et al.,* 2005; Schach and Creton, 2008). Chemical crosslinks are defined as covalent or ionic bonds which links one polymer chain to another (Doi and Edwards, 1986; Kobayashi and Müllen, 2014). Again, this impacts the physical properties of the gel (Zweifel *et al.,* 2009). The presence of crosslinking can increase elasticity and decrease viscosity.

This is due to crosslinking preventing the flow of polymer chains, causing them to be more rigid (Maitra and Shukla, 2014). The general rule is an increase in crosslinking – chemical or physical – leads to an increase in polymer elasticity.

Alongside crosslinking, rheological properties of a gel can also depend on the solvation effect. This is the interaction of a solvent with the dissolved molecules (Atkins and De Paula, 2014). Molecules may be ionised or uncharged, and when in the process of solvation leads to the molecule being surrounded by a concentric solvent shell. For example, depending on the strength of the charge this could lead to a secondary shell surrounding the first and possibly even a third. This increases the size of the sphere of solvation, also known as the Stokes radius (**Figure 3**).

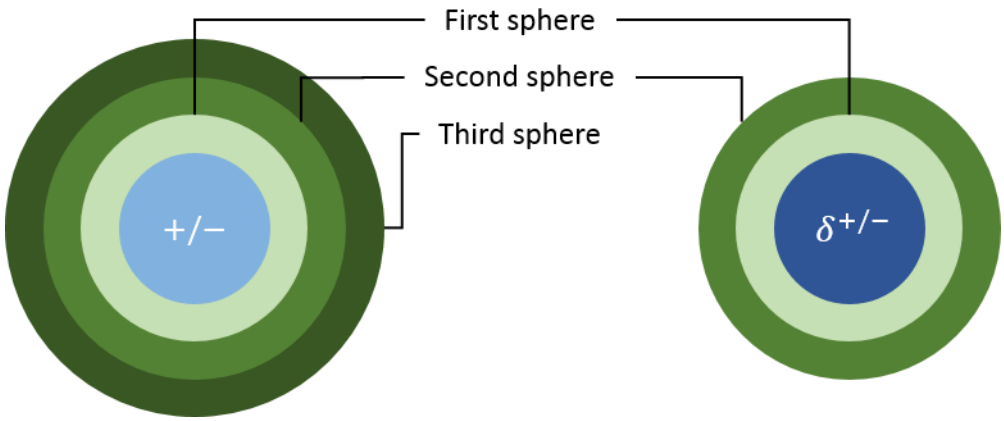

Figure 3: A diagram to show the sphere of solvation. In this example, the stronger charge (+/-) has a third sphere, increasing the general sphere of solvation.

The Stokes radius is the radius of a hard-sphere which diffuses at the same rate as the solute in relation to solute mobility (Atkins and De Paula, 2014). For example, a smaller ion with hydration may have a greater Stokes radius compared to a larger ion with hydration. An ion with a greater Stokes radius when in solution will "drag" a greater number of water molecules along with it as it moves through the solution (Atkins and De Paula, 2014). When discussing polymers, Stokes radius is known as "hydrodynamic volume". When the hydrodynamic volume of the polymer is raised – for example by introducing a co-solvent – this could lead to unfavourable packing of the polymer chains. This could then lead to hydrogen bonds being less likely to form, as well as a reduction in polymer-polymer interactions which could further interact with the polymer's properties (Kremer *et al.,* 2005).

Degree of substitution (DS) is also important in polymer chemistry. This is the average number of substituent groups attached per monomeric unit. Typically, a polymer with a higher DS will lead to less favourable chain alignment. Along with this, the substituents can have a similar impact as the general rule is that the larger substituents will occupy more space. The more space that is occupied, the less likely the chains are to pack

favourably which can similarly impact the polymer's properties to hydrodynamic volume. The unfavourable packing will mean that the chains are less likely to develop hydrogen bonds and polymer-polymer interactions. However, the chains may entangle and are less likely to "slide over each other" with ease, thus increasing elasticity (Bonet *et al.,* 2005).

Properties of a hydrogel can vary widely depending on the sample's composition. It is therefore important to characterise the stability of hydrogels. This can be done using three main parameters. The first parameter is the polymer volume fraction in the swollen state. This measures the amount of fluid absorbed and retained by the hydrogel. If the hydrogel does not contain ionic moieties then the structure can be analysed using the Flory-Rehner theory which states that a crosslinked or entangled gel immersed in a fluid, when allowed to reach equilibrium, is subject to only two opposing forces (Hamley, 2007). These forces are the thermodynamic forces of mixing and the retractive force of the polymer chains themselves; yet at equilibrium, the two forces are equal (Hamley, 2007). This is described using **Equation 4**:

$$\Delta G_{total} = \Delta G_{elastic} + \Delta G_{mixing}$$

Equation 4

The $\Delta G_{elastic}$ represents the elastic retractive forces which are developed inside of the gel. The ΔG_{mixing} is a result of the spontaneous mixing of the fluid molecules with the polymer chains. It is a measure of the compatibility of the polymer with the surrounding fluid molecules (Hamley, 2007).

The second parameter is that hydrogels can also be characterised using the molecular weight of the polymer chain between two neighbouring crosslinking points (Mc). These points can be chemical crosslinks or physical entanglements (Khan *et al.,* 2016). However, polymerisation is a process that has a random nature, therefore, only an average Mc value can be calculated.

Finally, the third parameter is mesh size which refers to the spacing within the 3D network. This can be found from the correlation distance between two adjacent crosslinks and provides a measure for the space available between macromolecular chains for drug diffusion. Again, due to the random nature of polymerisation, the mesh size given will be an average (Hamley, 2007; Khan *et al.,* 2016). This parameter is of interest in the pharmaceutical industry as a primary method of drug release from hydrogels. This is achieved through simple diffusion of the drug through the space between the macromolecular chain. The spacing – pores – can be controlled in terms of size and shape. This leads to hydrogels being classified as macro-porous, micro-porous or non-porous (Savina *et al.,* 2016).

1.1.1 Viscoelasticity

Viscoelasticity describes the behaviour or flow of matter. Materials may behave as a liquid (viscously) or as a solid (elastically). This is dependent on the material's properties and the conditions the material is subjected to, including the timescale of the rheological experiment (Kavanagh and Ross-Murphy, 1998; Sinko, 2017). A viscous material will undergo viscous flow to relieve the application of a force parallel to the face of the material. This is displayed in **Figure 4**. A material is considered as being made up of many parallel horizontal segments that are of an infinitesimal distance (dr) from each other. Force (F') is applied to the top segment, inducing the flow. The dashed lines indicate where the material once was, and the solid block is where the material has moved to. Therefore, the velocity between the two planes is dv. The force per area (A) is what is known as shear stress γ (Papanastasiou *et al.,* 2002). Purely viscous materials follow Newton's viscosity law (**Equation 5**) (Papanastasiou *et al.,* 2002; Sinko, 2017).

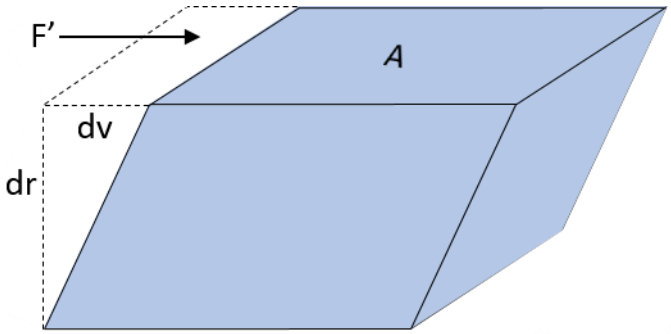

Figure 4: A representation of the shear force required to produce a velocity gradient between the parallel planes of a Newtonian liquid

Elastic materials, however, obey Hooke's law, meaning that under force, the molecules within a material will return to the initial state of equilibrium (**Equation 6**) (Sinko, 2017). This means the material will revert to their original shape after deformation like a spring. However, materials only follow Hooke's law when force is applied within the elastic range (Sinko, 2017). Once the material goes beyond the elastic range permanent deformation may occur (Sinko, 2017).

$$\sigma_s = \eta \frac{\mathrm{d}_{\varepsilon_s}}{dt}$$

Equation 5

$$\sigma = E_\varepsilon$$

Equation 6

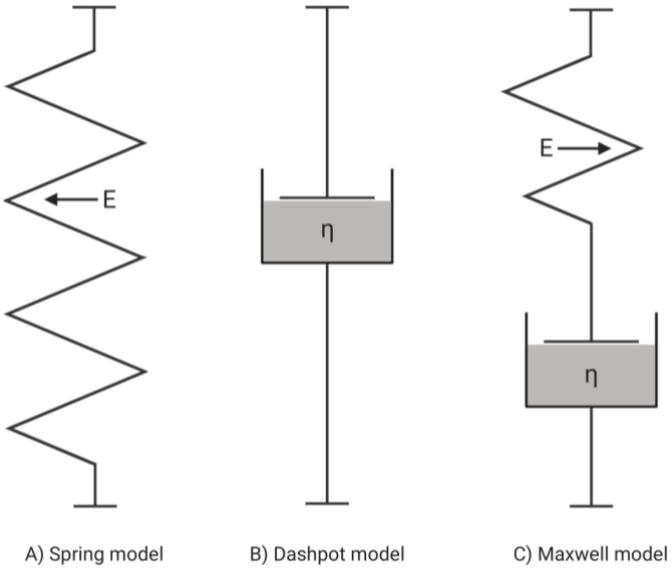

Figure 5: The spring model showing the behaviour of elastic materials. The dashpot model showing the behaviour of viscous materials. The Maxwell model showing the behaviour of viscoelastic materials.

The deformation timescale determines the ratio of viscous to elastic behaviour of a given material (Picout and Ross-Murphy, 2003). In mechanical models, Hookean deformation is represented by the spring model, showing that the force applied is proportional to its extension. It also means that objects which display only elastic behaviour will return to its original dimensions after this force or stress is removed, and the damage is non-permanent. Newtonian fluids displaying only viscous behaviour is shown through the dashpot model, in which the force is proportional to the extension rate. The Maxwell model is used for viscoelastic materials which display both the elastic modulus E and the viscosity coefficient η. The model includes the damper as a Newtonian fluid, with energy being dissipated, and the spring model with Hooke's law with energy being retained (**Figure 5**) (Flügge, 1975).

1.1.2 Hydroxypropyl Methylcellulose

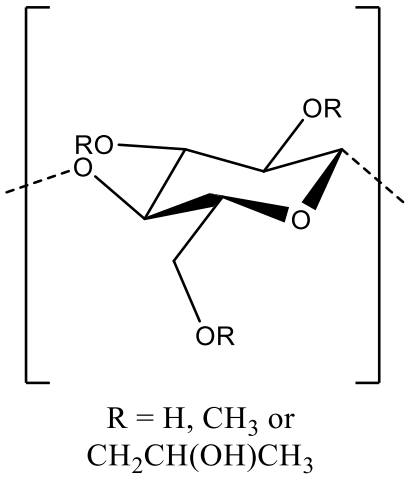

Figure 6: The structure of hydroxypropyl methylcellulose (HPMC). Drawn on ChemDraw Prime

Hydroxypropyl methylcellulose (HPMC) is a surface modified cellulose which is generally inert, non-toxic and viscoelastic, with multiple uses in food, cosmetics and the pharmaceutical industry (Kavanagh and Ross-Murphy, 1998; de Silva and Olver, 2005). HPMC is one of few water-soluble cellulose polymers and can rapidly form a uniform, strong and a viscous gel layer (Qui and Park, 2001). **Figure 6** shows the general structure of HPMC (Qui and Park, 2001). The monomeric units are linked by 1,4-β-glycosidic bonds and the R units contain substituents which are hydroxypropyl ($CH_2CH(OH)CH_3$), methoxy groups (CH_3), or hydrogen (H) (de Siva and Olver, 2005). The polymer's degree of substitution (DS), functional group substitution and chain length have an impact on the polymer's permeability, water solubility and mechanical properties such as tensile strength, elongation and rheology (Osorio *et al.,* 2011).

Some other water-soluble hydrogel-forming cellulose polymers include methylcellulose (MC), ethylcellulose (EC) and hydroxypropyl cellulose (HPC) which have different substituents as listed in **Table 1**, and this impacts the packing of the polymer chains (Gao *et al.,* 2011).

Table 1: Cellulose polymers and their substituents

Polymer	**R =**
MC	-H or -CH_3
EC	-H or -CH_2CH_3
HPC	-H or -$CH_2CH(OH)CH_3$
HPMC	-H, -CH_3 or -$CH_2CH(OH)CH_3$

Larger substituent groups will occupy more space, which causes the polymer chains to not align favourably, which can lead to two things occurring. The first being the presence of "pockets" amongst the polymer

chains. As the glycosidic backbones of the polymer are not near each other due to the large substituent groups this creates space among the chains as can be seen in **Figure 7**. MC has chains which are much closer together compared to HPMC which are further apart. Within these pockets it could be possible to introduce therapeutic agents. When this occurs, this leads to less polymer-polymer interactions and less hydrogen bonding (Serpe and Craig, 2007).

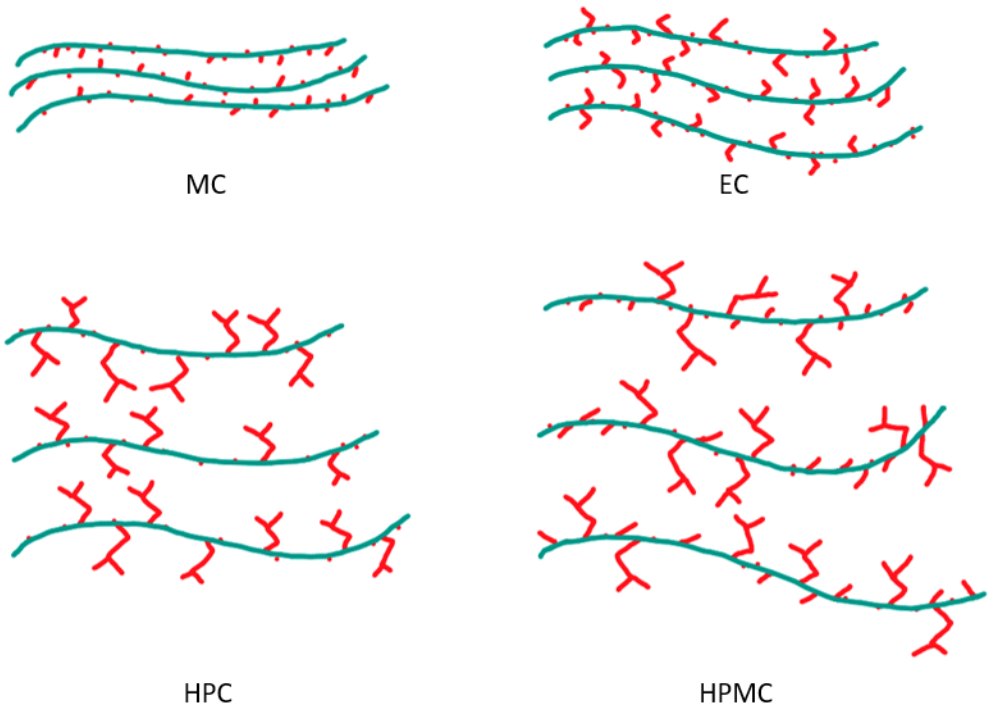

Figure 7: Schematic diagram of polymer chain packing of MC, EC, HPC and HPMC

Along with this, the larger substituent groups occupy more space, this means less polymer-polymer interactions occur as the chains are further apart. This also means fewer crosslinks and interactions are forming, leading to the chains being able to "slide over" each other and thus the polymer displaying viscous behaviour (Bonet *et al.,* 2005). This leads to an impact on a polymer's permeability with regards to Fick's first law. This relates to the diffusive flux of molecules from a region of high to low concentration along the concentration gradient, with the law written as **Equation 7**

$$J = -D\frac{dc}{dt}$$

Equation 7

J is the diffusion flux which is defined by the number or concentration of particles (c) moving past a region divided by the area of that region, multiplied by the time interval t. D is the diffusion coefficient which

depends on temperature, the viscosity of the polymer and the size of the particle. D will be greater at higher temperatures as the particles will have more thermal motion allowing for an increase in movement. In terms of viscosity, D will be greater when the polymer is displaying viscous behaviour as the molecules will have less resistance as it moves through and diffuses. With regards to particle size, ions at room temperature will generally have a D within the ranges of 0.6×10^{-9} - 2×10^{-9} m s^{-2}, and biological molecules – which are greater in size – typically have a D within the ranges of 10^{-11} - 10^{-10} m s^{-2} (Hamley, 2007). As the purpose of the polymer is to contain a biomacromolecule as a therapeutic agent, using HPMC due to its high viscosity will aid in the increasing of the overall diffusion (Atkins and De Paula, 2014).

As HPMC has been selected, the surface tension of this polymer would need to be considered. Surface tension is important for electrospinning, which will be discussed in further detail in **section 1.3.1**, as this can impact the morphology of the fibres. Surface tension is the tension of the film surface of a liquid which is caused by the attraction of the particles in the surface layer of the liquid, this tends to lead to minimised surface area and can be measured by the contact angle. Studies conducted by Riedl *et al* (2000) observed the effect of increasing HPMC concentration and the dynamic surface tension measured by the contact angle. They found that increasing the concentration of HPMC (1, 2, 3 and 4% w/w) increased the contact angle (85.30°, 91.60°, 94.30° and 113.80° respectively) as more polymer-polymer interactions formed (Riedl *et al.,* 2000). They introduced 1% poloxamer 407 as a plasticiser to the HPMC solutions and observed that the contact angle decreased to 23.00°, 62.50°, 67.70° and 100.90° respectively. This could be due to the poloxamer 407 molecules fitting between the HPMC polymer chains, leading to less polymer-polymer interactions and less attraction of the particles in the surface layer (Bonet *et al.,* 2005). Therefore, introducing a co-solvent could have the same impact.

1.2 RHEOLOGY

Rheology is the study of the deformation and flow of matter. This includes the classical extremes of Hookean solids and Newtonian liquids (Barnes *et al.,* 2005). Key parameters are stress (σ) - the force per unit area (**Equation 8**) - and strain (ε) – the deformation of the sample caused by stress (Hamley, 2007). In practice, viscosity η can be measured by applying an oscillating stress or strain, leading to defining shear rate ($\dot{\gamma}$) as **Equation 9**:

$$\sigma = \frac{F}{A}$$

Equation 8

$$\dot{\gamma} = \frac{dv_x}{dy}$$

Equation 9

Newtonian behaviour is when shear stress is proportional to the shear rate with viscosity being independent of shear rate (Hamley, 2007). However, if the viscosity is not constant nor independent of the shear rate the system is non-Newtonian, typical of many polymers (Hamley, 2007). This behaviour follows Hooke's law (Hamley, 2007). An important characteristic of a hydrogel is that it can display viscoelastic behaviour; at low deformation rates most polymers will exhibit viscous behaviour while at high deformation rates polymers will behave more elastically (Hamley, 2007).

One of the ways of observing properties of polymers is through characterisation using a rheometer, which can be done through an amplitude sweep and then a frequency sweep. An amplitude sweep is performed to determine the upper limit of the non-destructive range, the linear viscoelastic range (Kavanagh and Ross-Murphy, 1998; Wenchang *et al.,* 2003). This is done by increasing the stress applied to the sample incrementally while keeping the frequency consistent, this gives a stress/strain graph displaying strain rate ($\dot{\varepsilon}$). A stress is selected at the upper limit of this linear viscoelastic range and is used in the frequency sweep. A frequency sweep describes the time-dependent behaviour of the sample when that stress is applied. During this sweep, the oscillation frequency (w) is increased in a step-wise manner to allow for the measurement of different timescales (t) while keeping the stress constant. Low frequencies simulate slow motion on long timescales or at rest, while high frequencies simulate fast motion on short timescales (Barnes *et al.,* 2005).

In a frequency sweep for a viscoelastic system, an elastic portion will be in-phase with the strain, while the viscous portion will be out-of-phase with strain. This defines an in-phase shear modulus, known as the storage modulus and an out-of-phase shear modulus; also known as the loss modulus leading to **Equation 10**:

$$\sigma = \sigma_0' \sin \omega t + \sigma_0'' \cos \omega t$$

Equation 10

The in-phase storage modulus and the out-of-phase loss modulus can be defined mathematically as **Equations 11** (in-phase shear) and **12** (out of phase loss). So, stress in its entirety can be described as **Equation 13** with stress as σ and shear as γ.

$$G' = \frac{\sigma_0'}{\gamma_0}$$

Equation 11

$$G'' = \frac{\sigma_0''}{\gamma_0}$$

Equation 12

$$\sigma = G'\gamma_0 \, sin \, \omega t + G''\gamma_0 \, cos \, \omega t$$

Equation 13

The frequency sweep creates a rheogram of the storage modulus (G') and the loss modulus (G'') against frequency in Hz. The G'' characterises the viscous portion of the viscoelastic behaviour within the material (Barnes *et al.,* 2005). Viscous behaviours arises from the internal friction between the components of the flowing fluid – such as the molecules and particles (Sinko, 2017). Friction leads to the development of frictional heat within the sample; thus, deformation energy is transformed into heat (Sinko, 2017). Kinetic energy applied by the rheometer is absorbed by the sample and is used by the internal friction processes. Therefore, this energy is no longer available to further influence the sample (Sinko, 2017). This is an energy loss, also known as energy dissipation, and represents the G'' at each stage of the frequency sweep (Ewoldt *et al.,* 2008). Viscoelastic materials with dominant viscous behaviour will have a higher G'', mostly due to the lack of strong bonds between the individual molecules or lack of entanglements. This means there is little to no resistance between the polymer chains allowing them to slide past each other when stress is applied (Ewoldt *et al.,* 2008).

The G' represents the elastic portion of the viscoelastic behaviour within the material which describes the solid-state behaviour of the sample (Ewoldt *et al.,* 2008). In a viscoelastic sample, the elastic portion of energy is stored within the deformed material, so when stretching and extending the internal superstructures, the material is not destroyed (Doi and Edwards, 1986). When stress is removed the unused stored deformation energy becomes the driving force in reforming the sample to its original shape (Doi and Edwards, 1986). This stored energy is represented by the G'.

$$\tan \delta = \frac{G''}{G'}$$

Equation 14

The ratio between G' and G'' gives a value known as tan δ, also known as the loss tangent (**Equation 14**) and is a measure of the internal friction of the material within the conditions set and the energy loss per cycle (Hamley, 2007). When G'' is higher than G' – leading to tan δ being more than 1 – the viscous behaviours dominate, leading to a more liquid-like solution. If the G' is higher than the G'' – so tan δ being less than 1 – the sample displays a more gel-like consistency with elastic behaviour dominating. When tan δ equals 1, G' and G'' crossover and the solution undergoes a loss in fluidity and the formation of a 3D network leading to the formation of a gel; this point is known as gel point (Hamley, 2007; Rudin and Choi, 2013).

1.3 Polymer Nanofibers and Uses

1.3.1 Electrospinning

Developed by Cooley in 1902, electrospinning is a simple and cost-effective technique for the fabrication of nanofibers using electric force to draw them out from a polymer solution (Cooley, 1902). A wide range of polymers can be electrospun into nanofibers making this technique highly applicable and growing in popularity (Zamani *et al.,* 2013; Mouthuy *et al.,* 2015). This is a technique that can be compared to commercial processes for drawing fibres of the microscale in terms of results. However, electrospinning involves the use of electrostatic force to draw a reducing diameter viscoelastic jet, which will ultimately form a sub-micron scale fibre (Huang *et al.,* 2003; Li and Xia, 2004). The advantage of electrospinning over other mechanical drawing techniques is that it can generate much thinner fibres (Li and Xia, 2004). This is due to elongation being achieved via a contactless scheme through the application of an external electric field (Li and Xia, 2004) (**Figure 8**).

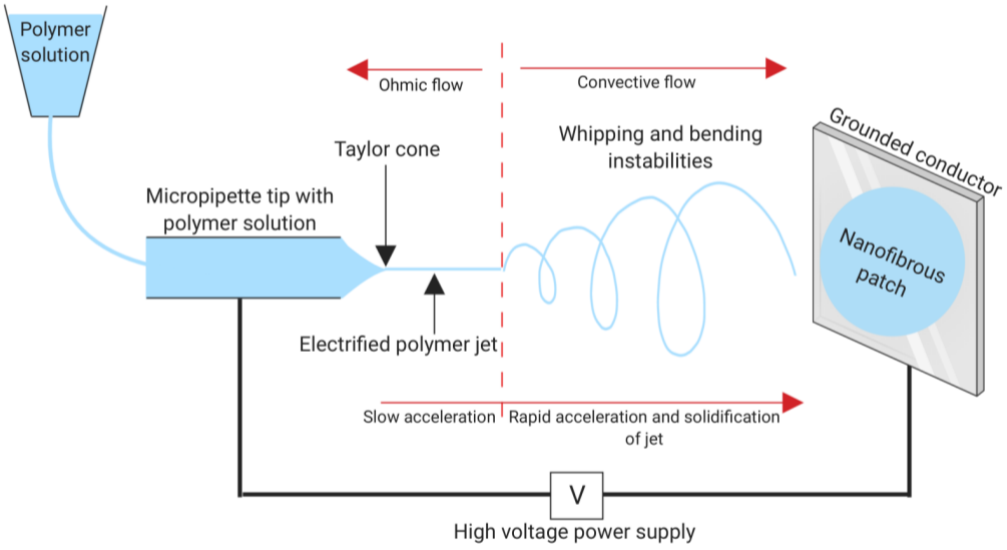

Figure 8: A schematic representation of the electrospinning process created by BioRender.com. The polymer solution (light blue) goes into the micropipette tip and once a high voltage is applied forms a Taylor cone. While in flight the electrified polymer jet undergoes whipping and bending instabilities; the solvent evaporates, and the jet solidifies and hits the grounded conductor to form a nanofibrous patch.

Figure 8 shows the three major components of an electrospinning device: a high voltage power supply, the micropipette tip and the grounded collector. The polymer solution is placed into the reservoir which travels down the tube, controlled by adjusting the height of the reservoir. During the spinning process, this impacts the replenishing rate of the polymer droplet as it is removed from the micropipette tip as a liquid jet (Reneker and Chun, 1996). A high voltage from the power supply is applied – typically in the range of 10 -

20 kV – which causes the polymer solution droplet at the end of the tip to become highly charged, and electrostatic repulsion induces the charge to be evenly distributed across the surface (Reneker and Chun, 1996; Li and Xia, 2004). The droplet experiences two types of electrostatic forces. The first being electrostatic repulsion between the surface charges and the second being Coulombic forces which are exerted by the external electric field (Reneker *et al.,* 2000). While under the influence of these electrostatic interactions, the polymer droplet is distorted into a conical shape known as the Taylor cone (Reneker *et al.,* 2000; Li and Xia, 2004). At the point of the Taylor cone, there is a high concentration of electrostatic stress, and once the strength of the electric field passes a threshold, the electrostatic forces overcome surface tension (Li and Xia, 2004). This causes the ejection of the charged jet of particles, which undergoes a stretching and whipping process, leading to the formation of a long, thin fibre (Li and Xia, 2004).

As the charged polymer solution jet continuously elongates in flight, the solvent evaporates and the polymer hits the grounded conductor to create a randomly orientated fibrous patch (Reneker and Chun, 1996). The grounded conductor can be modified to change the alignment of the nanofibers. For instance, a rolling drum can cause the fibres to be parallel while split electrodes cause the fibres to be perpendicular (Haider *et al.,* 2015).

The ideal fibrous patch would consist of one continuous nanofibre while being high in surface area (A) and uniform in diameter with little to no bead formation. The low diameter allows for a high surface area to volume ratio (A:V) and for more three-dimensional open pores within the nanofibre mesh and this allows for a more efficient drug delivery system (DDS) (Reneker and Yarin, 2008).

1.3.2 Factors Influencing Electrospinning

Different factors can influence different aspects in both the electrospinning process and the electrospun product. The factors can be divided into three categories as seen in **Table 2**.

Table 2: Parameters and factors that can impact electrospinning

Electrospinning parameters:	**Spinning solution properties:**	**Environmental factors:**
• Voltage applied • Flow-rate • Micropipette tip to collector distance	• Polymer concentration (viscosity) • Conductivity • Solvent volatility • Surface tension	• Relative humidity • Environmental temperature

The electrospinning parameters can influence the product, one example being the voltage applied to the polymer solution. The current from the high voltage power supply causes the polymer droplet to distort into

a Taylor cone and form the nanofibres when at a critical voltage (Haider *et al.,* 2015). This critical value needs to be met for the formation of nanofibers and this threshold varies between polymers. Generally, an increase in voltage leads to a decrease in the diameter of the nanofibres, thus increasing the A:V (Bhardwaj and Kundu, 2010). This is because an increase in voltage increases the electrostatic repulsion which favours the narrowing of the nanofibre diameter. Generally, a higher voltage causes a great stretching of the polymer solution as the Columbic forces in the jet are greater and the electric field is stronger, leading to a reduction in fibre diameter (Bhardwaj and Kundu, 2010; Haider *et al.,* 2015). When the applied voltage is above critical value this can lead to the formation of beads. This could be due to the high voltage decreasing the size of the Taylor cone and increasing the flow-rate. Deitzel *et al* (2001) conducted a study to determine how the voltage applied to a polymer can impact the morphology of an electrospun product. While working with poly(ethylene oxide) (PEO) it was found that the electric current, due to the ionic conduction of charge in the polymer, was assumed to be negligible (Deitzel *et al.,* 2001). However, when the voltage applied to the solution changed so did the nanofibre morphology. A voltage of 5.5 kV produced primarily straight nanofibres which were "defect-free". Yet when the voltage was increased to 7 kV and higher, the nanofibres had beads present; suggesting that voltage could be used for controlling bead density in the electrospun nanofibres (Deitzel *et al.,* 2001).

Another factor of the electrospinning process is the flow-rate. The flow of the polymeric solution through the apparatus can impact the morphology as a critical flow-rate allows for uniform bead-free nanofibres. A flow-rate above the critical value can lead to increased nanofibre diameter, increase in pore-size as well as the formation of beads (Haider *et al.,* 2015). These are linked with low evaporation rates of solvents and low stretching of the solution while in-flight. Therefore, a balance needs to be found as too low of a flow-rate will inhibit electrospinning (Bhardwaj and Kundu, 2010; Okutan *et al.,* 2014). Linking in with this, another possible factor is the distance between the micropipette tip and the collector. The distance can play an essential role in determining the morphology of the nanofibre (Haider *et al.,* 2015). A critical distance needs to be maintained to allow for uniform nanofibres, too large of a distance can result in nanofibres with large diameters, while too short of a distance will not allow for evaporation to fully occur leading to defects in the fibres (Matabola and Moutloali, 2013).

In terms of solution factors, the concentration of the polymer solution can have an impact on the morphology of the nanofibres as this can link with the solution's viscosity (Deitzel *et al.,* 2001; Okutan *et al.,* 2014). The electrospinning process relies on the stretching of the electrified jet. If the concentration is too low this can lead to the applied electric field and the surface tension causing the polymer chains to fragment before reaching the grounded conductor (Haider *et al.,* 2015). Too high a concentration may hinder solution

flow through the micropipette tip. It can cause blockage at the tip if the polymer solution dries and can lead to bead formation (Haider *et al.,* 2015).

Another solution factor is the conductivity as this can impact the Taylor cone formation as well as controlling the nanofibre diameters. Solutions with no or low conductivity will not be able to form a Taylor cone due to the lack of surface charge; thus, no electrospinning can take place (Bhardwaj and Kundu, 2010). If conductivity is above a critical value this can also hinder Taylor cone formation. When conductivity is at a critical value this allows for the formation of a Taylor cone as it increases the surface charge of the droplet, as well as decreasing the nanofibre diameter (Haider *et al.,* 2015). Another solution factor is the solvent itself and two aspects for selecting the solvents must be kept in mind. One of these is to ensure the polymer is completely soluble in the solvent. The other is that the chosen solvent has a moderate boiling point as this can give an indication of the solvent volatility (Sun *et al.,* 2014). In general, solvents with lower boiling points are preferred as the evaporation rate is quicker, therefore encouraging the solvent to evaporate while in-flight from the micropipette tip to the conductor. Too high a boiling point would mean the solvent would unlikely evaporate mid-flight leading to droplets on the conductor (Haider *et al.,* 2015). However, if a solvent is too volatile the evaporation rate would be too high, leading to blockage at the micropipette tip. Solvents with a high boiling point can still be electrospun. For example, dimethylformamide (DMF) is often used in electrospinning and has a high boiling point of 153 °C; it could just lead to nanofibres which are larger in diameter (Chai and Wu, 2013). The chosen solvent can also play a pivotal role in the fabrication of porous nanofibres, typically occurring if two solvents are involved. The different volatilities of the two solvents can lead to phase separation and will result in the formation of highly porous nanofibres (Haider *et al.,* 2015). Deionised water is a solvent that is typically used in electrospinning, and will allow HPMC – once incorporated – to be fully dissolved. Song *et al* (2017) observed the effects of deionised water and deionised water/ethanol mixes as solvent systems for poly(ethylene oxide) (PEO) nanofibres. It was observed that deionised water leads to smoother nanofibres which were lower in diameter compared to when ethanol was added, especially when the ethanol proportion increased. This could be because deionised water has a higher dielectric constant and dipole moment than ethanol which allows for a higher electrical susceptibility of the solution. This, in turn, leads to an increase in charge density of the electrified jet and while in flight the jet will undergo a stronger elongation force, causing the fibres to be smoother and lower in diameter (Song *et al.,* 2017). Therefore, using deionised water as the primary solvent would be beneficial.

The final electrospinning solution factor mentioned in **Table 2** is surface tension. Fridrikh *et al* (2003) predicted that the final in-flight jet diameter arises from a force balance between surface tension and electrostatic charge repulsion, which can vary between different polymers and different concentrations. The stability of the in-flight jet due to whipping is viewed as a competition between surface tension and

surface charge repulsion. During the beginning of the flight the surface tension will dominate leading to a stable and straight jet, and as the surface density grows the charge repulsion overcomes the surface tension causing the jet to bend and whip (Fridrikh *et al.,* 2003). As the jet undergoes bending and whipping instabilities this leads to the jet reducing in diameter while the solvent evaporates. As the instabilities are important in creating a low jet diameter, ensuring a low surface tension can result in obtaining nanofibres without beads, which could be achieved by introducing other solvents to the solution (Haghi and Akbari, 2007; Asiri *et al.,* 2018).

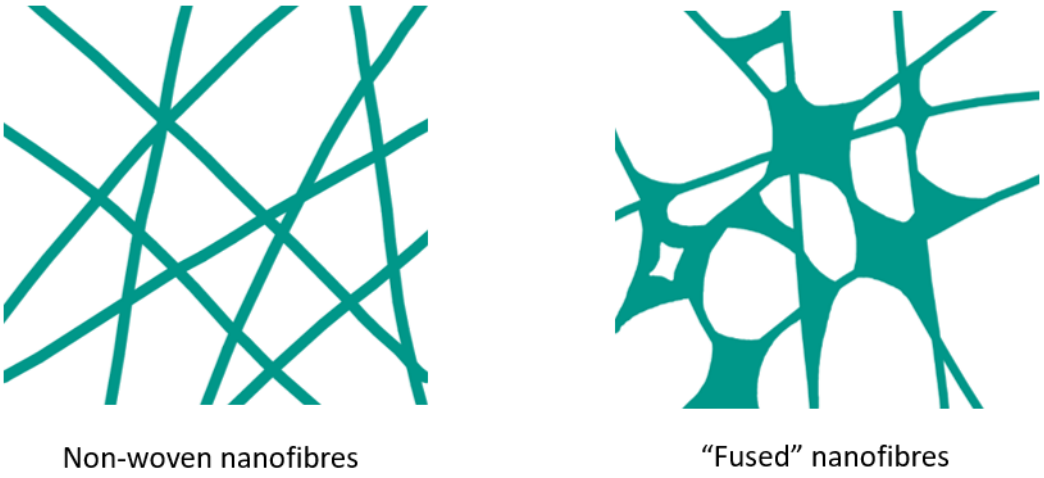

Figure 9: A schematic diagram to show the effects of high humidity on the formation of nanofibres, which can lead to "fused" nanofibres

With regards to environmental factors, two aspects are relative humidity and environmental temperature. Relative humidity can impact the solidification process of the electrified jet. High relative humidity can lead to the formation of fibres of lower diameters. However, too high of a relative humidity means there is higher partial pressure in the atmosphere which leads to incomplete drying of the jet as well as the possibility of "fused" fibres as shown in **Figure 9** (De Vrieze *et al.,* 2009). Temperature can impact the rate of evaporation of the solvent and the viscosity of the solution. The higher the environmental temperature the more likely the solvent is to evaporate whilst in-flight. With regards to viscosity, in general, the higher the temperature the more likely the polymer solution is to be viscous and flow. As previously mentioned, the evaporation rate and viscosity can impact the formation of nanofibres (Haider *et al.,* 2015).

1.3.3 Electrospinning and Drug Delivery

When compared with other pharmaceutical formulations and drug delivery systems (DDS), electrospinning offers great flexibility when it comes to selecting materials and the drugs for drug delivery application (Hu *et al.,* 2014). There are many advantages with electrospinning allowing for a greater method of DDS, for instance, electrospun products may offer:

- High A:V
- High loading capacity
- High encapsulation efficiency
- The possibility of simultaneous delivery of a range of therapies
- Cost-effectiveness
- The ease of operation

These are all appealing features for the use in DDS especially in the context of wound healing and prospective chemotherapy (Hu *et al.,* 2014). The drug release behaviour is determined by the diffusion of the drug from the matrix and the degradation of the carrier polymer used in electrospinning which can be dependent on the type of polymers (Hu *et al.,* 2014). In most cases, non-biodegradable polymers will rely solely on diffusion to play the leading role in drug delivery and display a sustained release profile. Biodegradable polymers, on the other hand, make drug delivery complicated as when the polymer degrades this could result in a burst release effect (**Figure TBC**) (Hu *et al.,* 2014).

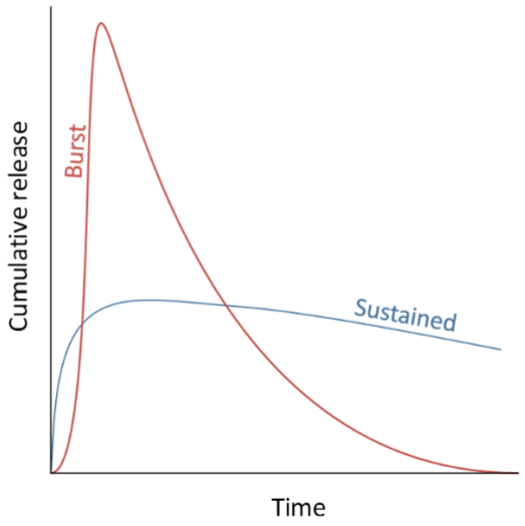

Figure 10: The generic release profiles from biodegradable polymers (burst release) and from non-biodegradable polymers (sustained-release).

This is unfavourable when constant release kinetics are desirable for the duration of therapeutic administration (Sinko, 2017). This is because a constant plasma-drug concentration is maintained for a prolonged period, which maximises the therapeutic effect of the drug while improving patient compliance (Gao *et al.,* 2011). Burst release profiles would result in a large proportion of the pharmaceutical intervention being released at once, so the target would get a large "hit" of the drug (**Figure 10**). As there is no sustained release, there is no slow continuous pharmaceutical intervention unless if the reservoir is replaced (Sinko, 2017). During a course of treatment, increasing the number of times which the reservoir must be replaced will reduce patient compliance. This will have a negative impact on the treatment (Sinko, 2017). Various carrier polymers have been used in electrospinning with a variety of drugs ranging from antibiotics, anticancer and even biomacromolecules such as proteins, DNA, RNA and growth factors (Zamani *et al.,* 2013). In terms of medical devices, antibiotics and antibacterial agents are the most preferred biocides to be encapsulated into electrospun nanofibers (Zamani *et al.,* 2013). Studies by Gilchrist *et al* (2013) incorporated rifampicin and fusidic acid into electrospun poly(D,L-lactic acid-co-glycolic acid) (PLGA) nanofibers to reduce implant-associated infections following invasive orthopaedic surgery. The electrospun PLGA loaded with antibiotics provided a localised delivery system with approximately 75-100% of the antibiotics being encapsulated within the fibres (Gilchrist *et al.,* 2013). The release profile observed was biphasic, meaning that there are two phases to the DDS (Jha *et al.,* 2015). For example, in terms of oral administration a biphasic release profile would be composed of a fast release layer and a sustained release layer; to allow for a more controlled release of the formulation (Jha *et al.,* 2015). Therefore, in terms of the electrospun PLGA, the antibiotics displayed antimicrobial activity against *Staphylococcus epidermidis* in both an immediate effect and a sustained effect (Gilchrist *et al.,* 2013). This was due to the polymer being biodegradable, so the burst release phase was over 1-2 days which was then followed by a slow, controlled release over 35 days (Gilchrist *et al.,* 2013).

It is possible to incorporate biomacromolecules such as proteins and growth factors into electrospun products. However, it is challenging to ensure the bioactivity or functional activity remains during the electrospinning process (Ji *et al.,* 2010). This is because electrospinning may result in the destabilisation of proteins. It has been reported that the high voltage and contact with certain organic solvents during electrospinning can result in the growth factors losing 20% of their bioactivity due to the loss of the α-helix in the secondary structure (Ji *et al.,* 2010). Incorporation of biomacromolecules through electrospinning can be accomplished through two methods: blend electrospinning or coaxial electrospinning (Ding *et al.,* 2019).

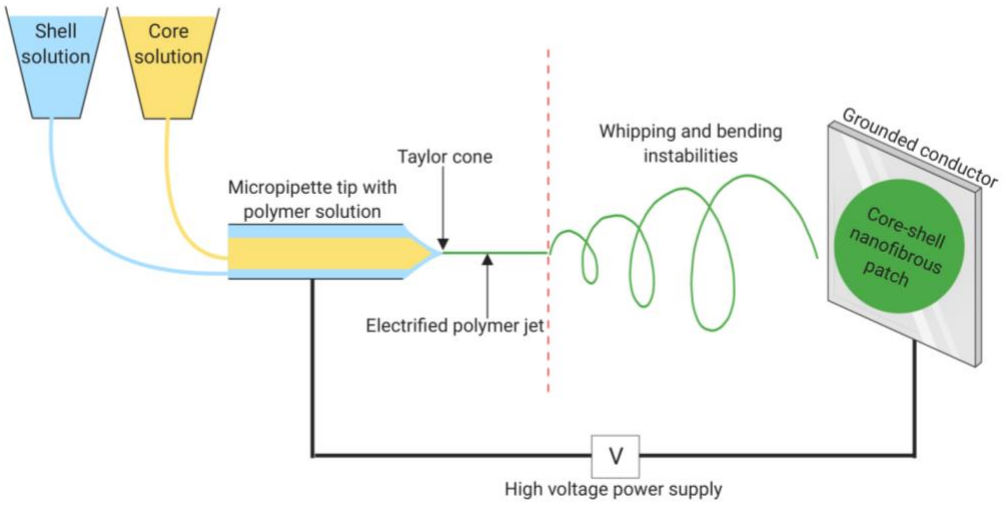

Figure 11: A schematic diagram of the general set-up for coaxial electrospinning.

Blend electrospinning allows for the biomacromolecules to be mixed into the polymer before electrospinning leading to localisation of them on the surface of the nanofibers; and consequently, leads to bioactivity reduction (Ji *et al.,* 2010). Coaxial electrospinning is a modification on the conventional method of electrospinning, allowing the incorporation of two or more polymers to form coaxial capillaries (Afshari, 2017). This method combines the polymers by injecting one solution into the other, forming nanofibres with a core-shell structure (**Figure 11**) (Qian *et al.,* 2014). The general coaxial electrospinning setup is similar to the standard set up. Two reservoirs are containing the polymers desired to be the outer shell and the inner core (a third solution can be involved if the outer and inner shells are desired to be different) and these are fed through to the micropipette tip. Like the conventional method, a high voltage is applied causing a high electrostatic field and the formation of a Taylor cone. The coaxial Taylor cone looks different as the core solution is pulled into and embedded within the shell solution, resulting in a compound fibre (Afshari, 2017). Once surpassing an electrical stress threshold, the solutions fire out as it would in standard electrospinning.

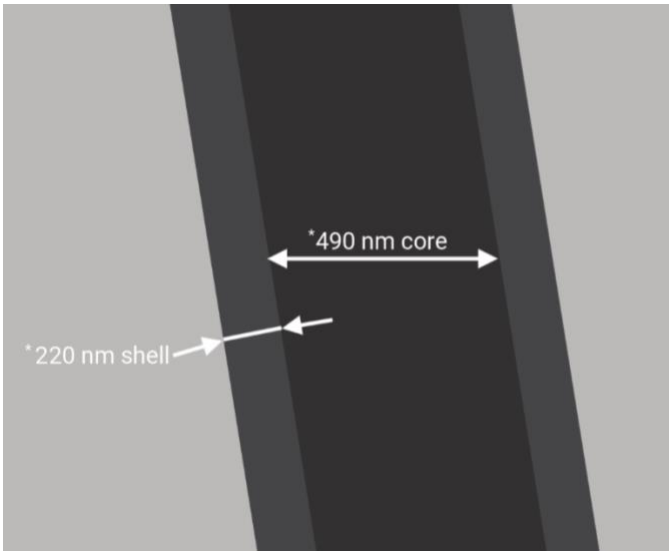

*Figure 12: Simulated core-shell nanofibres formed from coaxial electrospinning using poly(vinyl pyrrolidone) (PVP) as the shell and ethyl cellulose (EC) as the core polymer matrices. *Measurements taken from Qian et al (2014).*

Figure 12 shows an example of a fibre expected to be seen through coaxial electrospinning, with an outer shell and an inner, hollow core. This hollow-core can allow for safe and direct encapsulation of drugs and biomacromolecules into the electrospun nanofibres. Compounds which can be incorporated include:

- Hydrophobic drugs – such as rifampin
- Hydrophilic drugs – such as tetracycline
- Biomacromolecules – such as proteins.

The encapsulation of the therapeutic agent allows for local DDS (Luo *et al.,* 2012; Zamani *et al.,* 2013). These fibres can work for both sustained release and a biphasic release.

1.4 CO-SOLVENTS

1.4.1 Propylene glycol

Propylene glycol (PG) is an organic, low-toxic compound which is very elastic and has a long history use as a component in topical pharmaceutical interventions (Watkinson *et al.,* 2009). PG contains two alcohol groups, classing it as a diol, and this -OH groups makes PG a polar protic solvent that miscible with a broad range of solvents including water (**Figure 13**). Polar protic solvents are capable of hydrogen bonding, and this is an important aspect when incorporating PG with polymers (Atkins and De Paula, 2014).

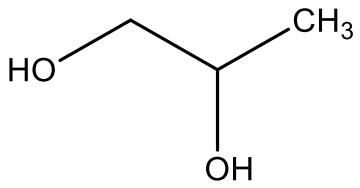

Figure 13: Structure of propylene glycol (PG). Drawn on ChemDraw Prime.

A study by Bendas *et al* (1995) determined how hydrogels with varying PG content influenced the *in vitro* penetration of topical glucocorticoids, and this was observed using solubility and partition coefficient tests. They observed that in general, an increase in PG content leads to an increase in solubility and a decrease in the partition coefficient between isopropyl myristate and the PG/water mixtures (Bendas *et al.,* 1995). Watkinson *et al* (2009) investigated the influence of PG on the solubility and the membrane permeability characteristics of ibuprofen on the stratum corneum using PG/water mixtures. PG/water mixtures were prepared from 10-100% PG in 10% (w/w) increments, and it was observed that ibuprofen flux increased as the concentration of PG increased and this increase of flux was particularly notable between 25-50% PG (Watkinson *et al.,* 2009). Both studies discussed that PG is beneficial for the release of the therapeutic agent, especially within higher concentrations. However, high concentrations of PG incorporated into HPMC will lead to the solution becoming too elastic, limiting spinnability. Karakatsani *et al* (2010) studied the use of different penetration enhancers with HPMC and used a lower concentration of PG. When 0.5% PG (w/v) was incorporated into HPMC only a mild enhancement effect was observed however there was a decrease in release rate as PG increased the elasticity of HPMC from 0.2676 Pa s to 0.3075 Pa s (Karakatsani *et al.,* 2010). Therefore, if incorporating PG into HPMC solutions, it would be beneficial to use low concentrations as this reduces the likelihood of the solution forming a gel while still interacting with the HPMC polymer in terms of hydrogen bonding and surface tension. As a low concentration of PG will not impact the enhancement of the therapeutic agent, a different penetration enhancer can also be incorporated.

1.4.2 Dimethyl sulfoxide

Dimethyl sulfoxide (DMSO) is an organosulfur compound that is also miscible in water. As DMSO is a polar aprotic solvent, the compound cannot form hydrogen bonds with itself due to the lack of O-H and N-H bonds (**Figure 14**) (Atkins and De Paula, 2014) The use of DMSO in medicine has predominately been used as a topical analgesic.

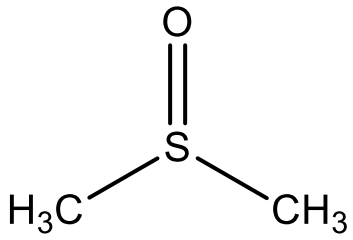

Figure 14: Structure of dimethyl sulfoxide (DMSO). Drawn on ChemDraw Prime.

While penetrating the skin, DMSO can carry other biological compounds through the skin without damaging them. It was found that DMSO acted as a powerful solvent as it denatures the proteins when applied to human skin as it results in changes from α-helices in the intercellular keratin to a β-sheet conformation (Karakatsani *et al.,* 2010). When incorporating DMSO into a therapeutic agent a safe concentration needs to be determined, which can be difficult as this can be dependent on the method of formulation/incorporation as well as use. Karakatsani *et al* (2010) used 0.5% DMSO (w/v) in HPMC and found that this did not improve the enhancement effect on the release rate, possibly because the concentration was too low.

If incorporating DMSO to the electrospun nanofibres, it is important to know how the solvent can interact with the skin. Gurtovenko and Anwar (2007) applied a range of concentrations to a 3.62 nm lipid bilayer system to determine how DMSO can interact with it. They determined that at concentrations of 2.5, 5.0 and 7.5% DMSO caused the membrane to thin to 3.42, 3.23 and 3.05 nm respectively. As well as membrane thinning, concentrations of 10, 12.5, 15 and 20% resulted in pore formation which could further lead to the disruption of ion transport across the cell membrane. Lastly, concentrations of 25-100% DMSO lead to membrane degradation (Gurtovenko and Anwar, 2007). Therefore, for the basis of preliminary results, 7.5% DMSO was used in this project to observe possible interactions with the bacteriocins once incorporated and if this would aid in release without severely damaging the skin.

1.5 ANTIBIOTICS

Antibiotics are a type of antimicrobial that is active against bacteria and are widely used for the treatment and prevention of bacterial infections. Typically, antibiotics used are semi-synthetically produced. For example, the first antibiotic – penicillin – was discovered through serendipity as Fleming accidentally left a *Staphylococci* plate near an open window with mould. After looking at the plate a "halo" of inhibited bacterial growth was seen – also known as a zone of inhibition – around the mould (Fleming, 1929). Fleming concluded the mould must have released a substance which repressed the growth and lysed the bacteria, acting as a natural antibiotic (Fleming, 1929; Tortora *et al.,* 2016). This natural antibiotic has been synthetically and semi-synthetically produced and altered for medical applications to form different generations. These different generations will be slightly different to the natural antibiotic but will have advantageous characteristics such as greater spectrum, greater activity, cause fewer side effects and be active against bacteria which may be resistant to the original. Depending on their mechanism of action, antibiotics may either display a bactericidal (killing) or bacteriostatic action (inhibiting reproduction).

1.5.1 Antibiotic Resistance

In the mid-1900s England's mortality rates from infectious diseases decreased from 25% to 1%, one of the reasons being the commercialisation of antibiotics and were regarded as a "medical miracle" (Smith *et al.,* 2012). This led to the 1940s-60s being known as the "antibiotic golden age". There was a rapid increase in the number of synthetic antibiotics being mass-produced with a variety of mode of actions. Most of the classes in use today were identified at this time (Ribeiro da Cunha *et al.,* 2019). It was believed that the high rate of antibiotic discovery meant that infectious diseases would soon be a controlled public health issue. Most antibiotics will lose their ability to kill disease-causing bacteria over time as bacteria evolve and adapt through natural selection, and the time between antibiotic deployment and resistance development can be short (**Figure 15**).

However, one of the reasons for the downfall of antibiotics and the appearance of antibiotic resistance (AR) stems from the high rate of discovery (Ribeiro da Cunha *et al.,* 2019). Alongside the rapid increase in antibiotic production, other factors also played a role in the rise in AR such as personal misuse, abuse and systematic over-prescription of antibiotics (Riley *et al.,* 2012; Lee *et al.,* 2015; Ribeiro da Cunha *et al.,* 2019). This includes self-medication of antibiotics, interruption of antibiotic therapy as well as the use of antibiotics as growth promoters in livestock farming (Rather *et al.,* 2017; Ribeiro da Cunha *et al.,* 2019).

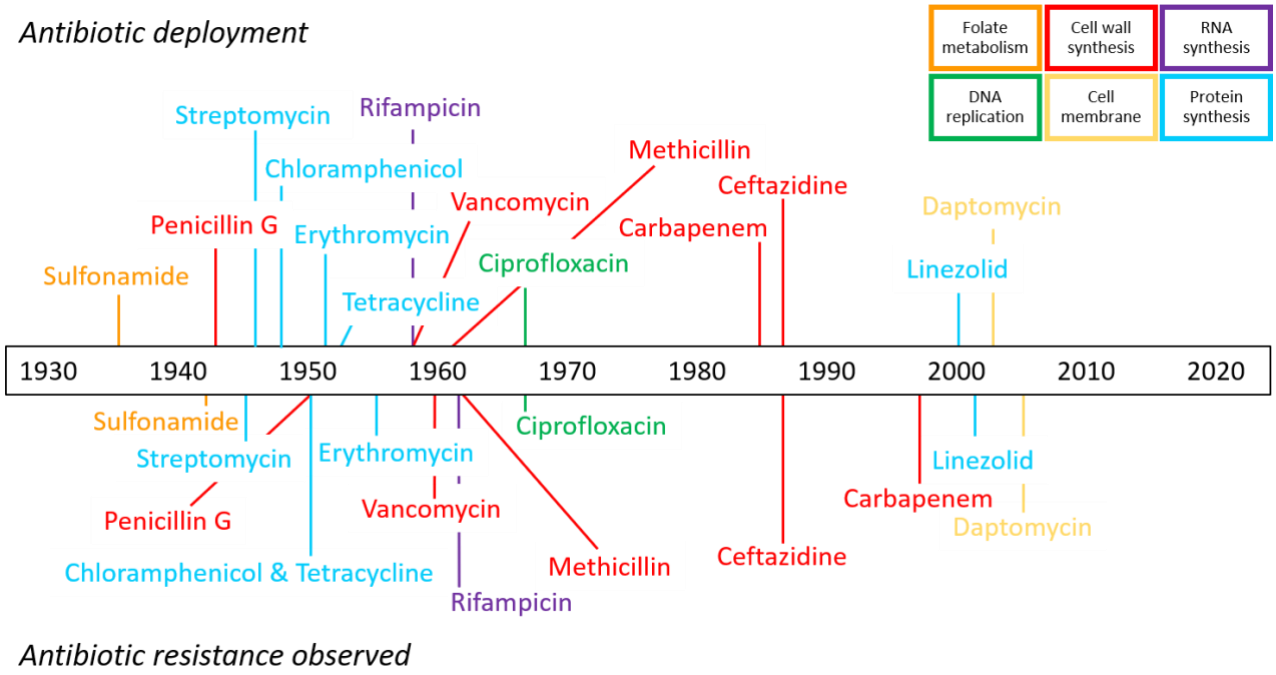

Figure 15: A combined timeline showing antibiotic deployment and resistance observed.

AR occurs when a pathogen develops immunity to its therapeutic agent (Riley *et al.,* 2012). This can lead to mutations occurring within the bacteria in a way which may interact with the drug (Riley *et al.,* 2012; Händel *et al.,* 2014). Examples include (Alanis, 2005; Kohanski *et al.,* 2010):

- Enzymatic degradation of the antibiotics
- Alteration of the proteins present within the bacteria that are the proposed target sites
- Changes in the membrane permeability of antibiotics
- Development of an active transport system in the bacteria causing the antibiotic to be pumped out of the cell

Any of these mutations can be passed to other bacteria through conjugation; a method in which the replicated plasmid travels through a conjugation tube. The plasmid DNA is then incorporated and replicated resulting in the formation of resistant bacteria (Nordmann *et al.,* 2007). If this method of mutation continues and the bacteria develops resistance to multiple antibiotics, this is then known as a "superbug". This is the reason why resistance has been found in *Staphylococcus aureus, Mycobacterium tuberculosis, Pseudomonas aeruginosa, Salmonella enterica* and *Enterococcus faecium* as well as many other common and clinically important bacteria (Arias and Murray, 2009).

1.6 BACTERIOCINS

Bacteria can produce proteinaceous toxins known as bacteriocins. These toxins are bacteriostatic or bactericidal towards other closely related species. However, they remain inactive against the producing bacteria (Dykes, 1995; Cascales *et al.,* 2007). Most bacteriocins are classed as displaying narrow-spectrum activity due to their high specificity towards their targets. Others have shown broad-spectrum activity as they are active across genera (Cotter *et al.,* 2005; Cui *et al.,* 2012; Dorit *et al.,* 2016). Bacteriocins are important mediators of microbial diversity and stability as they are used by bacteria in conditions of stress such as when as nutritional levels may be low (Nascimento *et al.,* 2004; Dorit *et al.,* 2016).

Typically, the name given to specific bacteriocins is derived from the producing bacterial species followed by the suffix "-cin" (Cascales *et al.,* 2007). Bacteriocins are abundant and diverse, produced by both Gram-positive and Gram-negative bacteria (Dorit *et al.,* 2016). The classification can then be broken down further based on the molecular weights of the bacteriocin, their structure and stability. An additional category is their interaction with the cell membranes of their targets (Dykes, 1995; Cotter *et al.,* 2012).

1.6.1 Cloacins

Cloacins (Cloacin DF13) are bacteriocins produced by strains of *E. coli* and *Enterobacter cloacae* which hold the bacteriogenic plasmid known as CloDF13 (Oudega *et al.,* 1984). They are classed as nuclease colicins, meaning they cleave nucleic acid substrates in *E. coli* (Papadakos *et al.,* 2011) and have a molecular weight of approximately 59 kDa (van der Elzen *et al.,* 1983).

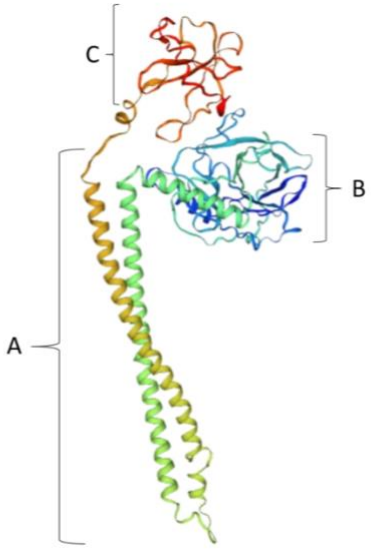

Figure 16: 3D ribbon structures from the Swiss-Model Database of cloacin DF13 (P00645 (CEAC_ECOLX)) from the organism: E. coli. With the receptor-binding domains (A), translocation domains (B) and the cytotoxic domains (C).

Cloacins display bactericidal effects to susceptible cells of *Enterobacter, E. coli* and *Klebsiella* species by first using the receptor-binding domain (**Figure 16 A**) and binding to the specific outer-membrane receptor proteins on the bacterial target (Oudega and de Graaf, 1976; Oudega *et al.,* 1984). After binding to the active site, the cloacin then crosses the membrane using the translocator domain (**Figure 16 B**) and translocator proteins in the bacteria, such as TolQ (Thomas and Valvano, 1992). The translocation domain is relatively large with some unstructured regions due to the composition of three β-sheets surrounded by two helical stretches (Dorit *et al.,* 2016). Afterwards, with the cytotoxic domain (**Figure 16 C**), the cloacin then displays bacteriostatic effects by hydrolysing the 16S rRNA, resulting in the inactivation of ribosomes. This inactivation leads to the inhibition of protein synthesis (Oudega and de Graaf, 1976). Thus, the target is unable to multiply. Along with impacting the target's gene expression, the cloacin molecule also induces a rapid efflux of potassium ions from the target's cytoplasmic membrane at a rate that is proportional to the concentration of cloacin (de Graaf, 1973). Once potassium efflux begins, this results in the uptake of sodium ions and then a gradual decrease in ATP levels, leading to cell death (de Graaf, 1973).

1.6.2 Bacteriocin Application and Resistance

A common use of bacteriocins is in the food industry. A well-known example is nisin, produced by *Lactococcus lactis,* which has been used in food preservation for years (Delves-Broughton *et al.,* 1996; Silva *et al.,* 2018). Nisin has shown antimicrobial activity against Gram-positive bacteria such as the *Listeria* and the *Staphylococcus* spp. as well as spore-forming bacteria such as the *Bacillus* and *Clostridium* spp. (Silva *et al.,* 2018). As they are sensitive to digestive enzymes if ingested the bacteriocins will degrade. This brings the benefit of not negatively impacting the natural gut microbiota, as traditional antibiotics would, and reducing the risk of side effects (Egan *et al.,* 2016; Silva *et al.,* 2018). Bacteriocins are also used in the pharmaceutical industry for treatment of pathogen-associated diseases and cancer therapy (Yang *et al.,* 2014). Bacteriocins are looked at as an alternative to traditional antibiotics.

As with all antimicrobial agents under investigation with views of clinical applications, there is the potential development of resistance. As a vital purpose of bacteriocins is to act as an alternative to traditional antibiotics, the frequency at which bacteriocin resistance develops would be considered an important issue; especially in a clinical sense. One method of resistance could be through spontaneous mutation of the target bacteria against the bacteriocins. Another method is through innate immunity where resistance is found intrinsically in a genus or species of bacteria (Dorit *et al.,* 2016). For example, a non-bacteriocin-producing bacterial strain may carry genes encoding for the immunity protein, thus providing protection from the bacteriocins; this is known as immune mimicry (Draper *et al.,* 2009; Dorit *et al.,* 2016).

Methods to combat resistance involve using bacteriocins in combinations. One example is through hurdle technology, in which bacteriocins are combined with chemical additives, heating or high-pressure treatments (Egan *et al.,* 2016). One example is the use of ethylenediaminetetraacetic acid (EDTA) with bacteriocins to aid in compromising the bacterial outer membrane (Stevens *et al.,* 1991; Chen and Hoover, 2003). Another includes using a combination of bacteriocins in a "cocktail" as this can be seen occurring naturally. For example, an *E. coli* cell may produce both colicin Ia and E1 and these interact with different receptor types. Although there is little understanding as to why certain bacteria can produce more than one bacteriocin type, one could argue this is to reduce resistance as simultaneous mutation in two different receptors is unlikely to occur (Dorit *et al.,* 2016). Therefore, in terms of clinical use, a cocktail of bacteriocins involving the use of multiple bacteriocins can be beneficial in ensuring resistance to less likely to occur.

1.7 Medical Sector Applications

From the moment of injury to full restoration, wound healing is a complex and highly developed series of events consisting of four phases: haemostasis, inflammation, proliferation and maturation (Childs and Murphy, 2017). The first stage is haemostasis, where the main objective is to stop the bleeding. Afterwards, in the inflammatory phase, platelets surround the wound to limit bleeding and begin cytokine signalling to initiate the coagulation cascade (Childs and Murphy, 2017). This promotes the release of growth factors and the attraction of neutrophils and macrophages to phagocytise dead tissue and bacterial particles (Childs and Murphy, 2017). In the proliferative phase, angiogenesis and extracellular matrix formation are encouraged. This then leads into the maturation phase where wound contraction and collagen remodelling occurs (Childs and Murphy, 2017). When selecting the appropriate treatment, it is vital it avoids hypoxia, infection, excessive oedema or introduces foreign bodies (Childs and Murphy, 2017). If common bacteria such as *Klebsiella pneumoniae* were to enter the wound this could cause a chronic wound or bacteremia if entering the bloodstream (Liu *et al.,* 2017).

Wound management costs the NHS an estimated £5.3 billion annually. Therefore, when developing treatments and dressings, cost-effectiveness needs to be considered (Guest *et al.,* 2017). The ideal wound dressing should (Liptak, 1997; Vowden and Vowden, 2017):

- Remove excess wound exudate while maintaining a moist environment
- Allow for effective oxygen saturation of the wound
- Protect against additional contamination or trauma
- Be non-toxic
- Conform to the wound's surface

Electrospun nanofibres have been used for dressings and offer great applications towards the wound healing process. Nanofibres have a large A:V, allowing to effectively absorb exudates to adjust wound moisture (Zamani *et al.,* 2013). The high porosity allows for effective air permeability, beneficial for cell respiration while preserving the wound from infection as the pores can be small (Zamani *et al.,* 2013). As mentioned previously, antibiotics have been incorporated into nanofibres and have displayed positive results. However, with the rise in AR, alternatives are sought.

2 AIMS AND OBJECTIVES

This project aimed to use electrospun HPMC nanofibres to deliver and control the release rate of isolated and purified bacteriocins in the context of a medical device. This was in the aim of developing alternatives to traditional antibiotics to combat infection for wound healing.

The steps necessary to achieve this aim included the following objectives:

- To formulate a range of HPMC solutions and rheologically characterise them
- To formulate a range of HPMC solutions to electrospin and observe their morphologies
- To optimise the electrospinning process and procedure to produce the ideal nanofibre
- To clone the cloacin bacteriocin gene
- To incorporate the cloacins into the electrospun nanofibre patch

3 EXPERIMENTAL

3.1 MATERIALS

3.1.1 Formulation of HPMC Samples

Dimethyl sulfoxide (DMSO) (Purity: ≥ 99.0%; Merck), Distilled water (ELGA PureLab® Option-S/R with a PureLab® Flex 1 Dispenser), Hydroxypropyl methylcellulose (HPMC) (CAS: 9004-65-3; Sigma Aldrich), Propylene glycol (PG) (Purity: ≥ 99.5%; Sigma Aldrich)

3.1.2 Electrospinning

200 µL T-200-Y micropipette tip (Axygen), Aluminium foil, Electrospinner (Model: ES1, Name: Adam, Power supply: 100 – 240 VAC 50/60 Hz, Current: 1.0 Amps; Electrospinz Ltd, New Zealand)

3.1.3 Cloning of Cloacin DF13

Agar (Acros Organics), Agarose (Acros Organics), Brain Heart Infusion broth (Sigma Aldrich), Distilled water (ELGA PureLab® Option-S/R with a PureLab® Flex 1 Dispenser), DNA extraction kit (containing buffers: AE (Elution buffer), AL (Lysis buffer), ATL (Tissue lysis buffer), AW1 (Wash buffer 1 – low concentration), AW2 (Wash buffer 2 – high concentration); Qiagen), Ethanol (Fisher Scientific), Gel extraction kit (containing buffers EB (Elution buffer), PE (Wash buffer); Qiagen), 1 kb Hyperladder (Bioline), Isoporponal (Fisher Scientific) *K. pneumoniae* 757 and 957 (University of Lincoln), Nuclease free water (Ambion), Phusion high-fidelity PCR kit (containing 5X Phusion buffer, 10 mM dNTPs (deoxyribonucleotide triphosphate), Phusion DNA polymerase; Thermo Scientific), pET 22b IC7 plasmid (Thermo Scientific), Primers (Forward and Reverse; Sigma Aldrich), PCR purficiation kit (containing buffers EB, PE; Qiagen), Restriction enzymes (NcoI 10 U mL^{-1}, NdeI 10 U mL^{-1}, XhoI 10 U mL^{-1}; Thermo Scientific), Syber safe (Thermo Scientific); TAE buffer (Tris base, acetic acid and EDTA buffer mixture) (Thermo Scientific), Tango buffer (10 X; Thermo Scientific), Ultrapure agarose (Thermo Scientific).

3.2 METHODOLOGY

3.2.1 HPMC Formulation and Characterisation

3.2.1.1 Formulation of HPMC solutions with Co-solvents

A range of 50 g HPMC concentrations was formed with PG, DMSO and distilled water (**Table 3**). The samples were magnetically stirred for 24 hours at room temperature and manually agitated 3 times throughout to break up clumps of HPMC. Samples were immediately tested after the 24 hours of stirring.

Table 3: Concentrations of hydroxypropyl methylcellulose (HPMC) formulated with the addition of propylene glycol (PG) and/or dimethyl sulfoxide (DMSO).

(w/w)

Code	HPMC	PG	DMSO	Distilled water	Total
A1	5	-	-	95	100
A2	5	2	-	93	100
A3	5	-	7.5	87.5	100
A4	5	2	7.5	85.5	100
B1	7.5	-	-	92.5	100
B2	7.5	2	-	90.5	100
B3	7.5	-	7.5	85	100
B4	7.5	2	7.5	83	100
C1	10	-	-	90	100
C2	10	2	-	88	100
C3	10	-	7.5	82.5	100
C4	10	2	7.5	80.5	100

3.2.1.2 Rheological Characterisation of HPMC Solutions

The samples of HPMC were subjected to rheological characterisation using a Discovery HR-2 rheometer (TA Instruments, UK) after stirring for 24 hours. A 60 mm stainless steel, parallel plate geometer with a 1 mm gap with solvent trap was used and tests were performed at 25 °C. The solution was applied onto the Peltier plate and amplitudes sweeps were performed at 0.1 Hz and 10 Hz between the stress of 0.1-20 Pa, with a consistent equilibration time of 3 minutes. From the stress/strain graph produced, a stress in the linear viscoelastic region was selected to perform a frequency sweep at frequencies 1-20 Hz. This gave the storage (G') and loss (G'') moduli of the sample plotted against frequency. The results were collected in quintuplicate on TA instruments Trios 4.1 and presented as averages using Microsoft Excel (with standard deviation shown in the appendices)

3.2.2 Nanofibre Formation and Nanofibre Morphology Determination

3.2.2.1 Nanofibre Formulation Through Electrospinning

The solutions were subjected to electrospinning using The Electrospinz electrospinner after 24 hours of mixing. The grounded conductor used was aluminium foil and was replaced after each run. The sample was transferred to the reservoir reaching the end of the capillary tip. Voltage was then applied and raised just below the point of electrical discharge (8-13 kV). Other parameters included the elevation of the reservoir (flow rate) (-2-4 mm) and the distance between the micropipette tip and the grounded conductor (80 mm). These parameters were kept as constant as possible to allow for the sample to act as the independent variable. Slight alterations were required to ensure ideal jet width and consistency, for example, thin and not spitting. The samples were electrospun for 20 minutes to form a patch on the grounded conductor.

3.2.2.2 Morphology Determination Through SEM

SEM images of the nanofibre patched were obtained using a NeoScope JCM-5000. An SEM stub with a conductive sticker was placed on the nanofibre patch for transfer of the sample. The samples were then imaged through SEM at a magnification of x5000. The SEM images were then analysed using ImageJ and 50 beads were measured to determine the average bead diameter.

3.2.3 Microbiology work

3.2.3.1 Growth of K. pneumoniae 957

K. pneumoniae 957 provided by the University of Lincoln was streaked onto a 1.2% brain heart infusion (BHI) agar plate. The plate was then incubated overnight at 37 °C, inverted. The plate was then checked for colonies. A colony was taken from the plate with an inoculating loop and mixed into autoclaved 20 mL 1.2% BHI broth to form an overnight culture which was incubated at 37 °C overnight. After incubation, the optical density (OD) of the broth was measured through photospectrometry at 590 nm. The OD for the overnight culture was 0.5 Abs.

3.2.3.2 K. pneumoniae 957 DNA Extraction

1 mL of *K. pneumoniae* 957 overnight culture was centrifuged for 10 minutes at 7,500 rpm (5406 x g). The supernatant was discarded, and the pellet was resuspended in 180 µL ATL buffer from the DNA extraction kit. 20 µL proteinase K was added and the sample was vortexed for 10 seconds. The sampled was incubated at 56 °C for 10 minutes while vortexing occasionally throughout incubation and a final 15-second vortex to ensure the pellet was fully resuspended. Afterwards, 200 µL of AL buffer was added to the sample and vortexed before adding 200 µL 95% ethanol and being vortexed again. The sample was transferred to a spin column with a collection tube. 500 µL AW1 buffer was added and the sample was centrifuged at 8,000 rpm

(6151 x g) for 60 seconds. Discarding the flow-through, 500 µL AW2 buffer was added and centrifuged at 13,300 rpm (17,000 x g) for 3 minutes. The spin column was transferred to a 2 mL microcentrifuge tube and 200 µL AE buffer was added, the sample was incubated at room temperature for 60 seconds. Afterwards, the sample was centrifuged at 8,000 rpm (6151 x g) for 60 seconds and the supernatant was collected. After collection, the concentration of the extracted *K. pneumoniae* 957 was determined using a Nanodrop (2,000/2,000C). 5 samples of the extracted DNA had concentrations of 6.8, 7.6, 11.1, 15.8 and 22.9 ng/mL with a baseline correction of 340 mm.

3.2.3.3 Cloning of cloacin

3.2.3.3.1 Polymerase Chain Reaction (PCR) of K. pneumoniae 957 DNA

The PCR procedure had been altered multiple times to obtain a pure sample shown by a clean band through gel electrophoresis. The changes made from the first standard procedure in **section 3.2.3.3.2** are shown in red. The temperature shown for "hold" automatically change by the thermal cycler, so are not shown in red.

3.2.3.3.2 Standard Methodology

For a 50 µL reaction, the following was added to a PCR tube: 33.5 µL nuclease-free water, 10 µL 5X Phusion buffer, 1 µL 10 mM dNTPs, 0.5 µL 10 µM forward primer, 0.5 µL 10 µM reverse primer, 0.5 µL Phusion DNA polymerase and 4 µL template *K. pneumoniae* 957 DNA. The sample was placed in a thermal cycler under the following conditions listed in **Table 4**:

Table 4: Standard PCR conditions

Stage	Temperature	Time
1. Heating	95°C	3 minutes
2. Denaturation	95°C	30 seconds
3. Annealing	55°C 65°C	30 seconds
4. Elongation	72°C	1 minute
5. Repeat stages 2-4	35 X	
6. Cooling	72°C	5 minutes
7. Hold	4°C	∞

After the PCR, the samples were viewed for bands using gel electrophoresis listed in **section 3.2.3.4**.

3.2.3.3.3 Final Methodology – 56.9°C

The 50 µL reaction was the same as listed in **section 3.2.3.3.2**. The sample was placed in the thermal cycler under the following conditions listed in **Table 5**:

Table 5: Final PCR conditions

Stage	Temperature	Time
1. Heating	95°C	3 minutes
2. Denaturation	95°C	1 minute
3. Annealing	56.9°C	1 minute
4. Elongation	72°C	1 minute
5. Repeat stages 2-4	35 X	
6. Cooling	72°C	5 minutes
7. Hold	12°C	∞

After the PCR, the samples were viewed for bands using gel electrophoresis listed in **section 3.2.3.4**.

3.2.3.4 Gel Electrophoresis

1% standard agarose gel was prepared using 100 mL 1X TAE buffer (10 mL 50X TAE buffer and 490 mL distilled water) and microwaved at 30-second bursts to ensure full incorporation. Once cooling to an appropriate temperature, 15 µL syber safe was added, swirled and poured into the electrophoresis case to set. 5 µL 1 kB hyperladder was transferred to the first well. 5 µL of the PCR sample mixed with 1 µL 6X loading buffer was transferred to the following respective wells. The gel was run at 110 V for approximately 60 minutes. The gel was imaged under UV light to observe bands.

3.2.3.5 Polymerase Chain Reaction Purification

5 volumes of PBI buffer was added to 1 volume of PCR mixture and mixed. The mixture was then transferred to a spin column with a collection tube and centrifuged at 13,000 rpm (16,242 x g) for 60 seconds. Flow-through discarded, 0.75 mL PE buffer was added and centrifuged at 13,000 rpm (16,242 x g) for 60 seconds. Flow-through discarded and the centrifuging process repeated to remove excess. The column was transferred to a microcentrifuge tube and 30 µL EB buffer was added to the membrane. The sample was centrifuged at 13,000 rpm (16,242 x g) for 60 seconds and flow-through collected.

Gel electrophoresis was performed as listed in **section 3.2.3.4**, with the alteration of 1.2% ultrapure agarose instead of 1% standard agarose.

3.2.3.6 Gel Extraction of Purified Polymerase Chain Reaction Sample

Under UV light the 2 kbp band was excised and 3 volumes of QC buffer was added to 1 volume of excised gel and stored at -4 °C overnight. 1 gel volume of 100% isopropanol was added, mixed and then the sample was transferred into a spin column and collection tube. The sample was centrifuged at 13,000 rpm for 60 seconds, and the flow-through was discarded. The column membrane was washed with 0.75 mL PE buffer and centrifuged at 13,000 rpm (16,242 x g) for 60 seconds. Flow-through was discarded and the centrifuging process repeated to remove excess. The spin column was transferred to a 2 mL microcentrifuge tube and 50 µL EB buffer was added. The sample was centrifuged at 13,000 rpm (16,242 x g) for 60 seconds and the flow-through collected.

3.2.3.7 Restriction Enzyme Digest

A vial of pET 22b IC7 plasmid was quantified using a nanodrop and diluted with EB buffer to be 2.4 µg mL^{-1}. The reactions were formed as listed in **Table 6**.

Table 6: Reactions prepared for the restriction enzyme digests using NdeI, XhoI and NcoI

Reaction name	**Reaction contents**
20 µL control reaction (Uncut pET 22b)	5 µl pET 22b plasmid, 4 µL Tango buffer & 11 µL nuclease-free water
20 µL pET 22b + NdeI reaction	5 µL pET 22b plasmid, 4 µL Tango buffer, 10 µL nuclease-free water & 1 µL NdeI enzyme
20 µL pET 22b + XhoI reaction	5 µL pET 22b plasmid, 4 µL Tango buffer, 10 µL nuclease-free water & 1 µL XhoI enzyme
20 µL pET 22b + NcoI reaction	5 µL pET 22b plasmid, 4 µL Tango buffer, 10 µL nuclease-free water and 1 µL NcoI enzyme
80 µL pET 22b + NdeI + XhoI reaction	5 µL pET 22b plasmid, 4 µL Tango buffer, 69 µL nuclease-free water, 1 µL NdeI enzyme, 1 µL XhoI enzyme
80 µL pET 22b + NcoI + XhoI reaction	5 µL pET 22b plasmid, 4 µL Tango buffer, 69 µL nuclease-free water, 1 µL NcoI enzyme, 1 µL XhoI enzyme
80 µL *K. pneumoniae* 957 (PCR product) + NdeI + XhoI reaction	50 µL *K. pneumoniae* 957 PCR product, 4 µL Tango buffer, 29 µL nuclease-free water, 1 µL NdeI enzyme, 1 µL XhoI enzyme
80 µL *K. pneumoniae* 957 (PCR product) + NcoI + XhoI reaction	50 µL *K. pneumoniae* 957 PCR product, 4 µL Tango buffer, 29 µL nuclease-free water, 1 µL NcoI enzyme, 1 µL XhoI enzyme

The reactions were mixed and incubated at 37 °C for 90 minutes. Gel electrophoresis was formed as listed in **section 3.2.3.4**.

3.2.4 Antimicrobial and Sterility Testing

3.2.4.1 HPMC Solutions Sterility Testing

3 wells of 5 mm diameter and approximately 1 mm thick were formed on one side of 1.2% BHI agar plates. In these, approximately 15 µL of the solution was pipetted into each well. On the other side of the plate 3 approximately 15 µL of the sample was pipetted straight onto the agar. The plates were then incubated at 37 °C overnight, with the agar facing upwards.

3.2.4.2 Electrospun Patches Sterility Testing

15 mm circles were cut from the electrospun patch and 5 of these were positioned so the patch touched the 1.2% BHI agar. This was repeated for each sample. The plates were incubated at 37 °C overnight, inverted. This was also performed with aluminium foil.

3.2.4.3 Growth of K. pneumoniae 757

K. pneumoniae 757 provided by the University of Lincoln was streaked onto a 1.2% BHI agar plate. The plate was then incubated overnight at 37 °C, inverted. The plate was then checked for colonies. A colony was taken from the plate with an inoculating loop and mixed into autoclaved 10 mL 1.2% BHI broth to form an overnight culture and was incubated at 37 °C overnight. After incubation, the optical density (OD) of the broth was measured through photospectrometry at 590 nm. The OD of the overnight culture was 0.5 Abs.

3.2.4.4 HPMC Solutions Antimicrobial Activity Testing

100 µL of *K. pneumoniae* 757 was added to 5 mL 0.8% soft agar, swirled and then poured on top of a 1.2% BHI agar plate, to form a bacterial overlay. 3 wells of 5 mm diameter and approximately 1 mm thick were formed on one side of these plates. In these were the approximately 15 µL of the solution was pipetted into each well. On the other side of the plate 3 approximately 15 µL of the sample was then pipetted straight onto the agar. The plates were then incubated at 37 °C overnight, with the agar facing upwards.

3.2.4.5 Electrospun Patches Antimicrobial Activity Testing

100 µL of *K. pneumoniae* 757 was added to 5 mL 0.8% soft agar, swirled and then poured on top of a 1.2% BHI agar plate, to form a bacterial overlay. 15 mm circles were cut from the electrospun patch and 5 of these were positioned so the patch touched the overlay. This was repeated for each sample. The plates were incubated at 37 °C overnight, inverted. This was also performed with aluminium foil.

4 RESULTS

4.1 RHEOGRAM OF A1, B1 AND C1

When electrospinning it is imperative that the solution is not a gel. Therefore, to determine how solid-like or solution-like the samples were, they were rheologically tested and observed for gel-point. If gel-point was reached this would mean the sample could not be used for electrospinning. Along with this, rheological characterisation was conducted to observe the solution's behaviour when the concentration of HPMC differs in terms of G' and G''. The results were obtained by performing amplitude sweeps at 0.1 Hz and 10 Hz between the stresses of 0.1-20 Pa. A stress value was then selected from the linear viscoelastic region to perform the frequency sweep and obtain G' and G''data. The 5% HPMC, 7.5% HPMC and 10% HPMC (w/w) are labelled as A1, B1 and C1 respectively.

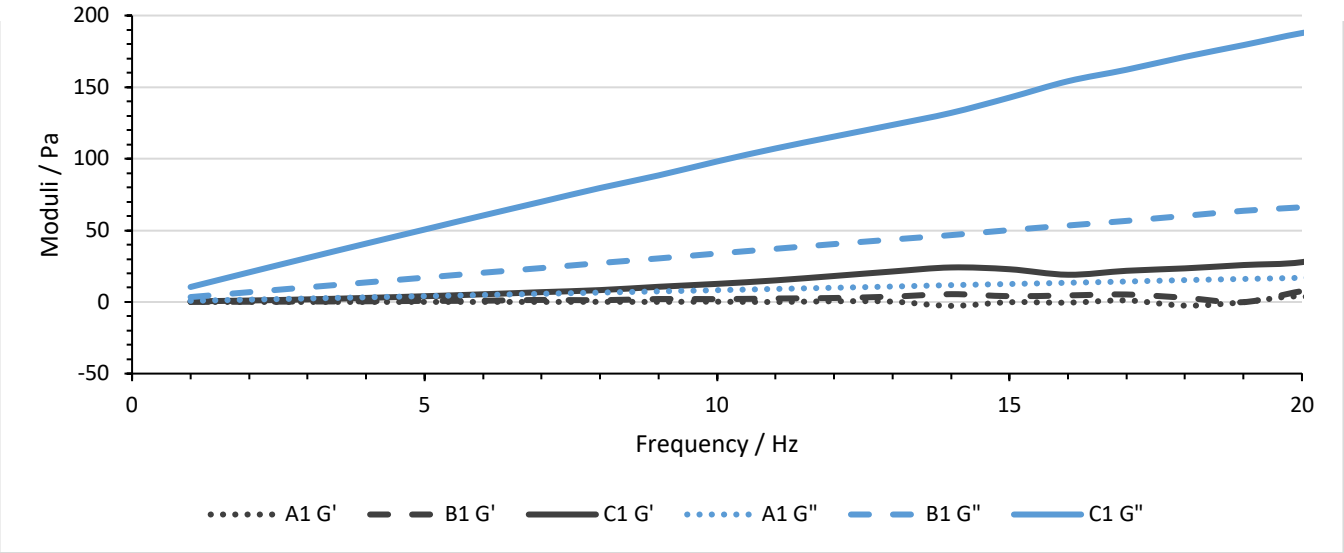

Figure 17: Rheogram of 5% HPMC (A1), 7.5% HPMC (B1) and 10% HPMC (C1) solutions (w/w) tested at 25 °C immediately after preparation from quintuplet readings.

Both moduli for A1, B1 and C1 increase as the frequencies increases from 1-20 Hz (**Figure 17**). The values for A1, B1 and C1 with standard deviation are tabled in **Appendix 1**. For each sample the G'' remains higher than the G', therefore each sample displays a dominant viscous behaviour. When comparing the solutions with each other it is observed that at a frequency of 20 Hz, A1 displayed a G' of 3.87 Pa, while B1 displayed an almost doubled value of 7.58 Pa. At 20 Hz, C1 displayed a value 7 times higher (27.80 Pa) than A1. When looking at the G'' at 20 Hz the B1 solution has an almost 4 times the higher value (66.13 Pa) than the A1 solution (16.87 Pa), and the C1 solution (187.78 Pa) has approximately an 11 times higher value than the A1 solution.

4.2 RHEOGRAM OF A2, B2 AND C2

To observe how the addition of PG impacted the rheological characterisation of HPMC at different concentrations, the samples were tested rheologically for their G' and G''data. The samples also needed to be observed for gel point as this would mean the sample could not be used for electrospinning. The results were obtained by performing amplitude sweeps at 0.1 Hz and 10 Hz between the stresses of 0.1-20 Pa. A stress value was then selected from the linear viscoelastic region to perform the frequency sweep and obtain G' and G''data. The 5% HPMC with 2% PG, 7.5% HPMC with 2% PG and 10% HPMC with 2% PG (w/w) are labelled as A2, B2 and C2 respectively.

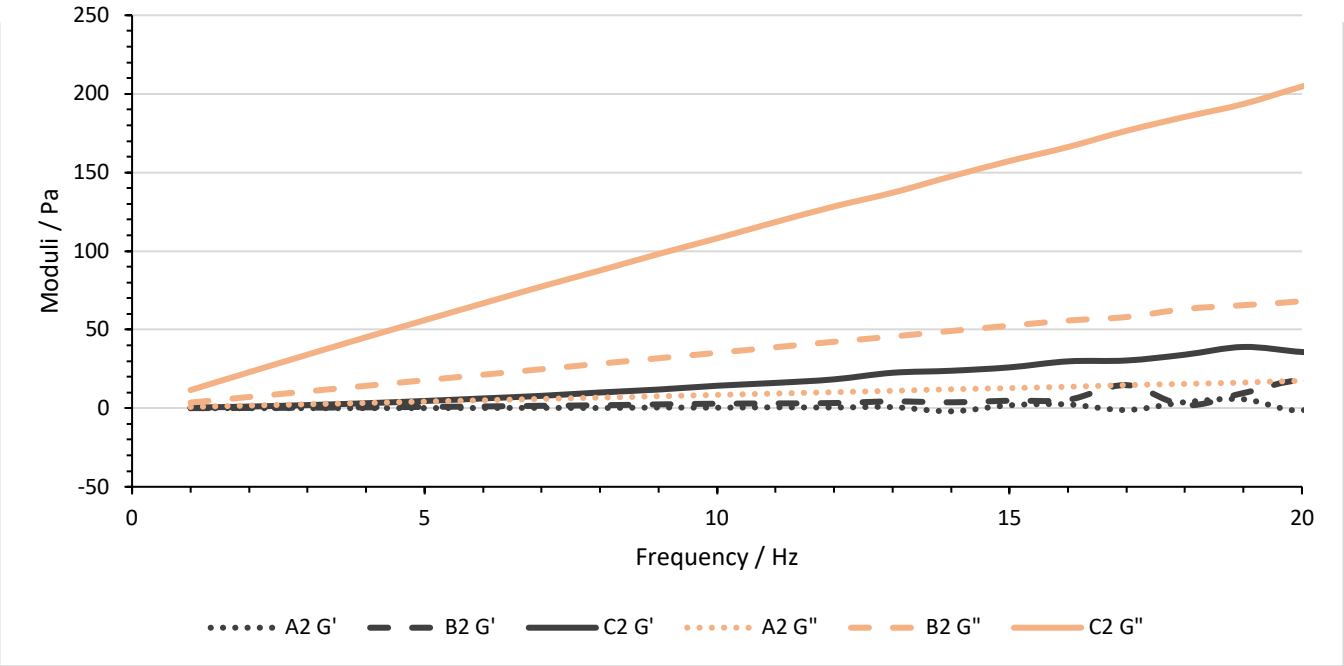

Figure 18: Rheogram of 5% HPMC with 2% PG (A2), 7.5% HPMC with 2% PG (B2) and 10% HPMC with 2% PG (C2) (w/w) solutions tested at 25 °C immediately after preparation from quintuplet readings.

Both moduli for A2, B2 and C2 increases as the frequency increases from 1-20 Hz (**Figure 18**). The values for A2, B2 and C2 with standard deviation are tabled in **Appendix 2**. For each sample the G''remains higher than the G', showing that the viscous behaviour remains dominant for each of the HPMC solutions even with the addition of PG. When comparing the G', at 20 Hz A2 displayed a value of -1.35 Pa which is approximately 13 times less than the B2 solution (17. 64 Pa). When comparing C2 with A2, at 20 Hz C2 displayed a 28 times increase (35.76 Pa) than A2. With regards to G'', 20 Hz the A2 solution displayed a value of 17.43 Pa which is approximately 4 times lower than the $G''$of B2 (68.08 Pa). In comparison to the A2 solution, the G'' of C2 is 11 times higher, with the value of 204.68 Pa.

4.3 RHEOGRAM OF A3, B3 AND C3

To observe how the addition of DMSO impacted the rheological characterisation of HPMC, the samples were tested rheologically for their G' and G''data. The samples also needed to be observed for gel point as this would mean the sample could not be used for electrospinning. The results were obtained by performing amplitude sweeps at 0.1 Hz and 10 Hz between the stresses of 0.1-20 Pa. A stress value was then selected from the linear viscoelastic region to perform the frequency sweep and obtain G' and G''data. The 5% HPMC with 7.5% DMSO, 7.5% HPMC with 7.5% DMSO and 10% HPMC with 7.5% DMSO (w/w) are labelled as A3, B3 and C3 respectively.

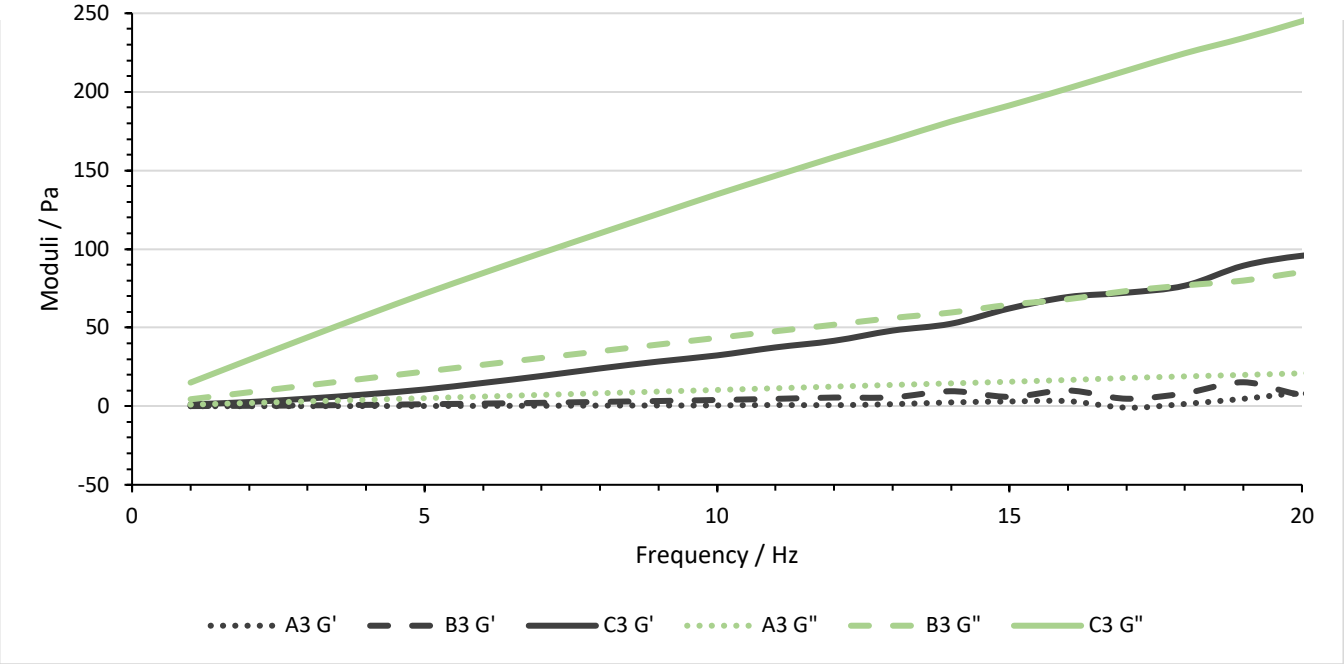

Figure 19: Rheogram of 5% HPMC with 7.5% DMSO (A3), 5% HPMC with 7.5% DMSO (B3) and 10% HPMC with 7.5% DMSO (w/w) (C3) solutions tested at 25 °C immediately after preparation from quintuplet readings

Both moduli for A3, B3, and C3 increases as the frequencies increases from 1-20 Hz (**Figure 19**). The values for A3, B3 and C3 with standard deviation are tabled in **Appendix 3**. For each sample the G''remains higher than the G', therefore each sample displayed a dominant viscous behaviour. At 20 Hz A3 displayed a G'value of 8.06 Pa which was only 1.1 times higher than B3 (7.32 Pa), showing that there is a minuscule difference in the solutions. However, when compared to C3, A3 had a G' value 11 times lower (95.74 Pa). With regards to the G''at 20 Hz A3 (20.93 Pa) was 4 times lower than B3 (85.31 Pa) and 11 times lower than C3 (244.93 Pa).

4.4 RHEOGRAM OF A4, B4 AND C4

With the addition of both co-solvents, there was a higher chance of gel point, therefore the samples were rheologically tested to ensure gel point was not reached. Alongside this, the test was conducted to observe how the two co-solvents interacted with the different concentrations of HPMC in terms of G' and G''data. The results were obtained by performing amplitude sweeps at 0.1 Hz and 10 Hz between the stresses of 0.1-20 Pa. A stress value was then selected from the linear viscoelastic region to perform the frequency sweep and obtain G' and G''data. The 5% HPMC with 2% PG and 7.5% DMSO, 7.5% HPMC with 2% PG and 7.5% DMSO and 10% HPMC with 2% PG and 7.5% DMSO (w/w) are labelled as A4, B4 and C4 respectively.

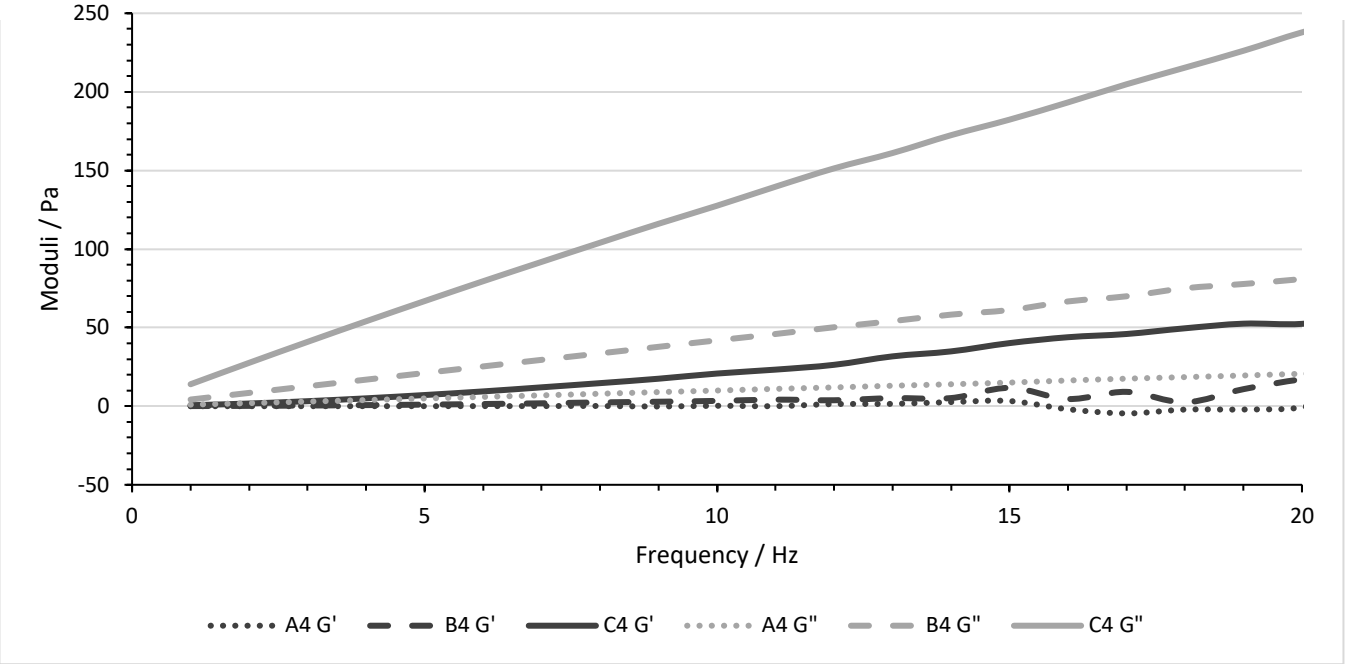

Figure 20: Rheogram of 5% HPMC with 2% PG and 7.5% DMSO (A4), 7.5% HPMC with 2% PG and 7.5% DMSO (B4) and 10% HPMC with 2% PG and 7.5% DMSO (C4) (w/w) solutions, tested at 25 °C immediately after preparation from quintuplet readings

Both moduli for A4, B4 and C4 increases as the frequencies increase from 1-20 Hz (**Figure 20**). The values for A4, B4 and C4 with standard deviation are tabled in **Appendix 4**. For each solution the G'' is dominant, therefore the viscous behaviour for each solution dominates. With regards to the G' at 20 Hz, A4 (-0.70 Pa) was 24 times lower than B4 (17.15 Pa) and 75 times lower than C4 (52.38 Pa). For the G'' at 20 Hz, A4 displayed a value of 20.62 Pa, which was approximately 4 times lower than B4 (80.91 Pa) and 11 times lower than C4 (237.84 Pa).

4.5 RHEOGRAM OF A1, A2, A3 AND A4

To observe how the absence and addition of the co-solvents impacted the rheological characterisation of 5% HPMC, the samples were rheologically compared for their G' and G''data. The results were obtained by performing amplitude sweeps at 0.1 Hz and 10 Hz between the stresses of 0.1-20 Pa. A stress value was then selected from the linear viscoelastic region to perform the frequency sweep and obtain G' and G''data. The 5% HPMC, 5% HPMC with 2% PG, 5% HPMC with 7.5% DMSO, and 5% HPMC with 2% PG and 7.5% DMSO (w/w) are labelled as A1, A2, A3 and A4 respectively.

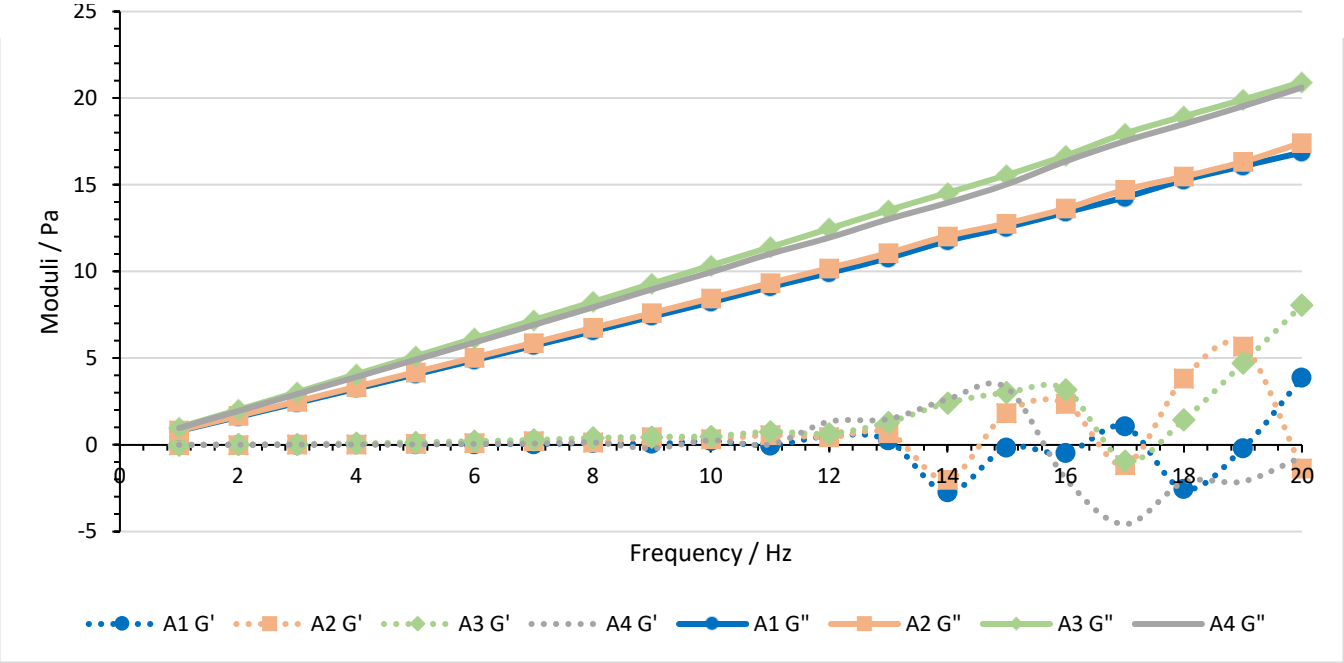

Figure 21: Rheological characterisation of 5% HPMC (A1), 5% HPMC with 2% PG (A2), 5% HPMC with 7.5% DMSO (A3) and 5% HPMC with 2% PG and 7.5% DMSO (A4) solutions (w/w), tested at 25 °C immediately after preparation from quintuplet readings.

Both moduli for A1, A2, A3 and A4 increases as the frequencies increase from 1-20 Hz (**Figure 21**). For each of the solutions G'' is dominant, therefore the viscous behaviour for each of the solutions dominates. The G'' at 20 Hz for A1 is approximately 2.8 times higher than A2, 2 times lower than A3 and only 0.18 times higher than A4. With regards to the G'at 20 Hz, A1 is only 1.03 times lower than A2, 1.24 times lower than A3 and 1.22 times lower than A4. However, as the readings from 12 Hz onwards fluctuate, thus the values at 20 Hz are not representative of the sample. Therefore, looking at the values at 10 Hz shows that G'A1 had a value of 0.21 Pa, which was 2.43 times lower than A2 (0.51 Pa), 1.57 times lower than A3 (0.33 Pa) and 1.24 times lower than A4 (0.26 Pa). The differences between these values are low and similar to each other.

4.6 RHEOGRAM OF B1, B2, B3 AND B4

To observe how the absence and addition of the co-solvents impacted the rheological characterisation of 7.5% HPMC, the samples were rheologically compared for their G' and G''data. The results were obtained by performing amplitude sweeps at 0.1 Hz and 10 Hz between the stresses of 0.1-20 Pa. A stress value was then selected from the linear viscoelastic region to perform the frequency sweep and obtain G' and G''data. The 7.5% HPMC, 7.5% HPMC with 2% PG, 7.5% HPMC with 7.5% DMSO, and 7.5% HPMC with 2% PG and 7.5% DMSO (w/w) are labelled as B1, B2, B3 and B4 respectively.

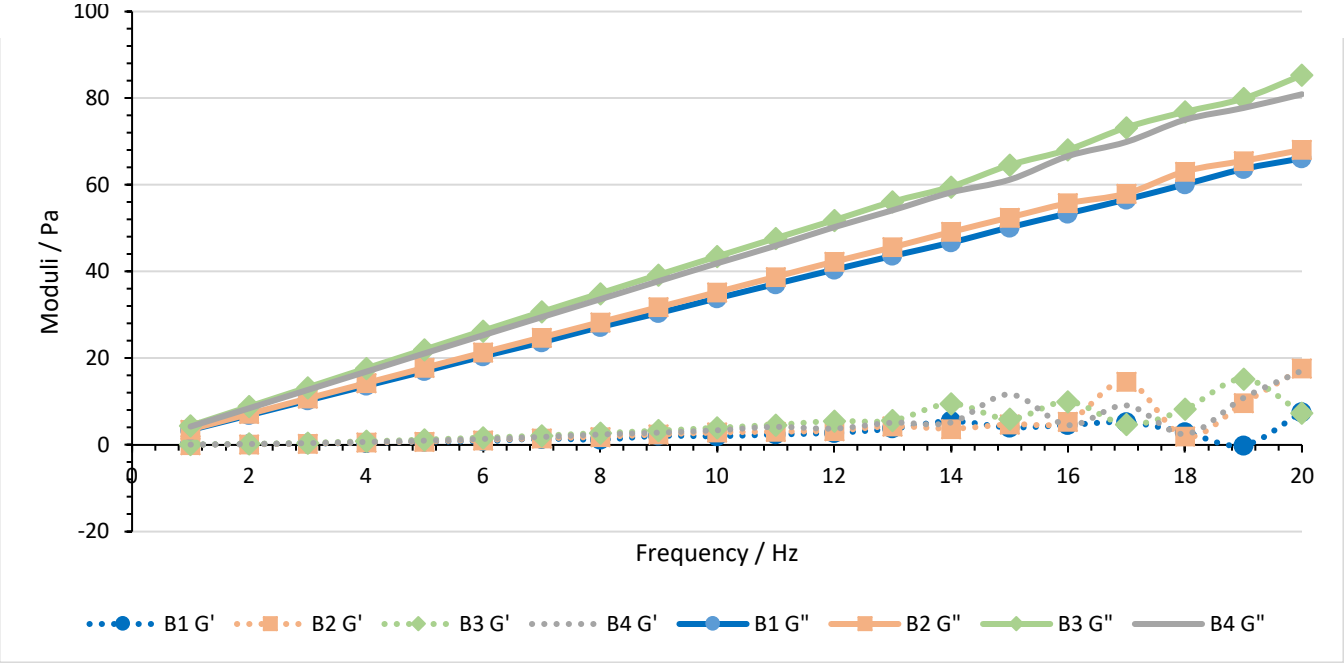

Figure 22: Rheogram of 7.5% HPMC (B1), 7.5% HPMC with 2% PG (B2), 7.5% HPMC with 7.5% DMSO (B3) and 7.5% HPMC with 2% PG and 7.5% DMSO (B4) (w/w) solutions, tested at 25 °C immediately after preparation from quintuplet readings.

Both moduli for B1, B2, B3 and B4 increases as the frequencies increase from 1-20 Hz (**Figure 22**), as was seen for **Figure 21**, along with the G''being dominant. At 20 Hz G' for B1 was 2.3 times lower than B2, 0.97 times lower than B3 and 2.26 lower than B4. However, as the G' fluctuate after 16 Hz this means the values are not representative of the sample. Looking at the readings for G' at 10 Hz, there is very little difference between the solutions. B1 displayed a value of 2.01 Pa which was 1.43 times lower than B2 (2.87 Pa), 2 times lower than B3 (3.98 Pa) and 1.69 times lower than B4. With regards to G'' values at 20 Hz as B1 was 1.02 times lower than B2, 1.29 times lower than B3 and 1.22 times lower than B4.

4.7 RHEOGRAM OF C1, C2, C3 AND C4

To observe how the absence and addition of the co-solvents impacted the rheological characterisation of 10% HPMC, the samples were rheologically compared for their G' and G''data. The results were obtained by performing amplitude sweeps at 0.1 Hz and 10 Hz between the stresses of 0.1-20 Pa. A stress value was then selected from the linear viscoelastic region to perform the frequency sweep and obtain G' and G''data. The 10% HPMC, 10% HPMC with 2% PG, 10% HPMC with 10% DMSO, and 10% HPMC with 2% PG and 10% DMSO (w/w) are labelled as C1, C2, C3 and C4 respectively.

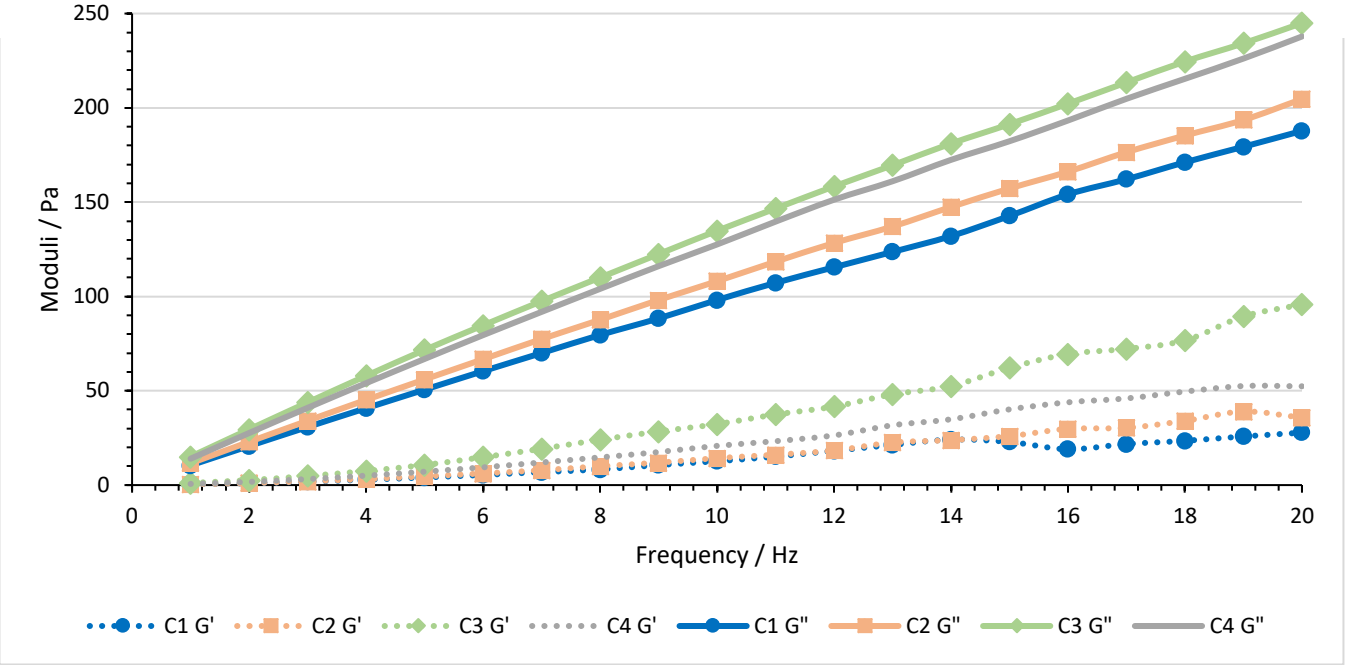

Figure 23: Rheogram of 10% HPMC (C1), 10% HPMC with 2% PG (C2), 10% HPMC with 7.5% DMSO (C3) and 10% HPMC with 2% PG and 7.5% DMSO (C4) (w/w) solutions, tested at 25 °C immediately after preparation from quintuplet readings.

Both moduli for C1, C2, C3 and C4 increases as the frequency increases from 1-20 Hz (**Figure 23**), as was seen in the previous two figures (**Figures 21** and **22**), along with G'' being the dominant modulus. At 20 Hz the G' for C1 was only 1.2 times lower than C2, 3.4 times lower than C3 and only 1.88 times lower than C4. Compared to the previous figures (**Figures 21** and **22**), the G' is much more stable and will be representative of the samples. For consistency G'at 10 Hz lead to C1 at 12.65 Pa, which was 1.13 times lower than C2 (14.28 Pa), 2.55 times lower than C3 (32.32 Pa) and 1.64 times lower than C4 (20.79 Pa). For the G'', at 20 Hz C1 was only 1.08 times lower than C2, 1.3 times lower than C3 and 1.27 times lower than C4.

4.8 10% HPMC SOLUTIONS TAN δ

As the 10% HPMC formulations (C1, C2, C3 and C4) showed the most stable rheological characterisation through $G'$and G''(**Figure 23**), the solutions' tan δ was then calculated to determine the ratio between the two moduli and how they relate to the solution's elasticity/viscosity and how this could impact fibre morphology.

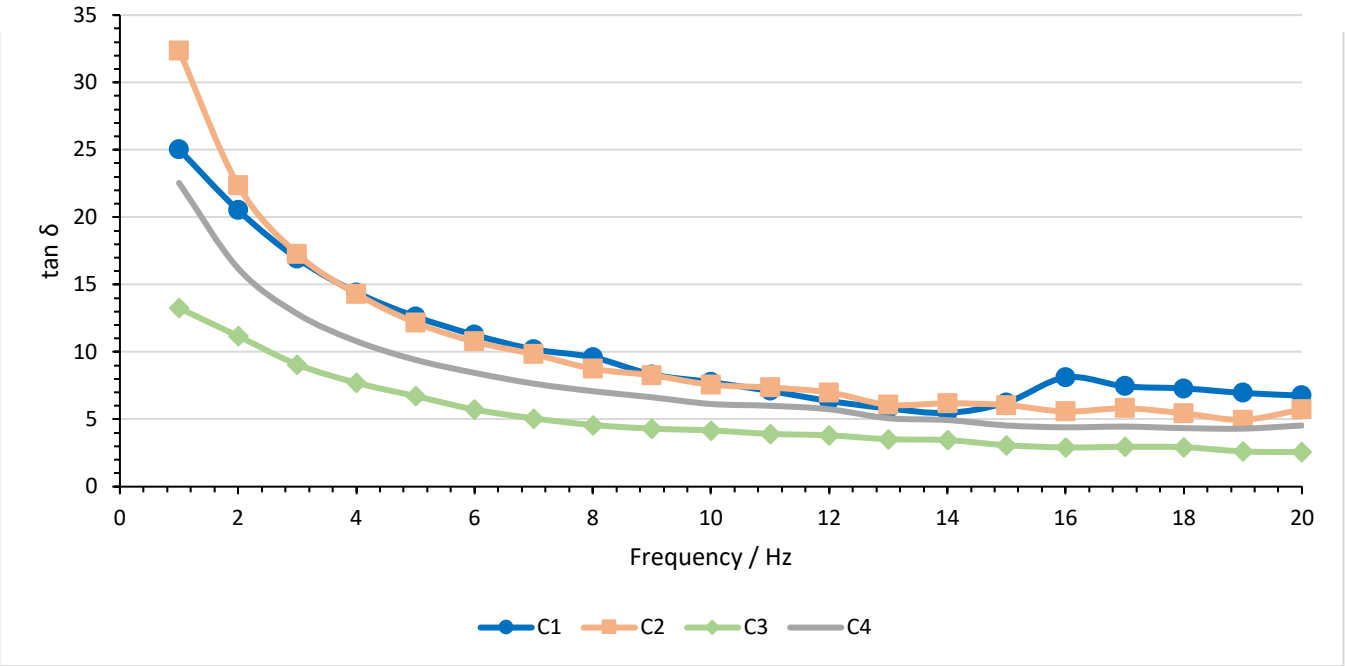

Figure 24: tan δ of 10% HPMC (C1), 10% HPMC with 2% PG (C2), 10% HPMC with 7.5% DMSO (C3) and 10% HPMC with 2% PG and 7.5% DMSO (C4) (w/w) solution, tested at 25 °C immediately after preparation from quintuplet readings.

The tan δ for C1, C2, C3 and C4 generally decreases as frequencies increase from 1-20 Hz (**Figure 24**). As none of the samples crossed 1 for tan δ, this showed that they during the frequencies they remained in the solution state. The higher the tan δ the more viscous-like behaviour is displayed by the sample, and C3 showed the most elastic-like behaviour out of the 4 samples.

4.9 SEM Images of Electrospun Patches

The morphology of the nanofibres was observed through SEM to determine the most ideal nanofibre from the solutions formed. The electrospinning parameters were kept as constant as possible to determine if the production and morphology of beads could be reduced and altered respectively. This meant for all of the solutions the voltage applied was around 8-13 kV, the elevation of the reservoir was -2-4 mm and the distance between the micropipette tip and the grounded conductor was 80 mm.

At x5000 magnification, all electrospun patches display the beaded nanofibres, however, some have different morphologies. **Figures 25 A1, B1 and C1** show that with the increase of HPMC concentration, the bead shape looks relatively similar in morphology, showing a normal droplet shape. The brightness intensity of the beads is due to the position of the beads and fibres. For instance, beads and fibres within the foreground of the SEM image will appear higher in light intensity compared to those in the background. **Figures 25 A2, B2 and C2** show that with the addition of PG to HPMC did not alter the overall shape of the beads. For each sample in **Figure 25,** there is the presence of nanofibres, however, this can be best seen in **Figure 25 C2** as there are "thread-like" nanofibres connecting between some beads within the middle of the image. **Figures 25 A3, B3 and C3** show the electrospun fibres with the addition of DMSO. When comparing these with each other, A3 (**Figure 25 A3**) show beads which are more elongated in shape compared to the beads present in B3 and C3 (**Figures 25 B3 and C3** respectively). **Figures 25 A4, B4 and C4** show very elongated beads when compared to **Figures 25 A-F**, and look to be non-uniform in shape.

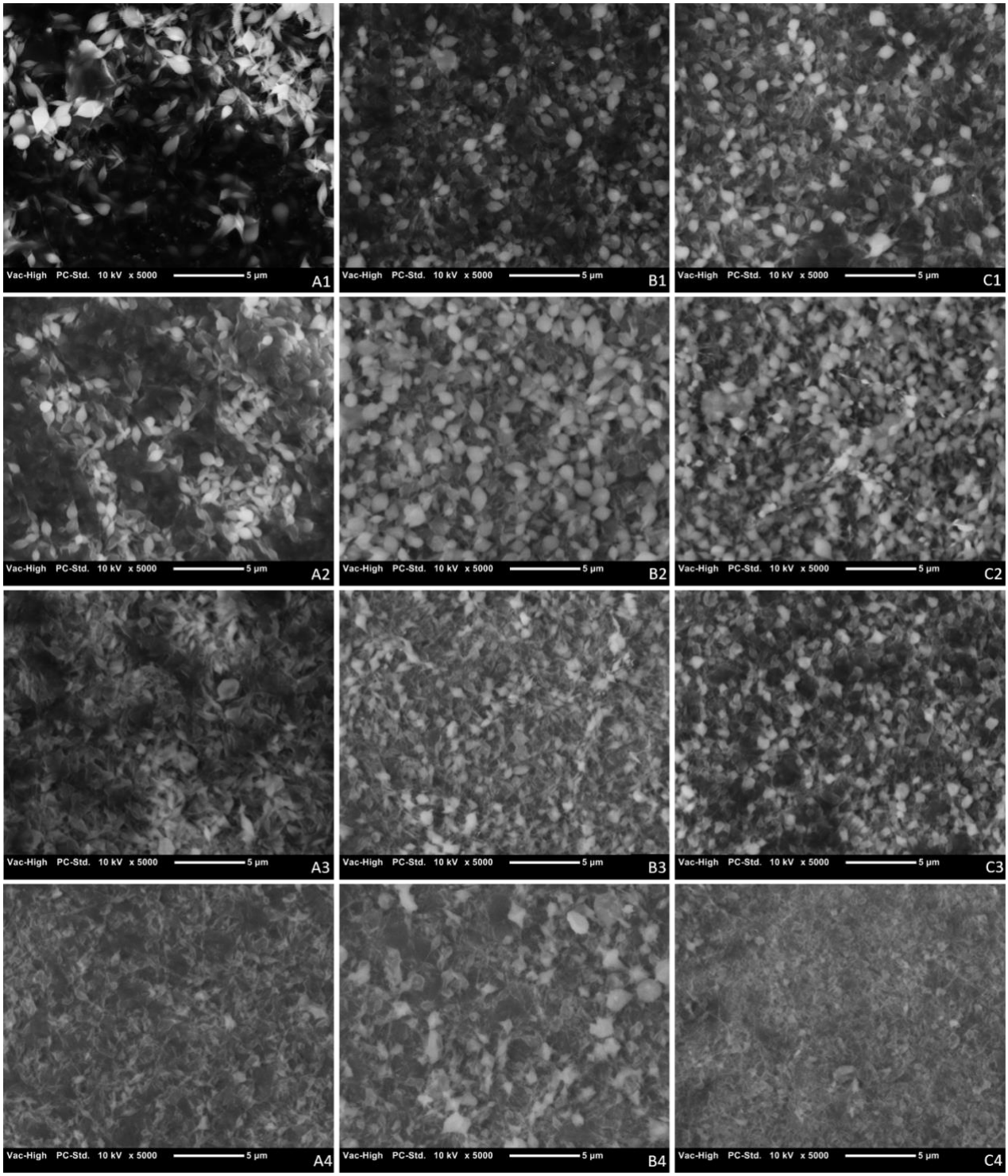

Figure 25: SEM images of electrospun solutions with x5000 magnification. A = 5% HPMC, B = 7.5% HPMC, C = 10% HPMC. The addition of the number indicates the lack of/addition of co-solvent, 1 = no co-solvent, 2 = addition of 2% PG, 3 = addition of 7.5% DMSO and 4 = addition of 2% PG and 7.5% DMSO (w/w).

4.10 Bead Diameter Measurements

The average bead diameters (**Figure 26**) were obtained through 50 readings for each electrospun patch (**Figure 25**).

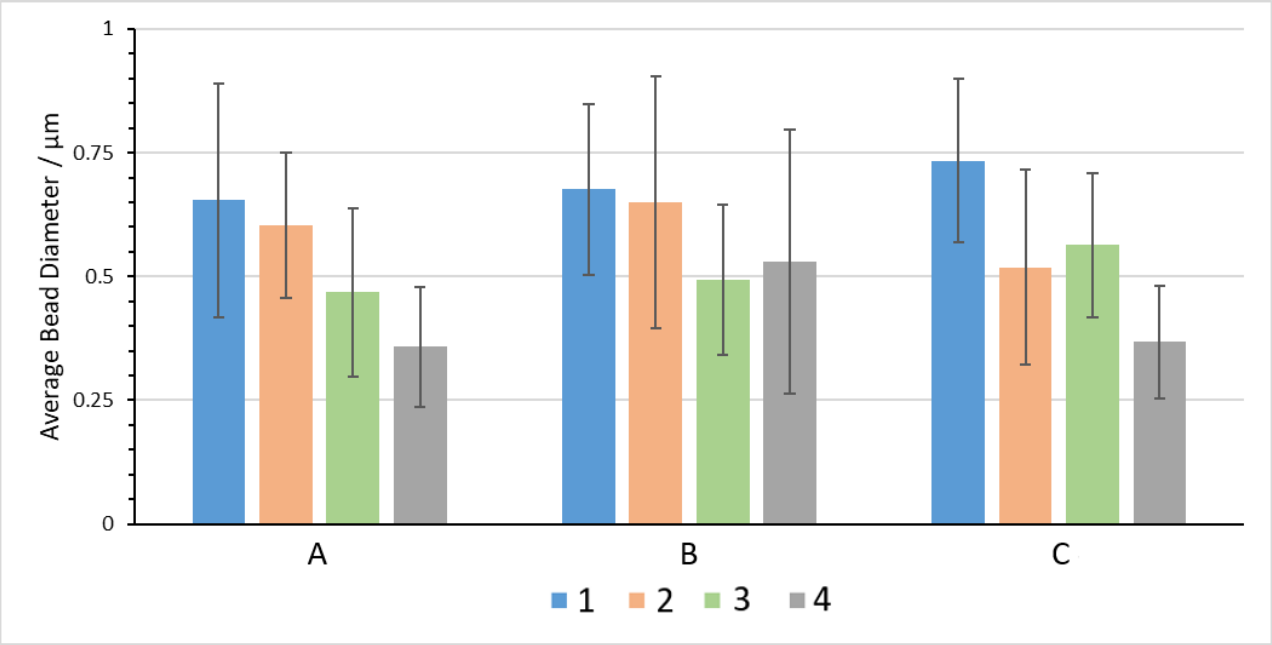

*Figure 26: Average bead diameter of electrospun patches obtained using 50 measurements from each SEM image in **Figure 23,** with error bars. A = 5% HPMC, B = 7.5% HPMC, C = 10% HPMC. The addition of the number indicates the lack of/addition of co-solvent, 1 = no co-solvent, 2 = addition of 2% PG, 3 = addition of 7.5% DMSO and 4 = addition of 2% PG and 7.5% DMSO (w/w).*

C3 produced the largest average bead diameter of 0.73 µm ± 0.17. When looking at the 5% solutions, a general decrease is seen with A2, A3 and then A4. The 10% solutions do not show a trend. The addition of PG (A2, A4, B2, B4, C2 and C4) showed a decrease in average bead diameter for each concentration. However, as the error bars overlap this means the results are not significantly different, therefore it cannot be concluded that the addition of 2% PG (w/w) as a co-solvent has a definite impact. From the solutions formulated and using the electrospinning parameters set, C4 provided the most ideal nanofibres with an average bead diameter of 0.37 µm ± 0.11. However, as mentioned before the error bars overlap, therefore the results are not significant.

4.11 Cloning of Cloacin DF13

4.11.1 Polymerase Chain Reaction - Standard Temperature Results

Polymerase chain reaction (PCR) is a method used to make millions of copies of a specific sample of DNA. This means a small sample of DNA can be amplified through this method of cloning and create a sample large enough to study in detail. The steps allow for the DNA strands to separate into two and for the primers and free nucleotides to join and form new DNA strands – thus a clone. The gel electrophoresis image (**Figure 27**) of the PCR protocol using the standard methodology (**section 3.2.3.3.2**) showed no bands present in **Gel 1**.

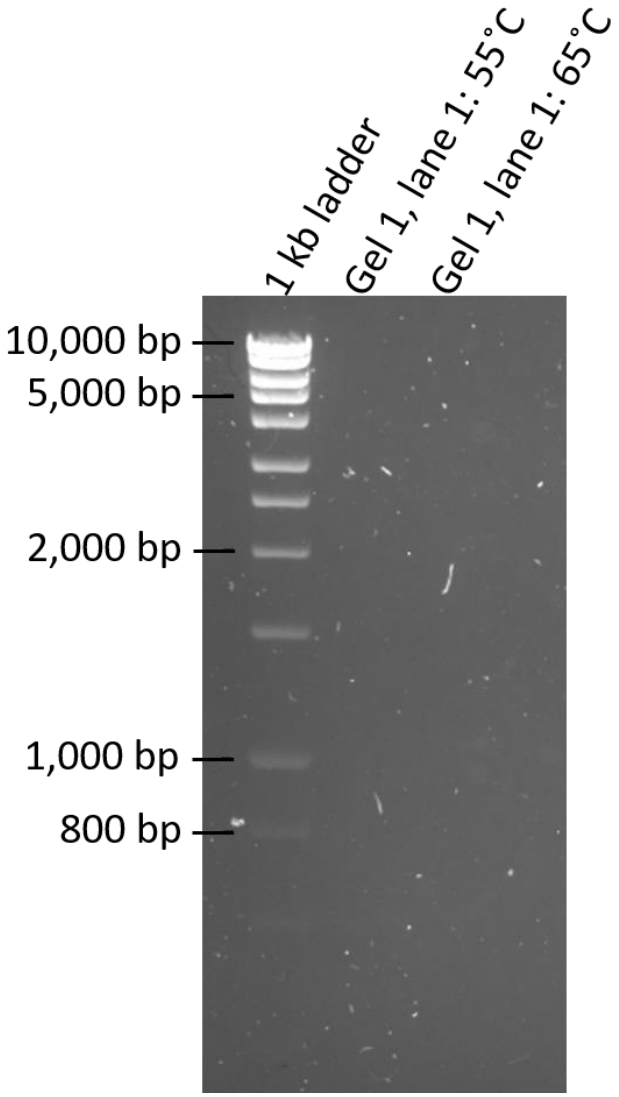

*Figure 27: Polymerase chain reaction gel image for the standard protocol and standard temperatures, listed in **section 3.2.3.3.2** run on 1% agarose gel with 1X TAE buffer at 110 V. PCR fragment of K. pneumoniae 957 in lane 1 and 1 kb ladder as indicated with key sizes highlighted. The gel image showed no bands, suggesting the reaction was unsuccessful.*

4.11.2 Polymerase Chain Reaction – 56.9°C Result

Through optimising the PCR procedure, the annealing stage was altered to 56.9 °C. Using the final methodology listed in **section 3.2.3.3.3** a gel electrophoresis image was produced with the PCR product of *K. pneumoniae* 957 (**Figure 28**). **Gel 2, lane 1** shows a clean band with the fragment at approximately 2 kbp and no contamination or unwanted product shown by the presence of other bands.

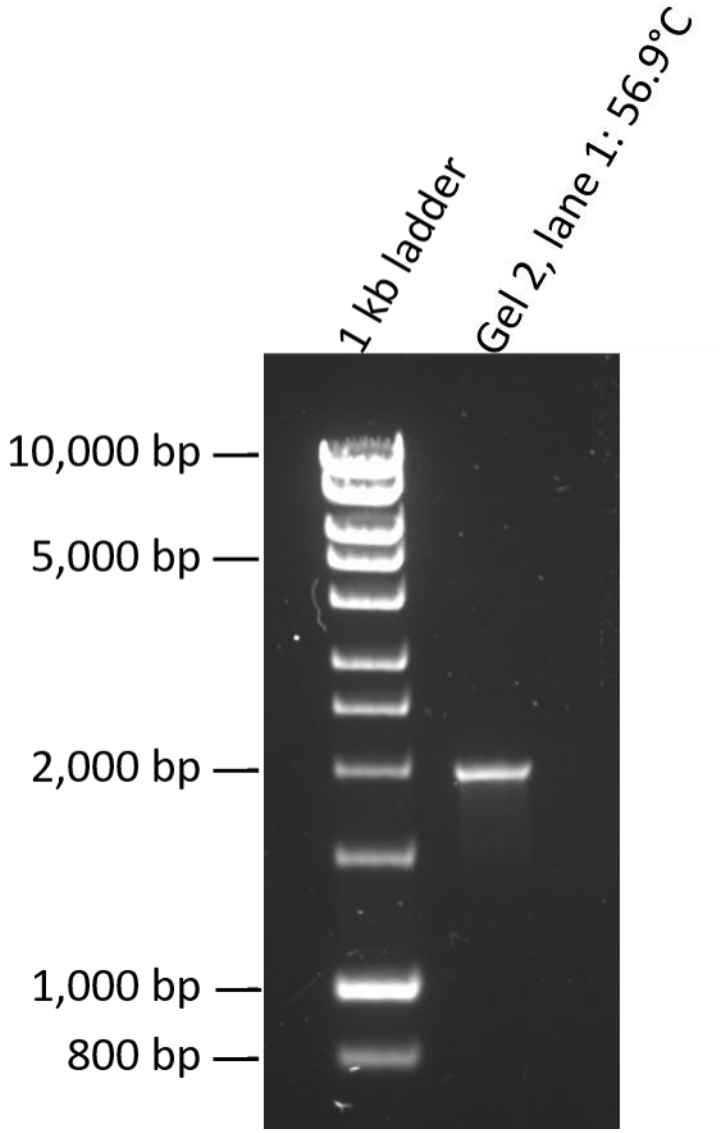

*Figure 28: Gel electrophoresis image of PCR product of K. pneumoniae 957 obtained from final PCR method (**section 3.2.3.3.3**) run on 1.2% ultrapure agarose gel with 1X TAE buffer at 110 V. PCR fragment of K. pneumoniae 957 in lane 1 and 1 kb ladder as indicated with key sizes highlighted. The PCR fragment shows the desired band size of 2,000 bp, matching the size of the cloacin gene.*

4.11.3 Restriction Enzyme Digest – NdeI, XhoI and NcoI Results

Restriction enzymes cleave DNA into fragments at specific recognition sites of the DNA. This method is used to cut both the pET 22b plasmid and the PCR product (cloacin bacteriocin gene) to create "sticky ends". These sticky ends can then be put together to form a pET 22b plasmid with the cloacin bacteriocin gene present.

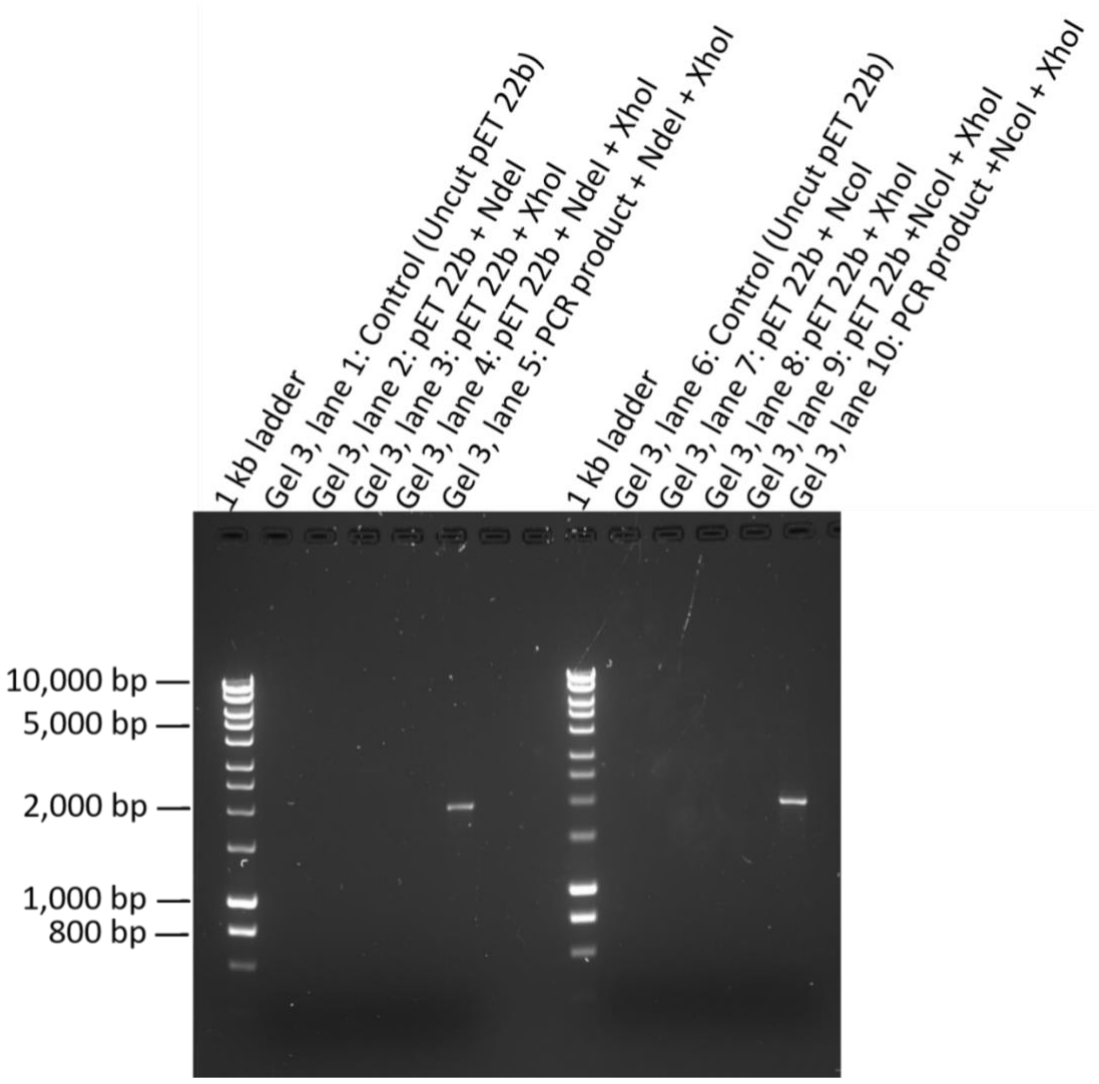

Figure 29: Gel electrophoresis image of restriction enzyme digestion using the restriction enzymes: NdeI, XhoI and NcoI as listed with the extracted PCR product and the pET 22b plasmid, with a control in lane 1 and 6; run on 1% agarose gel with 1X TAE buffer at 110 V. 1 kb ladder as indicated with key sizes highlighted.

Figure 29 shows the gel electrophoresis of the restriction enzyme digest performed using NdeI, XhoI and NcoI. The only bands present are the *K. pneumoniae* 957 PCR product, which was cut using NdeI & XhoI (**Gel 3, lane 5**) and NcoI & XhoI (**Gel 3, lane 10**). The band for this shows that the cut fragment remained at approximately 2 kbp. **Figure 29** also shows a lack of any other band for the other reactions, as well as lack of band for the controls, suggesting the pET 22b plasmid used may have been the issue.

4.12 Antimicrobial and Sterility Results

4.12.1 Sterility and Antimicrobial Activity of Aluminium Foil

This test was conducted to ensure that prove that the aluminium foil was not sterile and has the potential for microbial growth. The antimicrobial test was conducted to demonstrate if the foil had any antimicrobial action and to show the difference between the foil's antimicrobial action and the cloacin's antimicrobial activity.

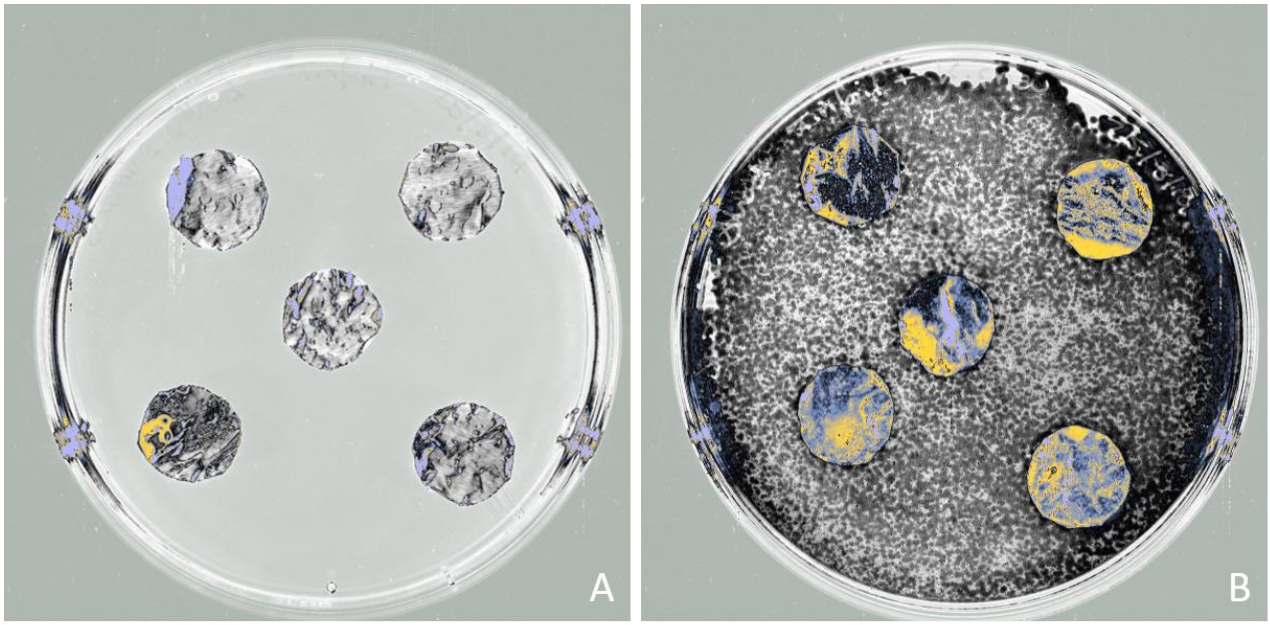

Figure 30: Sterility testing (A) of aluminium foil (15 mm diameter) using 1.2% BHI agar and antimicrobial activity testing (B) of aluminium foil (15 mm diameter) using 1.2% BHI agar with a 0.8% soft agar overlay with K. pneumoniae 757. Incubated overnight at 37 °C, inverted.

The sterility testing of aluminium foil (**Figure 30 A**) shows slight growth on the BHI agar (yellow markings on the foil). This showed that the aluminium foil itself is not sterile and when used for electrospinning is not present in a sterile environment. **Figure 30 B** shows that the aluminium foil does not produce an antimicrobial response to *K. pneumoniae* 757. This is seen through the yellow markings on the foil where bacteria were able to grow and the lack of zone of inhibition.

4.12.2 Sterility of Solution Results

This test was conducted to determine the sterility of each solution. This is so that the sterility of the production environment can be observed and if the solutions themselves have the potential for bacterial growth. Sterility would be observed by the lack of microbial growth which is seen in the formation of bacterial colonies. Bacterial colonies can appear in different sizes, colours and shape and this can aid towards identifying the bacterium causing the growth. However, to accurately identify the bacteria, further tests of the colonies would need to be conducted such as Gram staining, catalase and oxidase testing.

Figure 31 shows the sterility tests for each of the solutions on 1.2% BHI agar using the well method and the "placement" method. For the majority of the solutions, there appears to be no bacterial growth on the plates. This is seen through the lack of dark colouration seen on the agar plates. C1 (**Figure 31 C1**) was the only solution to show growth. This is seen in the "placement area" as there is one colony present but is not seen in the other solutions. The one white colony present is circular with an entire margin suggesting that the microorganism was not motile. However, as the colony measured approximately 5 mm in diameter, this could suggest the species was motile. The surface of the colony was raised in elevation, opaque, smooth and with a slight shine, suggesting the possibility of a biofilm present.

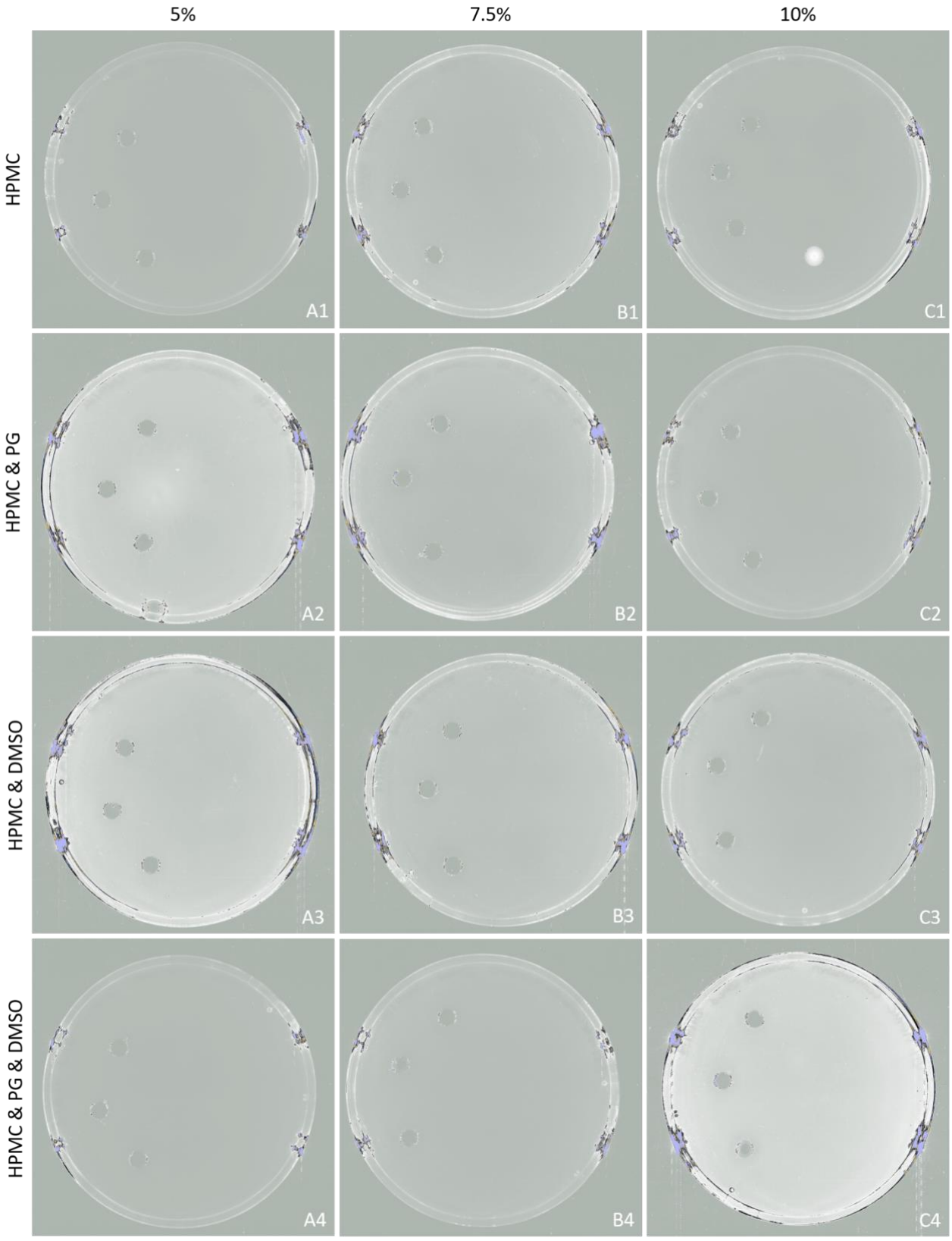

Figure 31: Sterility results of each solution used on plain 1.2% BHI agar using the "well" method and the "placement" method. Incubated overnight at 37 °C with the agar facing upwards. A = 5% HPMC, B = 7.5% HPMC, C = 10% HPMC. The addition of the number indicates the lack of/addition of co-solvent, 1 = no co-solvent, 2 = addition of 2% PG, 3 = addition of 7.5% DMSO and 4 = addition of 2% PG and 7.5% DMSO (w/w).

4.12.3 Sterility of Electrospun Patches Results

This test was conducted to determine the sterility of the solutions once they had been electrospun. This is because the solution may provide a different environment for bacteria compared to the electrospun patches. For example, the solutions could result in the lack of oxygen for bacterial growth while the electrospun patches may be more susceptible to contamination from the environment.

Each nanofibrous patch provided some bacterial growth, some to different degrees to others. Bacterial growth can be observed through the yellow colouration observed on the electrospun patches along with the dark colouration outside of the patches. A1, A3, A4, B1, B2, C3 and C4 (**Figures 32 A1, A3, A4, B1, B2, C3** and **C4** respectively) displayed bacterial growth outside of the electrospun patches. This bacterial growth seen outside of the patches were white and irregular in form and the margin was undulate. This could suggest the bacterial growth present was motile as the colony spreads over the agar. The surface was quite flat with a smooth, dull and opaque surface. **Figure 32 C3** also had a colony not connected to an electrospun patch present on the BHI agar. This colony is similar in appearance and size to the colony found in **Figure 32 C1** suggesting this could be the same bacteria and could be obtained from contamination. However, this cannot be concluded without further tests such as Gram staining, microscopy work, oxidase and catalase tests.

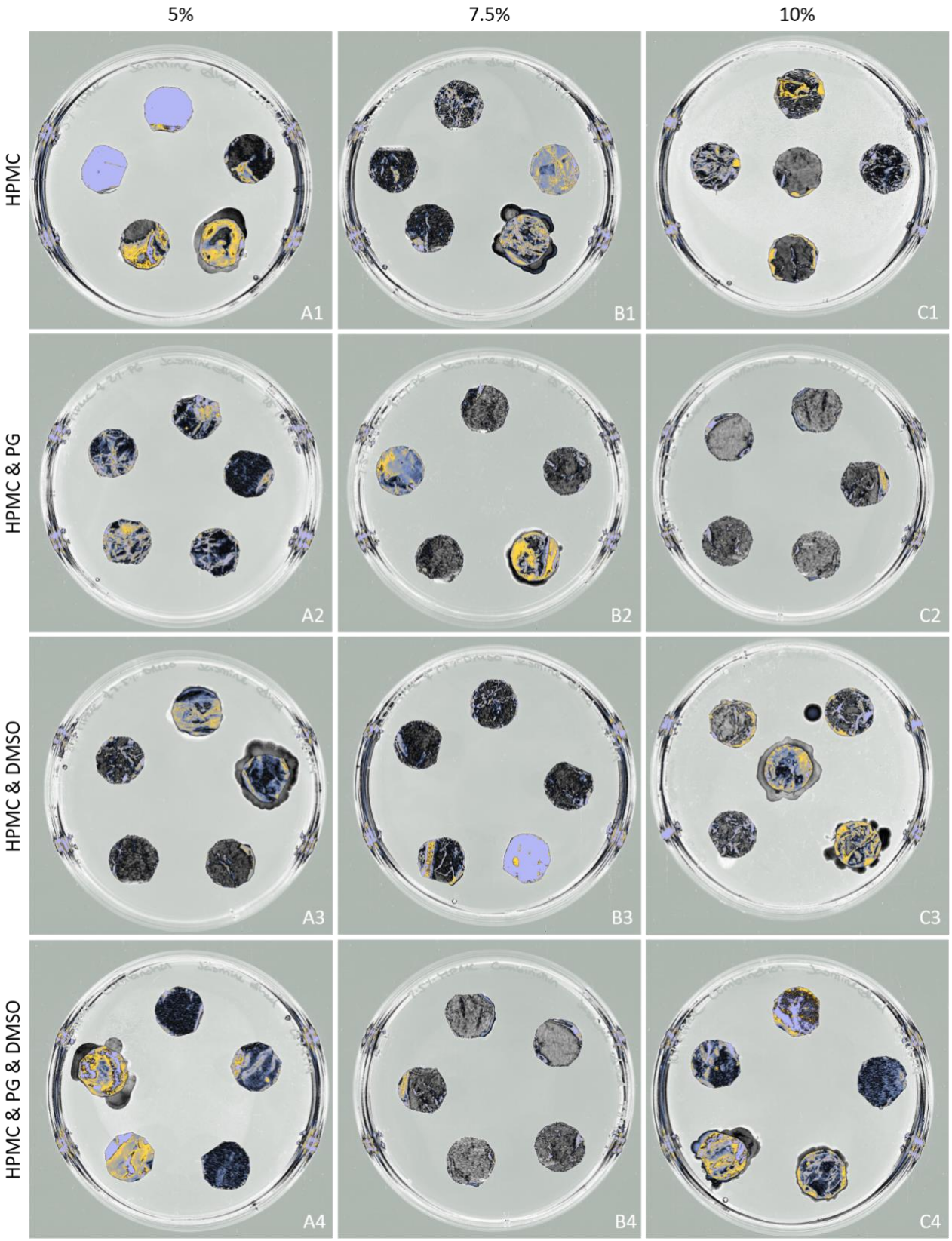

Figure 32: Sterility results of each electrospun product (15 mm diameter) on plain 1.2% BHI agar. Incubated overnight at 37 °C, inverted. . A = 5% HPMC, B = 7.5% HPMC, C = 10% HPMC. The addition of the number indicates the lack of/addition of co-solvent, 1 = no co-solvent, 2 = addition of 2% PG, 3 = addition of 7.5% DMSO and 4 = addition of 2% PG and 7.5% DMSO (w/w).

4.12.4 Antimicrobial Activity of Solutions Results

The antimicrobial activity of the solutions was conducted to determine if the solutions themselves displayed antimicrobial activity. As well as acting as a control or point of comparison against the cloacin, the co-solvents may also provide some antimicrobial activity. This would be seen through a zone of inhibition on the *K. pneumoniae* bacterial overlay.

For each of the agars in **Figure 33**, there was growth of *K. pneumoniae* 757 observed through the dark colouration of the agar, ranging in shades due to the imaging software and contrast adjustments. None of the solutions provided antimicrobial activity against *K. pneumoniae* and this is seen through the lack of zones of inhibition present. The slight change in colour of patterns seen on the agar is due to the "placement method" of the solutions as when they were placed this allowed them to spread across the agar. Therefore, when the plates were transported from the laminar airflow cabinet to the incubator some of the solutions could have moved and dried to form these patterns.

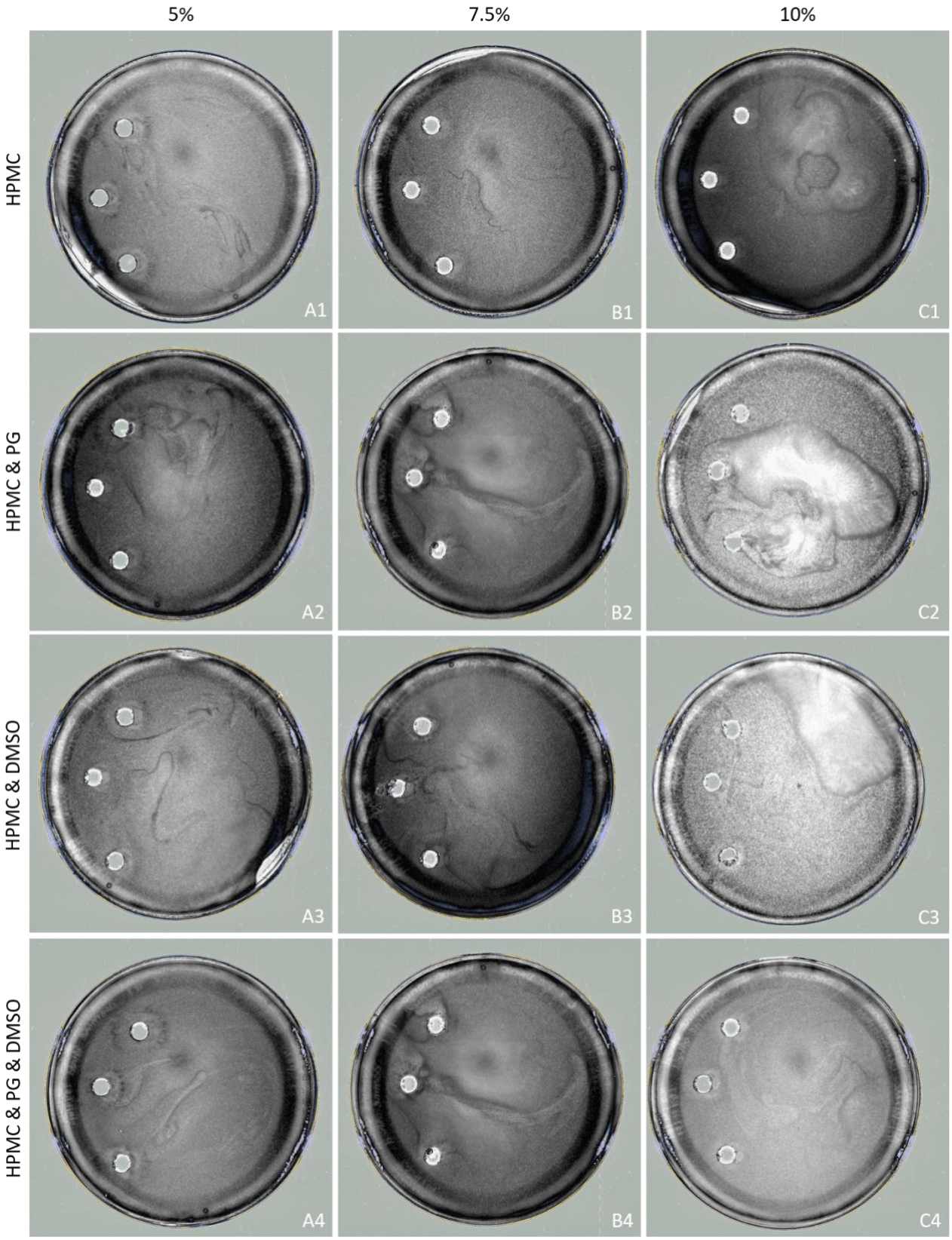

Figure 33: Antimicrobial activity results of each solution used on 1.2% BHI agar with 0.8% soft agar overlay of K. pneumoniae 757 using the "well" method and the "placement" method. Incubated overnight at 37 °C with the agar facing upwards. A = 5% HPMC, B = 7.5% HPMC, C = 10% HPMC. The addition of the number indicates the lack of/addition of co-solvent, 1 = no co-solvent, 2 = addition of 2% PG, 3 = addition of 7.5% DMSO and 4 = addition of 2% PG and 7.5% DMSO (w/w).

4.12.5 Antimicrobial Activity of Electrospun Patches Results

This test was conducted to determine if the solutions once electrospun produced an antimicrobial effect against *K. pneumoniae.* This was also to act as a control to compare against the electrospun fibres if they contained the cloacin to see how the cloacin produces an antimicrobial effect. As discussed before an antimicrobial activity is observed through the presence of a zone of inhibition on the bacterial overlay. In terms of the electrospun patches, the antimicrobial activity would be observed by a clear light grey circle surrounding the electrospun patch on the agar. This test was also important to observe if the co-solvents were present among the nanofibres and if they produced an antimicrobial effect as this could contribute towards the antimicrobial activity produced by the cloacin if they were incorporated in.

Growth of *K. pneumoniae* 757 can be seen by the dark colouration on the agar plates, different intensities are due to the saturation provided by the imaging software. C3 (**Figure 34 C3**) showed some "patchy" areas of the bacterial lawn. This could be due to the natural degradation that can occur with a bacterial broth, leading to a "patchy" bacterial lawn when placed on agar. For each of the electrospun nanofibrous patches, none of them produced any antimicrobial activity against *K. pneumoniae* 757. This was seen by the lack of zone of inhibition on the agar, as well as the yellow colouration under the patches indicating bacterial growth. B3 (**Figure 32 B3**) had an area with a lack of growth. It could be argued this may be antimicrobial activity. However, as there was not a clear zone circling the electrospun patch, this is likely an area where there is no bacterial overlay.

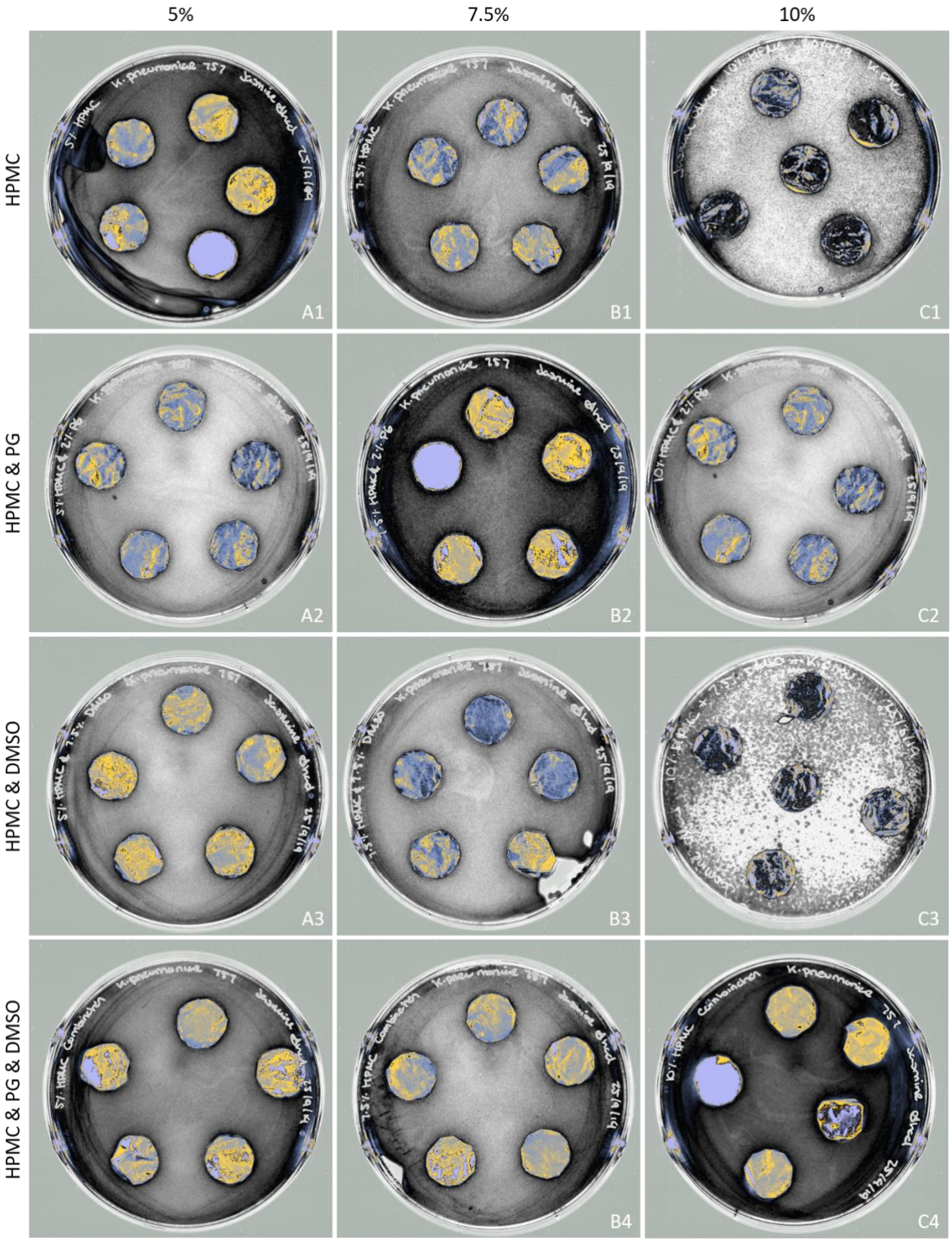

Figure 34: Antimicrobial activity results of the electrospun products (15 mm diameter) on 1.2% BHI agar with a K. pneumoniae 757. Incubated overnight at 37 °C, inverted. . A = 5% HPMC, B = 7.5% HPMC, C = 10% HPMC. The addition of the number indicates the lack of/addition of co-solvent, 1 = no co-solvent, 2 = addition of 2% PG, 3 = addition of 7.5% DMSO and 4 = addition of 2% PG and 7.5% DMSO (w/w).

5 DISCUSSION

5.1 RHEOLOGICAL CHARACTERISATION

All HPMC samples were rheologically characterised to compare their G' and G'' with each other. The samples were stirred for 24 hours and characterised immediately to replicate the rheological properties observed when electrospun as this also occurs immediately after 24 hours stirring. As all samples containing 10% HPMC (C1, C2, C3 and C4) had double the concentration of HPMC compared to the respective 5% HPMC samples (A1, A2, A3 and A4), it could have been expected that G' for the samples would also double. However, the samples did not show the 2-fold increase but instead increases which were higher. For example, at 20 Hz the storage modulus increases for A1 to C1 was 7 times. This shows that the increase in HPMC concentration leads to an increase in elasticity but not in a linear manner. The increase in elasticity could mean there is an increase in the likelihood of physical crosslinks – hydrogen bonding – between the polymer chains itself (Peppas *et al.,* 2000; Serpe and Craig, 2007). The presence and formation of physical crosslinks can create different physical properties within the polymer such as flexibility, hardness and the melting point. In terms of flexibility and hardness, this is with regards to the movement of the polymer chains, more physical crosslinks mean a restriction in movement of the chains, a reduction in flexibility, and an increase in hardness (Zweifel *et al.,* 2009; Maitra and Shukla, 2014). For all samples, as the concentration of HPMC increases as does the stability of the G' trendline. During the rheological characterisation samples containing 5% HPMC (w/w) had a lot of fluctuation of G' values beyond 12 Hz. This fluctuation was also seen with samples containing 7.5% HPMC (w/w) (**Figure 22**), however less than the 5% HPMC samples (**Figure 21**). This could be because at lower concentrations of HPMC there are less stable intermolecular forces present. The higher the frequencies applied, the more energy is applied to the system and of these leading to bonds breaking (Zweifel *et al.,* 2009). Thus, leading to samples containing 10% HPMC (C1, C2, C3 and C4) to have little G' fluctuation (**Figure 23**) as there were more hydrogen bonding.

The introduction of PG as a co-solvent was studied to determine the impact on the viscosity and the rheological characterisation. PG is often used as a plasticiser, which works by the molecule inserting itself in between the polymer chains. When in between the chains, this means they are less likely to form polymer-polymer interactions with each other (Bonet *et al.,* 2005). This allows the chains to flow over each other with greater ease, increasing flexibility and reducing the overall elasticity. This could also be seen through the solvation effect. The introduction of PG could have increased the Stokes radius or hydrodynamic volume causing the packing arrangement for the polymer chains to be unfavourable, so again fewer crosslinks can form. However, the results showed that there was a slight increase in elasticity (Atkins and De Paula, 2014)

(**Figure 18**). This could be since the PG solution itself is an elastic fluid, therefore, in general, increasing the overall elasticity of the HPMC samples (Karakatsani *et al.,* 2010). As well as this, the increase in elasticity could be due to the increase in hydrogen bonding – as PG is polar protic solvent – causing the polymer chains to decrease in flexibility (Atkins and De Paula, 2014).

The introduction of DMSO as a co-solvent was studied to determine the impact on the viscosity and the rheological characterisation of the HPMC samples. **Figure 19** showed the addition of 7.5% DMSO did increase the elasticity of the HPMC samples. As previously mentioned Karakatsani *et al* (2010) used a concentration that was 15 times lower than the concentration used in this project. This could suggest that a concentration of 0.5% is low enough that Stokes radius and the hydrodynamic volume does increase, allowing for unfavourable packing and reduction in polymer-polymer interactions (Atkins and De Paula, 2014). However, a concentration of 7.5% DMSO allows for an increase in the presence of hydrogen bonding.

The results also showed that the increase for both moduli from HPMC to the respective HPMC & PG and HPMC & DMSO samples were very similar. This could suggest that the co-solvents did provide an increase for both moduli values, however, the HPMC concentration is the main factor impacting the moduli values. This may be because HPMC is the main source for hydrogen bonding and polymer-polymer interaction and will, therefore, dictate how the viscoelastic behaviours will dominate.

5.2 ELECTROSPUN NANOFIBRES

The SEM images in **Figure 25** showed each sample produce beaded nanofibers. This is not considered ideal as the A:V is altered leading to be non-uniform throughout the fibres and if the bacteriocins were to be incorporated this would lead to the beads containing higher concentrations of the protein. Areas within the patch which contain higher areas of the therapeutic treatment would mean that the release would then be non-uniform as well. The concentration of the polymer solution was altered to observe how this could impact the nanofibre morphology. The concentration of the polymer and the elasticity or viscosity of this was an important aspect to the morphology of nanofibres. The electrospinning process relies on the stretching of the electrified jet and this can be impacted by the polymer solution concentration (Deitzel *et al.,* 2001; Okutan *et al.,* 2014). 5% HPMC, 7.5% HPMC and 10% HPMC (A1, B1 and C1 respectively) solutions were used as a range. This was because A1's concentration was not low, leading to the applied electric field and surface tension being "too strong", causing the polymer chains to fragment before reaching the conductor (Haider *et al.,* 2015). C1 was not a high concentration which would have led to a hindrance of flow and blockage of the micropipette tip (Haider *et al.,* 2015).

As the average bead diameters for A1, B1 and C1 were similar (0.65, 0.67 and 0.73 µm respectively), co-solvents PG and DMSO were added to assess the impact on the formation of nanofibres. The results showed that C4 displayed the closest to the "ideal" nanofibres as they contained the lowest average bead diameter (0.37 µm ± 0.11). This can also be seen in **Figure 25 C** as the beads looked to be more "drawn out" or more stretched in shape when compared to the other images. A4 (5% HPMC with 2% PG and 7.5% DMSO) had a similar average bead diameter to 10% HPMC with 2% PG and 7.5% DMSO denoted as C4 (0.36 µm ± 0.12). However, the standard deviation for A4 was higher than C4. Alongside this, A4's SEM image (**Figure 25 A**) showed bead morphology which was more droplet-like in shape compared to the more elongated beads for C4 (**Figure 25 C**). Therefore, C4 was seen as the "most ideal" in terms of nanofibres. The addition of co-solvents could have impacted the solvation effect by increasing the sphere of solvation, allowing for less polymer-polymer interactions to occur (Atkins and De Paula, 2014). This could allow the polymer chains to "slide over" each other with greater ease allowing for the electrospinning to be more "streamlined". So, when the polymer is being ejected there would be a reduced likelihood of areas containing high concentrations of the polymer. This is because the polymer chains would be spaced apart from each other as they cannot stack in a favourable manner (Bonet *et al.,* 2005). These co-solvents were added for different reasons; PG would lead to an increase in the viscous behaviour of the solution, by incorporating between the polymer chains. DMSO was added as this is a penetration enhancer, to "drag" the bacteriocins through the skin. Both PG and DMSO have boiling points which are higher than distilled water (188.2°C and 189°C respectively). An important factor to consider when using solvents in electrospinning is the solvent boiling

point as this can be considered as an estimate of the volatility (Sun *et al.,* 2014). In general, solvents with a low boiling point lead to nanofibres which are lower in diameter (Haider *et al.,* 2015). This is due to the quick evaporation rate, which leads to shorter drying time of the jet while in-flight, thus a continuing the elongation and thinning of the jet (Chai and Wu, 2013). As the solvents had relatively high boiling points this could explain why there was still the formation of beads as the solvents are unlikely to fully evaporate (Haider *et al.,* 2015). Incorporating a solvent with a lower boiling point could be beneficial to aid in evaporation such isopropanol, which has a boiling point of 82.5 °C. However not too low which would lead to blocking at the micropipette tip. The chosen solvents can also play a pivotal role in the fabrication of porous nanofibres. A study conducted by Megelski *et al* (2002) examined the properties of polystyrene nanofibres from solutions containing different ratios of dimethylformamide (DMF) and tetrahydrofuran (THF). Of the two solvents, THF was the more volatile with a boiling point of 66 °C while DMF has a higher boiling point of 153 °C. Solutions which were electrospun from 100% THF demonstrated a higher density of pores, leading to an increase in the A:V of the nanofibres by approximately 40% (Megelski *et al.,* 2002). Solutions which were spun with 100% DMF displayed loss of microtexture with the formation of smooth nanofibres. Megelski *et al* (2002) observed that between the two extremes: as the solvent volatility decreases the pore size increases and the pore depth decreases which leads to an overall decrease in pore density. This would be due to the lower boiling point being less likely to evaporate mid-flight, therefore more of the solvent would remain on the final product (Sill and von Recum, 2008; Haider *et al.,* 2015). If two solvents with different volatilities are involved this can lead to phase-separation due to one of the solvents behaving as a non-solvent (Haider *et al.,* 2015). This can lead to an increase in pore-density within the nanofibrous patch, which can be seen in **Figure 25.** However, if another solvent was involved with a lower boiling point this could further make DDS more efficient as it increases the A:V and aids in the release of the therapeutic agent.

The reduction of bead formation was critical because if the bacteriocins were to be incorporated within the nanofibres, beads could contain higher concentrations of the proteins. This could further mean the release of the bacteriocins from the nanofibres would be non-uniform and would make it difficult to determine the release accurately. As there is still the presence of beads in the nanofibres more factors need to be investigated to achieve the ideal nanofibres such as applied voltage, the distance between the micropipette tip and the conductor etc. (Bhardwaj and Kundu, 2010). However, during the experiments, environmental factors beyond control were the humidity and temperature. Humidity can impact nanofibre morphology as it can control the solidification process of the electrified jet; however, this is dependent upon the polymer. Working with a range of polymer blends Pelipenko *et al* (2013) observed with poly(vinyl alcohol) (PVA) a decrease in nanofibre diameter from 667 mm to 167 mm as the humidity was increased from 4% to 60%. A

further increase in humidity leads to bead formation with inhibition of electrospinning (Pelipenko *et al.,* 2013). Humidity may also impact the formation of pores on the nanofibrous patch. When a solution used two solvents with different volatilities, humidity causes a cooling effect that is similar to perspiration. This results in the condensation of water vapour into water droplets which could settle on the nanofibres, leading to the formation of pores (Haider *et al.,* 2015). Temperature can cause two opposing effects to change the average nanofibre diameter. An increase in temperature can increase the rate of evaporation of the solvent as well as decreasing the viscosity of the solution. As mentioned before, evaporation and viscosity can impact the formation of the nanofibres (Haider *et al.,* 2015)

5.3 RHEOLOGY AND ELECTROSPINNING

An important aspect of electrospinning is that the polymer must be formulated as a solution or as a melt if the sample is a gel it will not electrospin. One method of determining if the sample formulated is a gel would be to check the sample rheologically, ensuring that the sample does not reach gel point. This is the point at which G' would cross G'', as the character of the sample changed from the solution state into the gel state (Hamley, 2007; Rudin and Choi, 2013). As at the time it was not possible to simulate a frequency sweep mimicking the deformation which would be applied to the sample when electrospun, a range from 1-20 Hz was used to simulate slow and fast motions. Within this range, it was important to ensure the sample remains in the solution state to allow for a better chance for electrospinning, and this was seen through the product formation (**Figures 25**).

C4 showed the smallest bead diameter compared to the other solutions. Further comparing the samples containing 10% HPMC (C1 – 4), with regards to tan δ obtained through rheological characterisation; C1 and C2 showed similar tan δ trends (**Figure 24**). This matched with the G' and G'' that was seen in **Figure 23**. Therefore, the addition of 2% PG (w/w) did not alter the rheological properties but did decrease average bead diameter from 0.76 to 0.52 µm respectively (**Figure 26**). This could be due to the slight increase in solvation sphere the PG provided (Atkins and De Paula, 2014), however as the error bars overlap this is not a significant reduction. When looking at C3, **Figure 24**, showed that this displayed the most elastic-like behaviour as the lowest tan δ was observed. It was thought that the DMSO could also impact the solvation sphere, but DMSO allowed for more hydrogen bonding. If more hydrogen bonding were to occur this could allow for more favourable packing between the polymer chains (Barnes *et al.,* 2005). As C3 showed an average bead diameter of 0.56 µm, this could show that having a more elastic-like sample does aid in the reduction in bead diameter compared to C1. C4, however, had a tan δ which lay in between C2 and C3 (**Figure 25**) and produced the lowest average bead diameter of 0.38 µm. This suggests that the combination of PG and DMSO allowed for both an increase in hydrogen bonding with HPMC to allow the sample to be more stable while increasing the solvation sphere enough to reduce the polymer-polymer interactions to form (Atkins and De Paula, 2014). This could lead to the polymer chains to be more flexible and "slide over" each other as being electrospun (Barnes *et al.,* 2005). However, as the error bars for the bead diameter overlap the results are not significantly different.

Therefore, more factors need to be considered to be able to determine what other parameters may reduce bead diameter. Typically, when electrospinning, one may only know the morphology of the fibres through microscopy work afterwards, such as SEM. Therefore, it could be suggested that rheological characterisation could be beneficial in predicting the possible nanofibre outcome before electrospinning.

5.4 CLONING OF CLOACIN DF13

Phusion polymerase was chosen over Taq polymerase as Phusion is highly processive. This makes it much faster than Taq and can handle longer amplicons due to Phusion being less likely to dissociate. This is important as it allows to amplify the entire plasmid; something Taq may not be able to achieve. Alongside this, Phusion polymerase has an error rate 50-fold lower than Taq due to Phusion possessing a proof-reading domain. Taq does not have this domain which leads to a higher error rate especially with longer amplicons as there is a higher chance of introducing a mutation.

Figure 27 showed no bands while using standard PCR temperatures. After looking at the sequences of the primers it was found that the annealing temperatures of these were 40°C. However, setting the annealing stage at such a low temperature could have proved an issue for the polymerase as Phusion requires 75°C to be active. The protocol was altered to test a range of annealing temperatures and it was found that 59.6°C produced a band at the desired 2 kbp fragment length with no contaminants/unwanted fragments (**Figure 28**). This 2 kbp fragment is the estimated size of the bacteriocin and immunity protein section of the *K. pneumoniae* 957 plasmid. The sample then went through PCR purification to remove the components used during the reaction, such as dNTPs, buffers, primers and enzyme.

Restriction enzyme digests are an enzymatic technique used for the cleaving of DNA molecules at specific locations within the DNA – also known as restriction sites. The cut is made on both of the strands of DNA and depending on the recognition site, can lead to single-stranded DNA "overhangs". These overhangs produce "sticky ends", which are beneficial for performing a DNA ligase as DNA which complements the overhangs can link together, completing the sequence. As **Figure 29** showed no bands in the gel image besides **Gel 3 lanes 5** and **10**. As there were also no bands in the controls this could suggest that the pET 22b plasmid used had either degraded or that the concentration was too low.

5.5 STERILITY AND ANTIMICROBIAL TESTS

5.5.1 HPMC Solutions

Figures 31 and 33 show the sterility results and the antimicrobial activity results respectively. The sterility tests showed that for the majority of the plates there was no bacterial growth. As the samples were not formulated and prepared in a sterile environment, it was assumed bacterial growth would be present for most solutions. In literature, DMSO has displayed some antimicrobial activity. A study by Hassan (2014) tested the antimicrobial activity of DMSO with and without additional complexes they formulated. Using the agar well diffusion method – 8 mm in diameter – they demonstrated 20 µg mL^{-1} DMSO displayed activity against four human pathogenic bacteria (Hassan, 2014). Therefore, it could be argued that as 6 sample solutions contained DMSO (A3, A4, B3, B4, C3 and C4), these could prevent bacterial growth from the environment (**Figures 31 A3, A4, B3, B4, C3** and **C4**). However, as the other samples within **Figure 31** also did not show growth indicated through the well method or the placement method, it is likely that the DMSO did not impact bacterial growth in the samples. The lack of growth could instead be due to a lack of contamination from the environment during formulation. However, this could be unlikely as no methods to ensure sterility was used during formulation such as aseptic technique or the use of a laminar airflow cabinet. It could also be argued that if bacteria were to enter the sample from the environment, the solutions themselves could have in a sense "suffocated" the bacteria and provided little to no nutrients for them to survive.

Figure 31 C showed that C1 has one colony present in the area where the solution was placed. The motility of the organism in this colony is unknown as the margin present is entire – suggesting immotile – yet the diameter is approximately 5 mm in diameter – suggesting motility (Roth *et al.,* 2013). There was also a shine present on the colony which could suggest the presence of a biofilm. As there was only one colony present and this was only present from one of the samples, it could be argued that this appeared through contamination from the plating process.

The antimicrobial results showed that all of the samples did not produce an antimicrobial response to *K. pneumoniae* 757 (**Figure 33**). It was hypothesised that the 6 samples containing 7.5% DMSO could show some activity against *K. pneumoniae* 757 as in literature DMSO has displayed some activity against a range of organisms. When testing synthetic flavonoids, Babii *et al* (2018) used DMSO as a control during the antimicrobial activity test against 4 common microorganisms, one being *K. pneumoniae.* They found that a concentration of 125 µg mL^{-1} of DMSO was needed to produce minimum inhibitory results against *K. pneumoniae.* This could argue that the amount of DMSO used in the samples was not high enough to

produce an antimicrobial response in *K. pneumoniae* 757. As the samples did not produce a response this suggests that the components incorporated in the solutions do not display antimicrobial activity.

5.5.2 Electrospun patches

Figures 32 and **34** show the sterility results and the antimicrobial activity results respectively. The sterility tests showed that for all of the electrospun patches, microbial growth was observed through the yellow and dark colourations. This was expected as the solutions were not electrospun in a sterile environment. This could further suggest the samples in solution form inhibit the growth from the external environment. The growth was seen for the A1, A3, A4, B1, B2, C3 and C4 (**Figures 32 A1, A3, A4, B1, B2, C3** and **C4** respectively) could be motile bacteria as the colonies show undulate margins (Roth *et al.,* 2013).

With regards to the antimicrobial activity results, all samples show negative results (**Figure 34**). It could be argued that samples containing DMSO could have displayed some antimicrobial activity as DMSO in literature has shown some activity.

DMSO was added into the sample to act as a penetration enhancer as studies have shown this compound can readily cross most tissue membranes and penetrate the skin (Jacob and Herschler, 1986; Gurtovenko and Anwar, 2007; Hassan, 2014; Mi *et al.,* 2016). This resulted in changes from α-helices in the intercellular keratin to a β-sheet conformation (Karakatsani *et al.,* 2010). With this knowledge, DMSO was added to the electrospun samples in the hopes that the solvent would aid in the diffusion of bacteriocin. However, the main aspect of electrospinning which results in the formation of nanofibres is the aspect of the solvent evaporating during flight. As there was the formation of beads (**Figures 25**), this could suggest the presence of DMSO remaining in the nanofibres, however, one cannot easily determine the concentration of DMSO in the nanofibres. Yet it could be estimated that the concentration will be below 7.5%.

6 CONCLUSIONS AND FUTURE WORK

While formulating HPMC solutions, the effects of HPMC concentration and co-solvents (PG and DMSO) on rheological properties and electrospinnability were investigated. It was observed that increasing the concentration of HPMC increases the elasticity of the structured fluid due to the increase in physical entanglements. The introduction of co-solvents PG and DMSO allowed for a slight increase in elasticity while keeping the HPMC sample in a solution state. This was beneficial for electrospinning as the 10% HPMC with 2% PG and 7.5% DMSO solution provided the nanofibres with the lowest bead diameter of 0.36 µm, and thus the closest to the ideal fibre. The introduction of PG and DMSO provided a better DDS for the electrospun patches by increasing the presence of hydrogen bonding while increasing the solvation sphere and decreasing polymer-polymer interactions. DMSO would have also provided a penetration enhancement effect, allowing for the therapeutic agents to pass through the stratum corneum.

The electrospinning technique, as outlined above, holds promise towards the effective creation of non-woven HPMC patches for wound healing or other medical devices. However, as beads within the nanofibres were still observed, further work needs to be done to reduce or remove these. This would involve more experimentation with the different electrospinning parameters such altering the ratio of PG and DMSO used to understand how this can impact the bead diameter, as well as introducing solvents with lower boiling points such as DMF and THF as they have boiling points both higher and lower than water (153 °C and 66 °C respectively.

This project aimed to incorporate bacteriocins into the nanofibrous patch. This was not successful due to the microbiology work not progressing past the restriction enzyme digest of the plasmid pET 22b. The successful incorporation would have led to the patch, hopefully, exerting an antimicrobial effect. Future work would be successful incorporation of the bacteriocin and determining where they would present. For example, if they are inside the fibres or if they present on the surface, determining through SEM and fluorescence tagging. The efficiency of the antimicrobial patch could then be determined through antimicrobial activity tests used, by placing the patch on the *K. pneumoniae* bacterial lawn and observing zones of inhibition.

7 REFERENCES

Afshari, M. (2017) *Electrospun nanofibers*. Duxford: Woodhead Publishing.

Alanis, A. (2005) Resistance to Antibiotics: Are We in the Post-Antibiotic Era?. *Archives of Medical Research*, 36(6) 697-705.

Arias, C. and Murray, B. (2009) Antibiotic-Resistant Bugs in the 21st Century — A Clinical Super-Challenge. *New England Journal of Medicine*, 360(5) 439-443.

Asiri, A., Inamuddin. and Mohammad, A. (2018) *Applications of Nanocomposite Materials in Drug Delivery*, Duxford: Elsevier.

Atkins, P. and De Paula, J. (2014) *Atkins' Physical chemistry*, 10th edition. Oxford: Oxford University Press

Babii, C., Mihalache, G., Bahrin, L., Neagu, A., Gostin, I., Mihai, C., Sârbu, L., Birsa, L. and Stefan, M. (2018) A novel synthetic flavonoid with potent antibacterial properties: In vitro activity and proposed mode of action. *Plos One*, 13(4) 1-15.

Barnes, H., Hutton, J. and Walters, K. (2005) *An introduction to rheology*. Amsterdam: Elsevier.

Bendas, B., Schmalfuβ, U. and Neubert, R. (1995) Influence of propylene glycol as cosolvent on mechanisms of drug transport from hydrogels. *International Journal of Pharmaceutics*, 116(1) 19-30.

Bhardwaj, N. and Kundu, S. (2010) Electrospinning: A fascinating fiber fabrication technique. *Biotechnology Advances*, 28(3) 325-347.

Bonet, M., Quijada, C., Muñoz, S. and Cases, F. (2005) The roles of the degree of substitution and the degree of polymerization on the behaviour of cellulose ethers applied as adhesives for artwork conservation. *Journal of Adhesion Science and Technology*, 19(2) 95-108

Brostow, W., Drewniak, M. and Medvedev, N. (1995) Chain overlap and entanglements in dilute polymer solutions: Brownian dynamics simulation. *Macromolecular Theory and Simulations*, 4(4) 745-758.

Cascales, E., Buchanan, S., Duche, D., Kleanthous, C., Lloubes, R., Postle, K., Riley, M., Slatin, S. and Cavard, D. (2007) Colicin Biology. *Microbiology and Molecular Biology Reviews,* 71(1) 158-229.

Chai, J. and Wu, Q. (2013) Electrospinning preparation and electrical and biological properties of ferrocene/poly(vinylpyrrolidone) composite nanofibers. *Beilstein Journal of Nanotechnology,* 4(1) 189-197.

Chai, Q., Jiao, Y. and Yu, X. (2017) Hydrogels for Biomedical Applications: Their Characteristics and the Mechanisms behind Them. *Gels*, 3(1) 6.

Chen, H. and Hoover, D. (2003) Bacteriocins and their Food Applications. *Comprehensive Reviews in Food Science and Food Safety*, 2(3) 82-100.

Childs, D. and Murthy, A. (2017) Overview of Wound Healing and Management. *Surgical Clinics of North America*, 97(1) 189-207.

Cooley, J. (1902) *Apparatus for Electronically Dispersing Fluids.* US692631A. United States.

Cotter, P., Hill, C. and Ross, R. (2005) Bacteriocins: developing innate immunity for food. *Nature Reviews Microbiology*, 3(10) 777-788.

Cotter, P., Ross, R. and Hill, C. (2012) Bacteriocins – a viable alternative to antibiotics?. *Nature Reviews Microbiology,* 11(2) 95-105.

Cui, Y., Zhang, C., Wang, Y., Shi, J., Zhang, L., Ding, Z., Qu, X. and Cui, H. (2012) Class IIa Bacteriocins: Diversity and New Developments. *International Journal of Molecular Sciences*, 13(12) 16668-16707.

de Graaf, F. (1973) Effects of cloacin DF13 on the functioning of the cytoplasmic membrane. *Antonie van Leeuwenhoek*, 39(1) 109-119.

de Silva, D. and Olver, J. (2005) Hydroxypropyl Methylcellulose (HPMC) Lubricant Facilitates Insertion of Porous Spherical Orbital Implants. *Ophthalmic Plastic & Reconstructive Surgery*, 21(4) 301-302.

De Vrieze, S., Van Camp, T., Nelvig, A., Hagström, B., Westbroek, P. and De Clerck, K. (2009) The effect of temperature and humidity on electrospinning. *Journal of Materials Science*, 44(5) 1357-1362.

Deitzel, J., Kleinmeyer, J., Harris, D. and Beck Tan, N. (2001) The effect of processing variables on the morphology of electrospun nanofibers and textiles. *Polymer*, 42(1) 261-272.

Delves-Broughton, J., Blackburn, P., Evans, R. and Hugenholtz, J. (1996) Applications of the bacteriocin, nisin. *Antonie van Leeuwenhoek*, 69(2) 193-202.

Ding, J., Zhang, J., Li, J., Li, D., Xiao, C., Xiao, H., Yang, H., Zhuang, X. and Chen, X. (2019) Electrospun polymer biomaterials. *Progress in Polymer Science*, 90(1) 1-34.

Dorit, R., Roy, S. and Riley, M. (2016) *The Bacteriocins: Current Knowledge and Future Prospects*. Norfolk, UK: Caister Academic Press.

Draper, L., Grainger, K., Deegan, L., Cotter, P., Hill, C. and Ross, R. (2009) Cross-immunity and immune mimicry as mechanisms of resistance to the lantibiotic lacticin 3147. *Molecular Microbiology*, 71(4) 1043-1054.

Dykes, G. (1995) Bacteriocins: ecological and evolutionary significance. *Trends in Ecology & Evolution,* 10(5) 186-189.

Egan, K., Field, D., Rea, M., Ross, R., Hill, C. and Cotter, P. (2016) Bacteriocins: Novel Solutions to Age Old Spore-Related Problems?. *Frontiers in Microbiology*, 7(461) 1-21.

Ewoldt, R., Hosoi, A. and McKinley, G. (2008) New measures for characterizing nonlinear viscoelasticity in large amplitude oscillatory shear. *Journal of Rheology*, 52(6) 1427-1458.

Fleming, A. (1929) On the Antibacterial Action of Cultures of a Penicillium, with Special Reference to their Use in the Isolation of B. influenzæ. *British Journal of Experimental Pathology*, 10(3) 226-236.

Flügge, W. (1975) *Viscoelasticity*, 2nd edition. Berlin: Springer.

Fridrikh, S., Yu, J., Brenner, M. and Rutledge, G. (2003) Controlling the Fiber Diameter during Electrospinning. *Physical Review Letters*, 90(14) 1-4.

Gao, P., Nie, X., Zou, M., Shi, Y. and Cheng, G. (2011) Recent advances in materials for extended-release antibiotic delivery system. *The Journal of Antibiotics*, 64(9) 625-634.

Gilchrist, S., Lange, D., Letchford, K., Bach, H., Fazli, L. and Burt, H. (2013) Fusidic acid and rifampicin co-loaded PLGA nanofibers for the prevention of orthopedic implant associated infections. *Journal of Controlled Release*, 170(1) 64-73.

Graaf, F. and Klaasen-Boor, P. (1977) Purification and Characterization of a Complex between Cloacin and its Immunity Protein Isolated from Enterobacter cloacae (Clo DF13). Dissociation and Reconstruction of the Complex. *European Journal of Biochemistry*, 73(1) 107-114.

Guest, J., Vowden, K. and Vowden, P. (2017) The health economic burden that acute and chronic wounds impose on an average clinical commissioning group/health board in the UK. *Journal of Wound Care*, 26(6) 292-303.

Gurtovenko, A. and Anwar, J. (2011) Modulating the Structure and Properties of Cell Membranes: The Molecular Mechanism of Action of Dimethyl Sulfoxide. *The Journal of Physical Chemistry B*, 111(35) 10453-10460.

Haghi, A. and Akbari, M. (2007) Trends in electrospinning of natural nanofibers. *Physica Status Solidi (a)*, 204(6) 1830-1834.

Haider, A., Haider, S. and Kang, I. (2015) A comprehensive review summarizing the effect of electrospinning parameters and potential applications of nanofibers in biomedical and biotechnology. *Arabian Journal of Chemistry,* 11(8) 1165-1188.

Hamley, I. (2007) *Introduction to soft matter - revised edition*. Hoboken, N.J.: Wiley.

Händel, N., Schuurmans, J., Feng, Y., Brul, S. and ter Kuile, B. (2014) Interaction between Mutations and Regulation of Gene Expression during Development of De Novo Antibiotic Resistance. *Antimicrobial Agents and Chemotherapy*, 58(8) 4371-4379.

Hassan, A. (2014) The Antibacterial Activity of Dimethyl Sulfoxide (DMSO) with and without of Some Ligand Complexes of the Transitional Metal Ions of Ethyl Coumarin against Bacteria Isolate from Burn and Wound Infection. *Journal of Natural Sciences Research,* 4(19) 2224-3186

Hu, X., Liu, S., Zhou, G., Huang, Y., Xie, Z. and Jing, X. (2014) Electrospinning of polymeric nanofibers for drug delivery applications. *Journal of Controlled Release*, 185(1) 12-21.

Huang, Z., Zhang, Y., Kotaki, M. and Ramakrishna, S. (2003) A review on polymer nanofibers by electrospinning and their applications in nanocomposites. *Composites Science and Technology*. 63(15) 2223-2253.

Huang, W., Wang, M., Liu, C., You, J., Chen, S., Wang, Y. and Liu, Y. (2014) Phase separation in electrospun nanofibers controlled by crystallization induced self-assembly. *Journal of Materials Chemistry A*, 2(22) 8416.

Jacob, S. and Herschler, R. (1986) Pharmacology of DMSO. *Cryobiology*, 23(1) 14-27.

Jha, M., Rahman, H. and Rahman, M. (2015) Biphasic Drug Delivery In Controlled Release Formulations – A Review. *International Journal Of Pharmacy & Technology*, 6(4) 3046-3060.

Ji, W., Sun, Y., Yang, F., van den Beucken, J., Fan, M., Chen, Z. and Jansen, J. (2010) Bioactive Electrospun Scaffolds Delivering Growth Factors and Genes for Tissue Engineering Applications. *Pharmaceutical Research*, 28(6) 1259-1272.

Karakatsani, M., Dedhiya, M. and Plakogiannis, F. M. (2010). The effect of permeation enhancers on the viscosity and the release profile of transdermal hydroxypropyl methylcellulose gel formulations containing diltiazem HCl. *Drug Development and Industrial Pharmacy*, 36(10) 1195–1206.

Kavanagh, G. and Ross-Murphy, S. (1998) Rheological characterisation of polymer gels. *Progress in Polymer Science*, 23(3) 533-562.

Khan, S., Ullah, A., Ullah, K. and Rehman, N. (2016) Insight into hydrogels. *Designed Monomers and Polymers*, 19(5) 456-478.

Kohanski, M., Dwyer, D. and Collins, J. (2010) How antibiotics kill bacteria: from targets to networks. *Nature Reviews Microbiology*, 8(6) 423-435.

Lee, C., Lee, J., Park, K., Jeong, B. and Lee, S. (2015) Quantitative proteomic view associated with resistance to clinically important antibiotics in Gram-positive bacteria: a systematic review. *Frontiers in Microbiology*, 6(828).

Li, D. and Xia, Y. (2004) Electrospinning of Nanofibers: Reinventing the Wheel?. *Advanced Materials*, 16(14) 1151-1170.

Liptak, J. (1997) An overview of the topical management of wounds. *Australian Veterinary Journal*, 75(6) 408-413.

Liu, S., Long, Q., Xu, Y., Wang, J., Xu, Z., Wang, L., Zhou, M., Wu, Y., Chen, T. and Shaw, C. (2017) Assessment of antimicrobial and wound healing effects of Brevinin-2Ta against the bacterium Klebsiella pneumoniae in dermally-wounded rats. *Oncotarget*, 8(67) 111369-111385.

Luo, X., Xie, C., Wang, H., Liu, C., Yan, S. and Li, X. (2012) Antitumor activities of emulsion electrospun fibers with core loading of hydroxycamptothecin via intratumoral implantation. *International Journal of Pharmaceutics*, 425(1-2) 19-28.

Maitra, J. and Shukla, V. (2014) Cross-linking in Hydrogels - A Review. *American Journal of Polymer Science*, 4(2) 25-31.

Matabola, K. and Moutloali, R. (2013) The influences of electrospinning parameters on the morphology and diameter of poly(vinylidene fluoride) nanofibers – effect of sodium chloride. *Journal of Materials Science,* 48(16) 5475-5482.

Megelski, S., Stephens, J., Chase, D. and Rabolt, J. (2002) Micro- and Nanostructured Surface Morphology on Electrospun Polymer Fibers. *Macromolecules*, 35(22) 8456-8466.

Mi, H., Wang, D., Xue, Y., Zhang, Z., Niu, J., Hong, Y., Drlica, K. and Zhao, X. (2016) Dimethyl Sulfoxide Protects Escherichia coli from Rapid Antimicrobial-Mediated Killing. *Antimicrobial Agents and Chemotherapy*, 60(8) 5054-5058

Mouthuy, P., Groszkowski, L. and Ye, H. (2015) Performances of a portable electrospinning apparatus. *Biotechnology Letters*, 37(5) 1107-1116.

Nascimento, J., Abrantes, J., Giambiagi-deMarval, M. and Bastos, M. (2004) Growth conditions required for bacteriocin production by strains of Staphylococcus aureus. *World Journal of Microbiology & Biotechnology,* 20(9) 941-947.

Nordmann, P., Naas, T., Fortineau, N. and Poirel, L. (2007) Superbugs in the coming new decade; multidrug resistance and prospects for treatment of Staphylococcus aureus, Enterococcus spp. and Pseudomonas aeruginosa in 2010. *Current Opinion in Microbiology*, 10(5) 436-440.

Okutan, N., Terzi, P. and Altay, F. (2014) Affecting parameters on electrospinning process and characterization of electrospun gelatin nanofibers. *Food Hydrocolloids*, 39, 19-26.

Oudega, B. and de Graaf, F. (1976) Enzymatic properties of cloacin DF13 and kinetics of ribosome inactivation. *Biochimica et Biphysica Acta (BBA) – Nucleic Acids and Protein Synthesis*, 425(3) 296-304.

Oudega, B., Stegehuis, F. and Graaf, F. (1984) Effect of glucose fermentation of the functioning of protein H in the excretion of cloacin DF13 by Escherichia coli. *FEMS Microbiology Letters*, 21(1) 125-131.

Papadakos, G., Wojdyla, J. and Kleanthous, C. (2011) Nuclease colicins and their immunity proteins. *Quarterly Reviews of Biophysics*, 45(1) 57-103.

Papanastasiou, T., Alexandrou, A. and Georgiou, G. (2000) *Viscous fluid flow*. Boca Raton, FLa: CRC Press.

Pelipenko, J., Kristl, J., Janković, B., Baumgartner, S. and Kocbek, P. (2013) The impact of relative humidity during electrospinning on the morphology and mechanical properties of nanofibers. *International Journal of Pharmaceutics,* 456(1) 125-134.

Peppas, N. (2000) Hydrogels in pharmaceutical formulations. *Journal of Pharmaceutics and Biopharmaceutics.* 50(1) 27-46.

Picout, D. and Ross-Murphy, S. (2003) Rheology of Biopolymer Solutions and Gels. *The Scientific World Journal*, 3(1) 105-121.

Qian, W., Yu, D., Li, Y., Liao, Y., Wang, X. and Wang, L. (2014) Dual Drug Release Electrospun Core-Shell Nanofibers with Tunable Dose in the Second Phase. *International Journal of Molecular Sciences*, 15(1) 774-786.

Qui, Y. and Park, K. (2001) Environment-sensitive hydrogels for drug delivery. *Advanced Drug Delivery Reviews.* 53(3) 321-339.

Rather, I., Kim, B., Bajpai, V. and Park, Y. (2017) Self-medication and antibiotic resistance: Crisis, current challenges, and prevention. *Saudi Journal of Biological Sciences*, 24(4) 808-812.

Reneker, D. and Chun, I. (1996) Nanometre diameter fibres of polymer, produced by electrospinning. *Nanotechnology*, 7(3) 216-223.

Reneker, D. and Yarin, A. (2008) Electrospinning jets and polymer nanofibers. *Polymer*, 49(10) 2387-2425.

Reneker, D., Yarin, A., Fong, H. and Koombhongse, S. (2000) Bending instability of electrically charged liquid jets of polymer solutions in electrospinning. *Journal of Applied Physics*, 87(9) 4531-4547.

Ribeiro da Cunha, B., Fonseca, L. and Calado, C. (2019) Antibiotic Discovery: Where Have We Come from, Where Do We Go?. *Antibiotics*, 8(2) 45.

Riedl, Z., Szklenárik, G., Zelkó, R., Marton, S. and Rácz, I. (2000) The Effect of Temperature and Polymer Concentration on Dynamic Surface Tension and Wetting Ability of Hydroxypropylmethylcellulose Solutions. *Drug Development and Industrial Pharmacy*, 26(12) 1321-1323.

Riley, M., Robinson, S., Roy, C., Dennis, M., Liu, V. and Dorit, R. (2012) Resistance is futile: the bacteriocin model for addressing the antibiotic resistance challenge. *Biochemical Society Transactions*, 40(6) 1438-1442.

Roth, D., Finkelshtein, A., Ingham, C., Helman, Y., Sirota-Madi, A., Brodsky, L. and Ben-Jacob, E. (2013) Identification and characterization of a highly motile and antibiotic refractory subpopulation involved in the expansion of swarming colonies of Paenibacillus vortex. *Environmental Microbiology*, 15(9) 2532-2544.

Rudin, A. and Choi, P. (2012) *The elements of polymer science and engineering*, 3rd edition. Waltham, Mass.: Elsevier Science.

Schach, R. and Creton, C. (2008) Adhesion at interfaces between highly entangled polymer melts. *Journal of Rheology*, 52(3) 749-767.

Serpe, M. and Craig, S. (2007) Physical Organic Chemistry of Supramolecular Polymers. *Langmuir*, 23(4) 1626-1634.

Sill, T. and von Recum, H. (2008) Electrospinning: Applications in drug delivery and tissue engineering. *Biomaterials*, 29(13) 1989-2006.

Silva, C., Silva, S. and Ribeiro, S. (2018). Application of Bacteriocins and Protective Cultures in Dairy Food Preservation. *Frontiers in Microbiology*, 9(594).

Sinko, P. (2017) *Martin's physical pharmacy and pharmaceutical sciences*, 7th edition. Philadelphia: Wolters Kluwer.

Smith, P., Watkins, K. and Hewlett, A. (2012) Infection control through the ages. *American Journal of Infection Control*, 40(1) 35-42.

Song, Z., Chiang, S., Chu, X., Du, H., Li, J., Gan, L., Xu, C., Yao, Y., He, Y., Li, B. and Kang, F. (2017) Effects of solvent on structures and properties of electrospun poly(ethylene oxide) nanofibers. *Journal of Applied Polymer Science*, 135(5) 1-10.

Stevens, K., Sheldon, B., Klapes, N. and Klaenhammer, T. (1991) Nisin treatment for inactivation of Salmonella species and other gram-negative bacteria. *Applied and Environmental Microbiology*, 57(12) 3613–3615.

Sun, B., Long, Y., Zhang, H., Li, M., Duvail, J., Jiang, X. and Yin, H. (2014) Advances in three-dimensional nanofibrous macrostructures via electrospinning. *Progress in Polymer Science,* 39(5) 862-890.

Tangcharoensathien, V., Sattayawutthipong, W., Kanjanapimai, S., Kanpravidth, W., Brown, R. and Sommanustweechai, A. (2017) Antimicrobial resistance: from global agenda to national strategic plan, Thailand. *Bulletin of the World Health Organization*, 95(8) 599-603.

Thomas, J. and Valvano, M. (1992). TolQ is required for cloacin DF13 susceptibility in Escherichia coli expressing the aerobactin/cloacin DF13 receptor IutA. *FEMS Microbiology Letters*, 91(2), 107-112.

Tortora, G., Funke, B. and Case, C. (2016) *Microbiology*, 12th edition. Upper Saddle River: Pearson Education Limited

van den Elzen, P., Walters, H., Veltkamp, E. and Nijkamp, H. (1983) Molecular structure and function of the bacteriocin gene and bacteriocin protein of plasmid Clo DF13. *Nucleic Acids Research*, 11(8) 2465-2477.

Vashist, A., Kaushik, A., Vashist, A., Jayant, R., Tomitaka, A., Ahmad, S., Gupta, Y. and Nair, M. (2016) Recent trends on hydrogel based drug delivery systems for infectious diseases. *Biomaterials Science*, 4(11) 1535-1553.

Vowden, K. and Vowden, P. (2017) Wound dressings: principles and practice. *Surgery (Oxford)*, 35(9) 489-494.

Watkinson, R., Guy, R., Hadgraft, J. and Lane, M. (2009) Optimisation of Cosolvent Concentration for Topical Drug Delivery – II: Influence of Propylene Glycol on Ibuprofen Permeation. *Skin Pharmacology and Physiology*, 22(4) 225-230.

Wenchang, T., Wenxiao, P. and Mingyu, X. (2003) A note on unsteady flows of a viscoelastic fluid with the fractional Maxwell model between two parallel plates. *International Journal of Non-Linear Mechanics*, 38(5) 645-650.

Xiao, H., Luo, C., Yan, D. and Sommer, J. (2017) Molecular Dynamics Simulation of Crystallization Cyclic Polymer Melts As Compared to Their Linear Counterparts. *Macromolecules*, 50(24) 9796-9806.

Yang, S., Lin, C., Sung, C. and Fang, J. (2014) Antibacterial activities of bacteriocins: application in foods and pharmaceuticals. *Frontiers in Microbiology*, 5(241) 1-10.

Zamani, M., Prabhakaran, M. and Ramakrishna, S. (2013) Advances in drug delivery via electrospun and electrosprayed nanomaterials. *International Journal of Nanomedicine*, 8(1) 2997-3017.

Zweifel, H., Maier, R. and Schiller, M. (2009) *Plastics additives handbook*. Munich: Hanser.

8 APPENDIX 1

Table 7: Rheological data for 5% HPMC (A1), 7.5% HPMC (B1) and 10% HPMC (C1) (w/w) solutions from quintuplet readings with standard deviation

Frequency / Hz	A1 G'/ Pa	B1 G'/ Pa	C1 G'/ Pa	A1 G''/ Pa	B1 G''/ Pa	C1 G''/ Pa
1	0.0011 ± 0.0025	0.0630 ± 0.0363	0.4180 ± 0.0837	0.8077 ± 0.0467	3.4333 ± 0.1721	10.4638 ± 0.7925
2	0.0056 ± 0.0094	0.1616 ± 0.0632	1.0082 ± 0.2164	1.6187 ± 0.0950	6.8373 ± 0.3317	20.6920 ± 1.5324
3	0.0114 ± 0.0197	0.2977 ± 0.0881	1.8172 ± 0.3904	2.4306 ± 01428	10.2394 ± 0.4906	30.7892 ± 2.2079
4	0.0239 ± 0.0374	0.4802 ± 0.1298	2.8266 ± 0.5710	3.2460 ± 0.1894	13.6299 ± 0.6514	40.7602 ± 2.8673
5	0.0354 ± 0.0617	0.7431 ± 0.2337	4.0049 ± 0.8376	4.0669 ± 0.2364	16.9970 ± 0.7868	50.5798 ± 3.3715
6	0.0535 ± 0.0825	0.8700 ± 0.1760	5.3618 ± 0.9430	4.8921 ± 0.2796	20.4328 ± 0.9846	60.3947 ± 4.0777
7	0.0499 ± 0.1322	1.4415 ± 0.7967	6.8662 ± 1.1875	5.7217 ± 0.3295	23.6983 ± 1.0237	69.9961 ± 4.5631
8	0.1100 ± 0.3516	1.2217 ± 0.2724	8.2856 ± 1.5501	6.5550 ± 0.3841	27.2124 ± 1.2454	79.5794 ± 49823
9	0.0636 ± 0.2195	2.0795 ± 1.8893	10.6063 ± 2.0741	7.3997 ± 0.4300	30.4179 ± 1.4852	88.3654 ± 5.1891
10	0.2085 ± 0.1430	2.0093 ± 0.7886	12.6476 ± 2.8534	8.2321 ± 0.4618	33.8289 ± 1.5713	98.1126 ± 5.6427
11	-0.0232 ± 0.8431	2.4120 ± 2.3878	15.0955 ± 4.0467	9.1065 ± 0.5347	37.1305 ± 1.7331	107.2001 ± 6.2320
12	0.5107 ± 0.8047	2.7879 ± 2.4690	18.1513 ± 2.9164	9.9220 ± 0.5323	40.4252 ± 1.6515	115.4796 ± 6.5206
13	0.2595 ± 3.4500	3.7585 ± 4.3932	21.2832 ± 4.0362	10.7822 ± 0.5116	43.6096 ± 1.8053	123.6240 ± 6.6463
14	-2.7183 ± 1.3789	5.4696 ± 3.6745	24.1094 ± 4.9430	11.7653 ± 0.5796	46.6832 ± 2.2001	132.0242 ± 8.0066
15	-0.1628 ± 5.8685	4.0498 ± 3.4436	22.8541 ± 7.6554	12.5510 ± 0.8405	50.1918 ± 2.1971	142.7068 ± 7.6347
16	-0.4822 ± 5.2689	4.5958 ± 6.4997	19.0128 ± 4.5046	13.4117 ± 0.6511	53.4110 ± 2.7441	154.1442 ± 8.3072
17	1.0703 ± 6.1655	5.2424 ± 6.7816	21.7669 ± 5.8834	14.2825 ± 0.8874	56.6367 ± 2.5204	162.1512 ± 8.8501
18	-2.5520 ± 9.8743	2.9039 ± 7.8312	23.4744 ± 5.4612	15.2776 ± 0.9449	60.1216 ± 2.2958	171.1552 ± 9.3830
19	-0.1960 ± 7.6832	-0.0966 ± 5.4957	25.7877 ± 3.4407	16.0838 ± 0.8416	63.6739 ± 2.2991	179.3668 ± 10.3763
20	3.8651 ± 13.9026	7.5750 ± 10.2151	27.7966 ± 3.5092	16.8688 ± 1.0440	66.1261 ± 2.7286	187.7806 ± 10.7806

9 APPENDIX 2

Table 8: Rheological data for 5% HPMC with 2% PG (A2), 7.5% HPMC with 2% PG (B2) and 10% HPMC with 2% PG (C2) (w/w) solutions from quintuplet readings and with standard deviations

Frequency / Hz	A2 G' / Pa	B2 G' / Pa	C2 G' / Pa	A2 G'' / Pa	B2 G'' / Pa	C2 G'' / Pa
1	0.0029 ± 0.0008	0.0483 ± 0.0178	0.3565 ± 0.0475	0.8353 ± 0.0677	3.5760 ± 0.5428	11.5455 ± 0.6206
2	0.0114 ± 0.0026	0.1552 ± 0.0508	1.0233 ± 0.1232	1.6731 ± 0.1364	7.1440 ± 1.0855	22.8953 ± 1.2010
3	0.0262 ± 0.0064	0.3201 ± 0.0977	1.9733 ± 0.2151	2.5124 ± 0.2054	10.7035 ± 1.6223	34.0928 ± 1.7645
4	0.0470 ± 0.0129	0.5361 ± 0.1529	3.1557 ± 0.3230	3.3543 ± 0.2753	14.2533 ± 2.1537	45.1610 ± 2.3013
5	0.0855 ± 0.0332	0.8107 ± 0.2162	4.5984 ± 0.4546	4.1988 ± 0.3461	17.7873 ± 2.6772	55.9885 ± 2.7833
6	0.1278 ± 0.0335	1.1237 ± 0.2958	6.1997 ± 0.5645	5.0471 ± 0.4159	21.3131 ± 3.1898	66.7296 ± 3.3043
7	0.2295 ± 0.0577	1.5316 ± 0.3884	7.8758 ± 0.6104	5.8942 ± 0.4881	24.8066 ± 3.6930	77.4242 ± 3.8915
8	0.1338 ± 0.2277	1.8590 ± 0.4873	10.0136 ± 0.9959	6.7520 ± 0.5629	28.3249 ± 4.1996	87.6236 ± 4.1292
9	0.4528 ± 0.3452	2.4165 ± 0.7087	11.8728 ± 0.8426	7.6004 ± 0.6366	31.7824 ± 4.6960	98.1129 ± 4.8148
10	0.3321 ± 0.0312	2.8659 ± 0.6651	14.2846 ± 1.1646	8.4718 ± 0.6992	35.2551 ± 5.1823	108.0770 ± 5.1205
11	0.5671 ± 0.4112	3.0549 ± 0.9805	16.1002 ± 1.4414	9.3321 ± 0.7754	38.7743 ± 5.6630	118.4260 ± 5.6711
12	0.4422 ± 1.5102	3.2809 ± 1.1037	18.3458 ± 3.0573	10.1969 ± 0.8158	42.2790 ± 6.3355	128.3404 ± 5.4867
13	0.6863 ± 2.0365	4.3121 ± 3.2256	22.5477 ± 3.6967	11.0657 ± 0.9277	45.5971 ± 6.7289	137.0874 ± 6.3468
14	-1.9892 ± 4.0779	3.7534 ± 4.0586	23.8192 ± 5.4665	12.0510 ± 0.9762	49.1361 ± 6.9226	147.4432 ± 6.4903
15	1.8481 ± 6.1045	4.7673 ± 5.4900	25.9792 ± 5.1356	12.7761 ± 1.0463	52.4870 ± 7.6661	157.2586 ± 7.6457
16	2.3894 ± 5.8604	5.3768 ± 6.3769	29.8132 ± 4.6109	13.6350 ± 0.9525	55.7720 ± 7.4171	166.1814 ± 9.5656
17	-1.1474 ± 10.0589	14.6687 ± 3.1568	30.3429 ± 6.6355	14.7101 ± 1.4269	58.0115 ± 8.1675	176.4870 ± 10.7139
18	3.8331 ± 10.3052	1.9243 ± 7.2784	34.0586 ± 7.6453	15.4770 ± 1.4128	63.1117 ± 9.0296	185.3312 ± 11.8713
19	5.6995 ± 9.2482	9.6455 ± 11.7399	38.9744 ± 12.0304	16.3314 ± 1.4041	65.5481 ± 8.8779	193.5678 ± 11.1802
20	-1.3485 ± 17.8007	17.6384 ± 9.6263	35.7604 ± 12.2126	17.4325 ± 1.2457	68.0849 ± 9.6083	204.6784 ± 9.8026

10 APPENDIX 3

Table 9: Rheological data for 5% HPMC with 7.5% DMSO (A3), 7.5% HPMC with 7.5% DMSO (B3) and 10% HPMC with 7.5% DMSO (C3) (w/w) solutions from quintuplet readings and with standard deviation

Frequency / Hz	A3 G' / Pa	B3 G' / Pa	C3 G' / Pa	A3 G'' / Pa	B3 G'' / Pa	C3 G'' / Pa
1	0.0098 ± 0.0060	0.0866 ± 0.0226	1.1357 ± 0.4502	1.0123 ± 0.0766	4.4314 ± 0.5509	15.0507 ± 1.3452
2	0.0240 ± 0.0128	0.2507 ± 0.0771	2.6415 ± 0.8448	2.0233 ± 0.1532	8.8510 ± 1.1011	29.5110 ± 2.4668
3	0.0520 ± 0.0277	0.5070 ± 0.1601	4.8301 ± 1.4043	3.0466 ± 0.2358	13.2633 ± 1.6369	43.8069 ± 3.5584
4	0.0953 ± 0.0499	0.8357 ± 0.2630	7.5084 ± 2.1206	4.0777 ± 0.3230	17.6525 ± 2.1542	57.9018 ± 4.4671
5	0.1494 ± 0.0827	1.2300 ± 0.3950	10.6563 ± 3.5581	5.1152 ± 0.4122	22.0194 ± 2.6490	71.6288 ± 5.1178
6	0.2220 ± 0.0867	1.6794 ± 0.5247	14.7931 ± 5.3642	6.1550 ± 0.5027	26.3634 ± 3.1436	84.6882 ± 5.8128
7	0.2913 ± 0.1939	2.1532 ± 0.6990	19.2376 ± 7.3917	7.2050 ± 0.5888	30.6891 ± 3.6024	97.4854 ± 6.2874
8	0.4056 ± 0.2474	2.7507 ± 0.7922	24.0404 ± 9.1081	8.2463 ± 0.6746	34.9700 ± 4.0970	110.0182 ± 6.7217
9	0.4745 ± 0.3012	3.2938 ± 1.0489	28.4196 ± 11.2518	9.3032 ± 0. 7761	39.2461 ± 4.5169	122.4468 ± 7.0722
10	0.5073 ± 0.2029	3.9704 ± 1.1772	32.3222 ± 14.9167	10.3524 ± 0.8506	43.4763 ± 4.9675	134.8218 ± 7.2974
11	0.7619 ± 0.8621	4.6536 ± 1.3237	37.4002 ± 16.4550	11.4090 ± 0.9210	47.6843 ± 5.4117	146.6312 ± 7.6680
12	0.6588 ± 1.8014	5.5179 ± 1.4024	41.6066 ± 19.8703	12.4760 ± 0.9578	51.8484 ± 5.9371	158.3544 ± 7.9678
13	1.3039 ± 2.8537	5.6287 ± 3.5566	48.0986 ± 20.6609	13.5380 ± 1.2498	56.1165 ± 6.1164	169.5596 ± 8.5007
14	2.4226 ± 2.5099	9.5264 ± 3.1322	52.4717 ± 24.0299	14.5420 ± 1.2132	59.5936 ± 6.3715	181.0742 ± 8.9016
15	3.0154 ± 3.7080	5.9553 ± 6.6104	62.1938 ± 22.7500	15.5627 ± 1.1972	64.5692 ± 6.4677	191.3438 ± 10.1197
16	3.2013 ± 5.7514	10.0104 ± 7.1336	69.4780 ± 25.1172	16.6890 ± 1.3240	68.1136 ± 6.9455	202.2216 ± 10.7952
17	-0.9112 ± 5.8911	4.7515 ± 2.3865	72.2005 ± 28.7264	17.9571 ± 1.4176	73.2680 ± 8.0713	213.4762 ± 10.9145
18	1.4410 ± 10.6844	8.2343 ± 10.4707	76.6942 ± 32.0265	18.9600 ± 1.4750	76.8456 ± 8.5039	224.5644 ± 10.7795
19	4.7189 ± 9.2464	15.2230 ± 8.3270	89.4132 ± 34.6490	19.9165 ± 1.4952	79.9394 ± 7.8472	234.2240 ± 12.5469
20	8.0578 ± 9.7212	7.3197 ± 6.6999	95.7365 ± 41.1475	20.9322 ± 1.7390	85.3072 ± 9.5695	244.9334 ± 12.9659

11 APPENDIX 4

Table 10: Rheological data of 5% HPMC with 2% PG and 7.5% DMSO (A4), 7.5% HPMC with 2% PG and 7.5% DMSO (B4) and 10% HPMC with 2% PG and 7.5% DMSO (C4) (w/w) solutions from quintuplet readings and with standard deviation

Frequency / Hz	A4 G' / Pa	B4 G' / Pa	C4 G' / Pa	A4 G'' / Pa	B4 G'' / Pa	C4 G'' / Pa
1	0.0037 ± 0.0027	0.0749 ± 0.0241	0.6198 ± 0.1560	0.9735 ± 0.1388	4.2371 ± 0.3528	13.9741 ± 1.6088
2	0.0113 ± 0.0079	0.2084 ± 0.0564	1.7026 ± 0.4633	1.9521 ± 0.2838	8.4567 ± 0.7039	27.5903 ± 3.0806
3	0.0186 ± 0.0161	0.4131 ± 0.1032	3.1908 ± 0.8418	2.9347 ± 0.4266	12.6801 ± 1.0607	40.9401 ± 4.4499
4	0.0229 ± 0.0289	0.6903 ± 0.1645	5.0034 ± 1.2631	3.9206 ± 0.5695	16.8890 ± 1.4162	54.0319 ± 5.7433
5	0.0302 ± 0.0433	0.9921 ± 0.2378	7.1028 ± 1.6946	4.9145 ± 0.5695	21.1160 ± 1.7766	66.8644 ± 7.0109
6	0.0645 ± 0.0551	1.3913 ± 0.3252	9.4129 ± 2.1664	5.9124 ± 0.8572	25.3026 ± 2.1346	79.4985 ± 8.1522
7	0.0772 ± 0.1121	1.8396 ± 0.4169	12.0028 ± 2.6454	6.9224 ± 1.0088	29.4756 ± 2.4877	91.8049 ± 9.2659
8	0.1462 ± 0.0863	2.4179 ± 0.5187	14.6788 ± 3.2078	7.9336 ± 1.1506	33.6037 ± 2.8458	104.0202 ± 10.2354
9	-0.1948 ± 0.3167	2.8427 ± 0.6250	17.4913 ± 3.6993	8.9754 ± 1.3029	37.7752 ± 3.2137	116.0610 ± 11.3115
10	0.2624 ± 0.1731	3.3770 ± 0.6758	20.7869 ± 4.2361	9.9642 ± 1.4505	41.9020 ± 3.5435	127.5650 ± 12.2530
11	0.0296 ± 0.9594	4.1682 ± 0.8712	23.2699 ± 5.4936	11.0228 ± 1.6121	45.9376 ± 3.8804	139.6686 ± 12.6376
12	1.3457 ± 2.0073	3.7789 ± 1.3345	26.3320 ± 4.9176	11.9565 ± 1.7850	50.2361 ± 4.2228	151.2940 ± 14.7907
13	1.4845 ± 3.0017	5.1234 ± 3.8208	31.7053 ± 5.4586	13.0199 ± 1.9902	54.1352 ± 4.6669	161.0752 ± 15.3107
14	2.6304 ± 3.6529	5.1679 ± 2.5186	34.8711 ± 7.1725	13.9680 ± 1.8859	58.2654 ± 4.7067	172.4268 ± 16.4590
15	3.2977 ± 3.0111	11.6605 ± 2.9481	40.1390 ± 8.5899	15.0312 ± 2.2282	61.1851 ± 4.9663	182.3146 ± 16.3558
16	-1.9320 ± 4.4677	4.5805 ± 4.4864	43.8834 ± 8.4351	16.3603 ± 2.4081	66.6506 ± 6.1218	193.2906 ± 18.6217
17	-4.5720 ± 2.3452	9.1156 ± 6.1877	45.9402 ± 10.0858	17.5168 ± 2.4756	69.9221 ± 5.7820	204.8124 ± 19.2209
18	-2.1496 ± 5.0006	2.5028 ± 1.7979	49.5792 ± 10.9594	18.5087 ± 2.5944	75.0310 ± 6.3827	215.4144 ± 20.1928
19	-2.1117 ± 7.3336	10.8349 ± 13.9865	52.5128 ± 14.3721	19.5376 ± 2.9494	77.7526 ± 5.9474	226.1342 ± 19.3499
20	-0.6954 ± 10.8701	17.1481 ± 13.9609	52.3828 ± 20.3265	20.6197 ± 3.1651	80.9130 ± 6.1295	237.8446 ± 17.2952